Chemomechanics of Self-Oscillating Gels

by

Irene Chou Chen

B.S. Chemical & Biological Engineering, University of Wisconsin, Madison (2006)

Submitted to the Department of Chemical Engineering
in partial fulfillment of the requirements for the degree of

Doctor of Philosophy in Chemical Engineering

at the

MASSACHUSETTS INSTITUTE OF TECHNOLOGY

June 2013

Author .....
Department of Chemical Engineering
May 9, 2013

Certified by .....
Krystyn J. Van Vliet
Paul M. Cook Career Development Associate Professor
Thesis Supervisor

Certified by .....
Paula Hammond
David H. Koch Professor
Thesis Supervisor

Accepted by .....
Patrick S. Doyle
Professor of Chemical Engineering, Department Committee for Graduate Students

Chemomechanics of Self-Oscillating Gels

by

Irene Chou Chen

Submitted to the Department of Chemical Engineering
on May 9, 2013, in partial fulfillment of the
requirements for the degree of
Doctor of Philosophy in Chemical Engineering

Abstract

Biological materials such as cardiac and skin tissue exhibit the unique capacity to transduce mechanical stimuli into propagating electrical and chemical signals throughout the body. Few synthetic materials have been engineered to produce communicative chemical signals in response to mechanical input, though such synthetic material analogues could enable devices that mimic biological tissues and pressure sensitive processes whereby molecular mechanoreceptors enable rapid and localized transmission of chemical signals. In this thesis, self-oscillating polymer gels comprising N-isopropylacrylamide-co-Ru(bpy)$_3$ are synthesized in order to elucidate chemical and mechanical (chemomechanical) coupling in synthetic, stimuli-responsive materials, and to design mechanically induced, oscillatory signaling systems.

N-isopropylacrylamide-co-Ru(bpy)$_3$ gels represent a unique class of polymeric materials known as BZ gels, that are capable of undergoing the Belousov-Zhabotinsky (BZ) self-oscillating reaction. When submerged in stagnant solution containing chemical reactants, and in the absence of continuously applied external perturbation, the BZ gels exhibit sustained, colorful oscillations due to the changing oxidation state of Ru(bpy)$_3$ transition metal complex. By measuring temperature profiles of the BZ gel, we showed that the swelling behavior and hydrophobicity of the gel depend on the oxidation state of covalently bound Ru(bpy)$_3$. Using timelapse microscopy, we recorded the BZ oscillations and tracked the far from equilibrium chemical behavior exhibited by the gels. At constant system temperature, the BZ reaction induced cyclic changes in the osmotic pressure of the gel, resulting in periodic gel swelling and shrinking. Such volumetric changes, driven by the BZ reaction, are largest (22 %) when the edge length of the gel is relatively short (0.6 mm), and pattern formation is dominated by slow kinetics. Therefore, by quantifying the chemomechanical behavior of BZ gels, we demonstrated that the gels convert chemical oscillations into mechanical actuation.

Next, we sought to design novel stimuli-responsive behavior in BZ gels by devising methods for mechanically triggering oscillations in quiescent gels. When sufficient macroscopic compressive stress was applied to submerged, non-oscillating gels, BZ oscillations were triggered and persisted until the stress was removed. To our knowledge, BZ gels represent the first synthetic hydrogel capable of producing oscillations in response to mechanical stimuli. To establish the conditions conducive to mechanical triggering, we quantified the chemical regimes for which BZ gels spontaneously oscillate or fail to oscillate. In doing so, we demonstrated that such regimes are governed

by the ratio of inhibitor to activator species, which are both intermediate species that are produced throughout the reaction, providing negative and positive chemical feedback, respectively. Mechanically triggerable conditions corresponded to an intermediate ratio of reactant to inhibitor species, such that mechanical compression enabled transitions near the boundary dividing the non-oscillatory and oscillatory regimes. By varying the crosslinking density of the material, we also showed that both the required stress and strain for inducing oscillations in BZ gels increased with decreasing polymer volume fraction. Application of macroscopic, compressive stress to BZ gels caused a decrease in overall gel volume and an increase in the concentration of $Ru(bpy)_3$, and oscillations were triggered at a critical concentration of $Ru(bpy)_3$. In demonstrating that BZ gels can sense mechanical pressure and respond by transducing such energy into chemical oscillations, we have opened up new avenues of research based on mechanical sensing in BZ gels.

Finally, we explore the mechanisms of synthetic "communication" in which discrete BZ gels sense mechanical stress and transmit chemical signals to neighboring gels. Specifically, we designed arrays of closely spaced gels (0.2 mm gap distance) that communicate via diffusion of activator species. We demonstrated that mechanical triggering can induce wave directionality to a set of gels that would otherwise exhibit disorder, and can propagate signals that change directions by migrating around bends without decay in signal amplitude. By introducing a node to a set of BZ gels, we showed that the BZ signal can split without attenuation, effectively doubling the system output. Last, we quantified the collision of two mechanically induced signals to show that wave collision occurs without amplification, and results in signal extinction. Taken altogether, these studies of signal propagation in BZ gels demonstrate that the underlying mechanism of BZ gel communication is governed by the diffusion of activator species. In addition to demonstrating for the first time a synthetic hydrogel that is capable of generating oscillations in response to mechanical compression, we have shown that BZ gels can propagate mechanically induced signals over long ranges and complex trajectories. Our results can be used to facilitate understanding of complex biological phenomena involving chemomechanical coupling and mechanotransduction, or to design advanced, functional materials that act as pulsating chemical or pressure sensors.

Thesis Supervisor: Krystyn J. Van Vliet
Title: Paul M. Cook Career Development Associate Professor

Thesis Supervisor: Paula Hammond
Title: David H. Koch Professor

In memory of Lian Fan Chou, my grandmother (waipo),
who taught me to always be thankful,
and to appreciate the small things in life.

Acknowledgments

I feel extremely fortunate to have completed both a challenging and fulfilling Ph.D. thesis, and am grateful for the assistance and support of many individuals. First, I would like to thank my advisor, Professor Krystyn Van Vliet, whose persistence and enthusiasm provided constant inspiration and guidance.

I am also grateful for my co-advisor, Professor Paula Hammond, and my committee members, Professor Robert Cohen and Professor Michael Rubner, whose insightful questions greatly improved this thesis.

Much of this work would not have been possible without the scientific expertise and foundational contributions by our collaborators at the University of Pittsburgh. I am deeply indebted to Professor Anna Balazs, Dr. Olga Kuksenok, and Dr. Victor Yashin. It has been a terrific opportunity and true pleasure to work with such creative researchers!

I would like to acknowledge Professor Eric Shusta of UW-Madison. Eric was my first research advisor, and taught me that good research requires creativity, open-mindedness, and scrupulous note taking.

I would also like to thank the entire Van Vliet lab, both past and present members. I was lucky to be surrounded by clever and intelligent colleagues, many of whom have become great friends. Together, we shared many laughs and adventures, both inside and outside the lab!

I also feel fortunate to have met great friends at MIT, and I would like to thank all of them for the wonderful times that have made graduate school so memorable.

I would like to extend my deepest appreciation to Joshua Bialkowski, for having so much confidence in me, and for patiently helping me with my math. Josh provided immeasurable support and encouragement, and constantly inspired me to learn new things.

I am also lucky to have an encouraging and understanding family. I especially thank my parents and my sister for their love and support.

Finally, I would like to thank the MRSEC program of the National Science Foundation (DMR-0819762) for funding my thesis project. I greatly enjoyed interacting with researchers and collaborators through the CMSE IRG-II.

Contents

List of Figures

List of Tables

Chapter 1

Background and Motivation

1.1 Introduction

Most engineered materials, such as cement, steel, and glass, have been designed to withstand changes in temperature, mechanical impact, and chemical exposure. Such materials are used to construct buildings and roads as well as clocks and household applicances, and consistent physical properties over a broad range of environmental conditions are desired. By contrast, an emerging class of synthetic materials, for which the physical properties change in response to environmental stimuli, are being developed to design adaptable and efficient materials of the future.[9–11]

One of the limitations of current synthetic materials is that these materials lack functionality. As a result, devices fabricated from such materials require repeated or sustained stimuli, such as electrical input. Biological materials, on the other hand, can directly convert chemical energy into macroscopic motion, with efficiencies that are sometimes three times as high as synthetic devices.[12,13] Natural materials achieve such efficiency because they are structurally complex and hydrated, rather than uniform and dry. As a result, biological materials can often harness chemical energy from their aqueous environment and translate such molecular reactions into macroscopic motion. In other words, chemomechanics, or chemical and mechanical coupling, underlies the physical processes of many biological phenomena, although the mechanisms are not always well understood.

One method for designing synthetic materials involves mimicking existing biological materials or processes. In unique instances, such bio-inspired materials not only have technological applications, but also contribute to scientific knowledge by helping to elucidate complex, biological phenomena. In this thesis, polymeric hydrogels exhibiting the Belousov-Zhabotinsky (BZ) self-oscillating reaction, are fabricated in order to elucidate chemomechanics in synthetic and natural systems. By mimicking aspects of biological processes, these materials exhibit functional properties with potential applications as sensors and actuators. This chapter introduces the BZ reaction and provides motivation for studying BZ gels and the unique, biomimetic attributes exhibited by such gels.

1.2 Belousov-Zhabotinsky Reaction

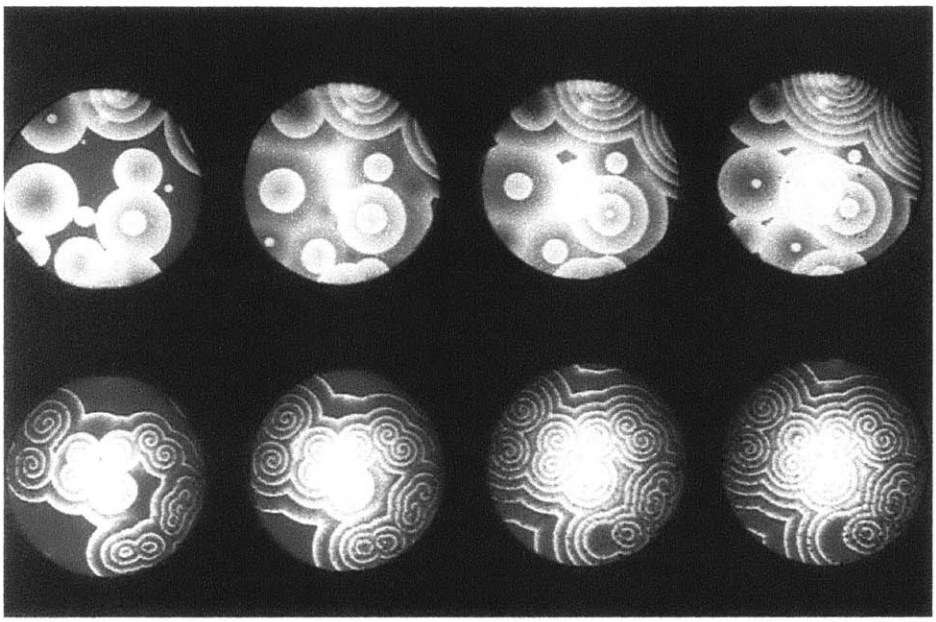

Figure 1-1: BZ patterns in an unstirred solution. Top row illustrates target waves, and bottom row illustrates spiral waves. Both rows represent snapshots taken every 60 seconds (from left to right). Reprinted with permission from Winfree, A.T. *Prog. Theor. Chem, 4*, 1, 1978. Copyright by American Press, 1978.

The BZ reaction is an aqueous phase, oscillating reduction-oxidation (redox) reaction that was discovered in the 1950s by Boris P. Belousov.[14] At the time, Belousov was seeking to mimic the Krebs cycle using inorganic chemicals, when he observed colorful oscillations from a mixture of sulfuric acid, bromate, citric acid, and cerium ions. Belousov's manuscript reporting his discovery of a self-oscillating chemical mixture was rejected due to scientific skepticism, as critics claimed that a well-mixed, homogeneous reaction occuring in a closed system violated the Second Law of Thermodynamics. Later, in 1964, Anatol Zhabotinsky confirmed Belousov's results and characterized the reaction along with the underlying mechanism. He was able to publish his results on the self-oscillating chemical reaction that is now known as the Belousov-Zhabotinsky (BZ) reaction.[14,15]

As shown in Figure 1-1, the BZ reaction is typically characterized by colorful target or spiral shaped chemical waves that spontaneously initiate and propagate throughout the solution. Such wave propagation occurs in an unstirred solution containing BZ reactants, where no chemicals are being added or removed from the system. Target patterns characterized by concentric waves often prevail in BZ solutions occuring without disturbances (see top row in Figure 1-1), however small disturbances that disrupt uniform diffusion, such as solution inhomogeneities (e.g., dust) result in the formation of spiral patterns (see bottom row in Figure 1-1).[14]

Although various combinations of chemical reactants can result in the

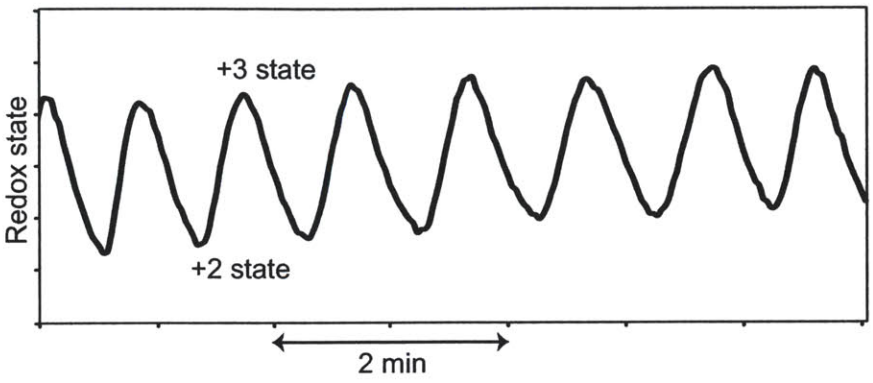

Figure 1-2: BZ oscillations in an unstirred solution. Image analysis was performed at a single location within a BZ solution comprised of 0.2 M MA, 0.3 M $NaBrO_3$, 5 mM ferroin, and 0.3 M H_2SO_4.

BZ reaction, typical reactants include malonic acid (MA), bromate (BrO_3), a transition metal complex, and sulfuric acid (H_2SO_4) or nitric acid (HNO_3). During the reaction, the transition metal complex acts as a catalyst for the BZ reaction and alternates between an oxidized and reduced state due to regulatory, feedback mechanisms. Figure 1-2 shows oscillations in an unstirred BZ solution containing ferroin transition metal complex.

BZ chemical waves are readily visualized via color changes because transition metals (e.g., ferroin complex, cerium ions, or ruthenium complex) exhibit unique colors that depend on the oxidation state of the compound.[14,16] For instance, cerium ions are colorless in the reduced (+3) state and yellow in the oxidized (+4) state. In contrast, the ferroin complex appears red in the reduced (+2) state and blue in the oxidized (+3) state, while the ruthenium complex appears orange in the reduced (+2) state and green in the oxidized (+3) state (also see Figure 1-3). Note that color is not necessarily a binary measurement, and changes in chemical concentration can affect the perceived color saturation of the compound.

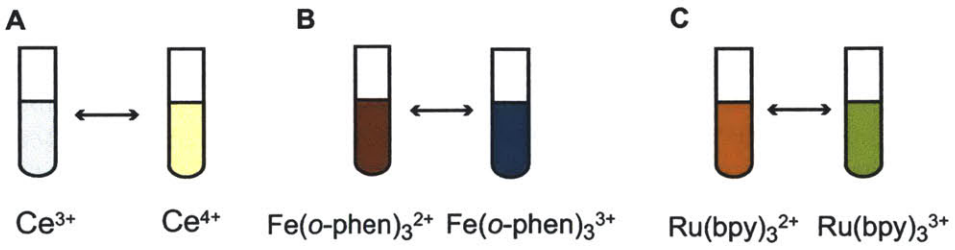

Figure 1-3: Colors exhibited by transition metals at different oxidation states. (A) Cerium ions are colorless or clear in the reduced state and pale yellow in the oxidized state. (B) Ferroin complex is red in the reduced state and blue in the oxidized state. (C) Ruthenium complex is orange in the reduced state and green in the oxidized state.

The kinetics of the BZ reaction are quite complex, involving dozens of chemical species and reaction steps. However, Field, Koros, and Noyes (FKN) developed a simplified reaction mechanism to describe the BZ chemistry:[17,18]

$$BrO_3^- + 2Br^- + 3H^+ \rightarrow 3HOBr, \tag{1.1}$$

$$BrO_3^- + HBrO_2 + 2Ru(bpy)_3^{2+} + 3H^+ \rightarrow 2HBrO_2 + 2Ru(bpy)_3^{3+} + H_2O, \tag{1.2}$$

$$2Ru(bpy)_3^{3+} + MA + BrMA \rightarrow fBr^- + 2Ru(bpy)_3^{2+} + byproducts. \tag{1.3}$$

Here, we have written the reaction in terms of a ruthenium complex ($Ru(bpy)_3$) because this BZ catalyst is employed during most of this thesis work. The variable f is a stoichiometric parameter of the BZ reaction that represents the moles of Br^- produced for every two moles of $Ru(bpy)_3$ that are reduced by MA. Although the value of f depends on the concentration of bromate and other chemical species, oscillations cannot occur when f is greater than 2.[19]

In the above equations, BrO_3^- oxidizes the $Ru(bpy)_3$ catalyst while producing bromous acid ($HBrO_2$), which is the activator species for reaction 1.2. MA then reduces the $Ru(bpy)_3$ catalyst while producing bromide (Br^-), which is an inhibitor species for the reaction step given by reaction 1.2. The FKN mechanism represents a simplified BZ mechanism that aids in understanding of the basic concepts and main processes involved in BZ self-oscillations. It should be noted that each of the reaction steps actually involves many other elementary reactions. Figure 1-4 shows a simplified flowchart for the BZ reaction. Within the entire cycle, $HBrO_2$ and Br^- act as regulatory compounds that provide the necessary feedback for sustained oscillations. Specifically, Br^- provides negative, chemical feedback while $HBrO_2$ provides positive, chemical feedback. This combination of positive and negative feedback results in sustained chemical oscillations.

Without a detailed understanding of the reaction chemistry, the BZ reaction appears to violate the Second Law of Thermodynamics, which states that all chemical reactions proceed in a direction that decreases the Gibbs free energy of the system. A common misconception of the BZ reaction is that oscillations occur around the equilibrium state of the solution. In fact, it is not possible for a closed homogeneous system that lacks diffusion gradients to oscillate around its equilibrium state while approaching a steady-state equilibrium (see Figure 1-5A).[16] However, it is possible for a closed homogeneous system to experience oscillations while approaching equilibrium when these oscillations occur around quasi-steady states (this scenario is depicted in Figure 1-5B). In other words, the BZ reaction operates far from equilibrium, and oscillations occur around quasi-steady states.[16]

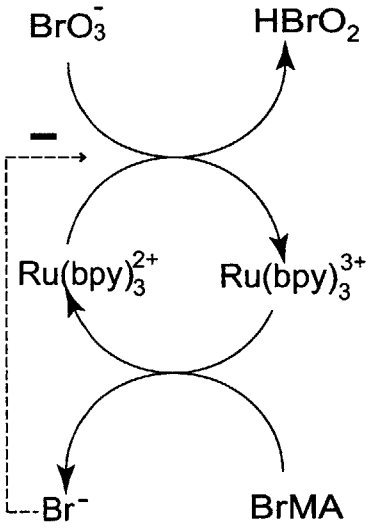

Figure 1-4: Flowchart for the BZ reaction.

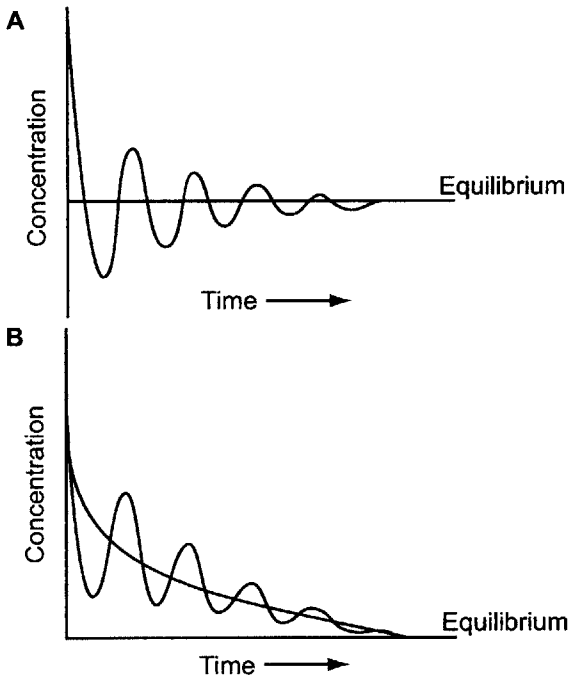

Figure 1-5: Oscillations in a closed, uniform aqueous solution. (A) Oscillations proceed around equilibrium. Note that this is not possible for closed, unstirred BZ solutions. (B) Oscillations proceed around quasi-steady states. Adapted with permission from (Degn, H., *J. Chem. Educ., 49* (5), p 302). Copyright (1972) American Chemical Society.

An additional level of complexity is introduced within the BZ system when considering thermal feedback. Altogether, the overall BZ reaction is exothermic. As heat is released during a reaction step, the kinetic constants

of all other individual reaction steps will change. In fact, the redox oscillations driven by the BZ reactions are intimately coupled to temperature oscillations within the system.[20] While various BZ systems exist with different rate constants, the reduction of the transition metal complex is typically the slowest reaction step. On the other hand, the generation of HOBr due to Br^- is several orders of magnitude faster than the other reaction steps.[20]

1.2.1 Nonlinear chemical dynamics and biological analogies

Previously, the BZ reaction and other chemical oscillators have been used to experimentally study systems that similarly exhibit nonlinear dynamics, sensitive initial conditions, or potentially chaotic behavior. Such studies have allowed researchers to develop methods for stabilizing chaotic output by controlling system feedback.[21] The advantage of using the BZ reaction to model such chaotic systems is because color output facilitates measurements of both spatial and temporal oscillations.

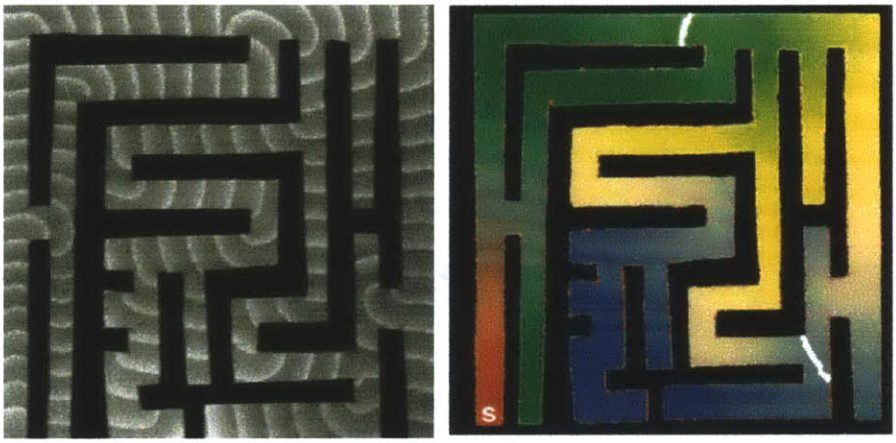

Figure 1-6: Applying BZ wave propagation to determine the optimal path in a maze. Left image is a snapshot of the experiment, and right image is a color map illustrating the time difference between initiation and wave observation at different locations. Red, green, yellow, and blue represent increasing times, and white lines indicate points of wave collision. Adapted from (Steinbock, O., *Science, 267*, p 869, 1995) Reprinted with permission from AAAS.

The BZ reaction has also been applied to problems in path planning. Shown in Figure 1-6 is a maze with tangible obstacles that has been immersed in the BZ solution. While typical path planning problems are solved computationally using iterative methods,[22] Figure 1-6 shows that the chemical waves of the BZ reaction can be imaged to identify the optimal path through a maze.[23] In addition to providing interesting applications, the process of path optimization using BZ waves is a potential analogy to path planning in biological systems governed by reaction and diffusion. Understanding the mechanisms of path planning in synthetic chemical systems may provide important hypotheses regarding unknown mechanisms of path optimization in chemically driven systems such as neuronal networks.[23]

Indeed, simplified chemical systems such as the BZ reaction have been

used to study a variety of complex biological phenomena. Ultimately, the aims of developing simplified models of complicated processes are (1) to gain insights into the underlying mechanisms of difficult problems, and (2) to develop treatments or solutions.[24,25] For instance, Winfree used BZ chemical waves to understand spiral pattern formation and how such patterns affect cardiac defects. In particular, ventricular fibrillation has been associated with cardiac tissue inhomogeneities that disrupt the propagation of normal, concentric electrochemical waves. In cardiac tissue, wave disruption results in uncoordinated, spiral waves. As discussed previously, inhomogeneities in the BZ solution reaction also lead to target wave breakup and the formation of spiral patterns.[25,26] Thus, the simple nature of the model BZ system facilitated identification of the underlying mechanism causing wave breakup in complex, biological systems.

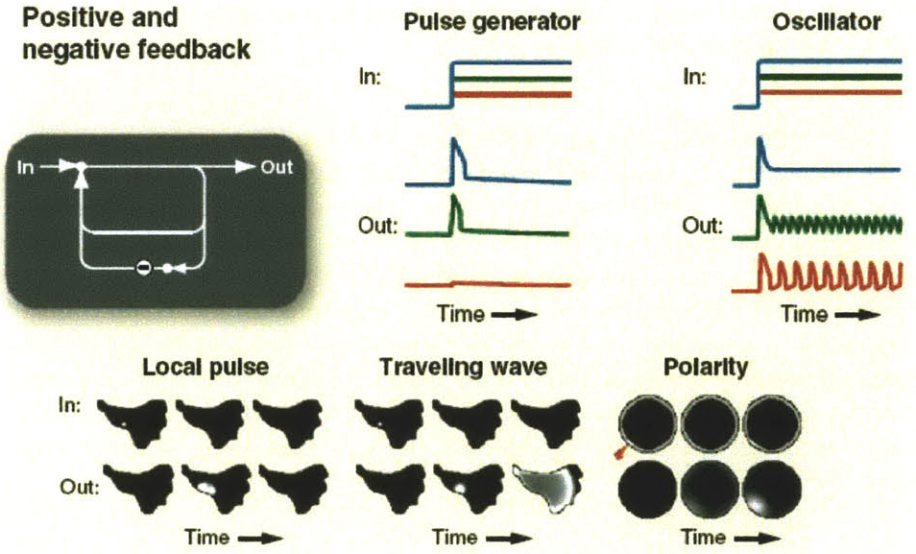

Figure 1-7: Coupled positive and negative feedback in biological cells can lead to a local pulse, traveling wave, cell polarization, and oscillations. Reprinted from (Brandman, O. *Science Signalling, 322*, p 390, 2008) with permission from AAAS.

In fact, the human body undergoes various oscillatory processes, such as circadian rhythms, the Krebs cycle, and intercellular Ca^{2+} signaling, to name a few.[27,28] Intimately linked with such oscillations are regulatory feedback loops and release of signaling molecules. Specifically, oscillations often occur as a result of coupled positive and negative system feedback. As shown in Figure 1-7, feedback can even give rise to self-oscillating chemical waves in biological cells. Often, these waves are Ca^{2+} gradients that can be transmitted across gap junctions to communicate with other cells.[28] Altogether, the BZ reaction mimics coupled positive and negative feedback, oscillatory output, wave patterns, and signal propagation observed in biological phenomena.

In many instances, the chemical dynamics of biological systems are analogous to the BZ dynamics, and similarities can be visually striking. As shown in Figure 1-8, the spatial patterns observed in the BZ reaction are actually comparable to the visual patterns observed in aggregating Dictyostelium Dis-

Figure 1-8: Pattern formation in the BZ reaction (left image) and in Dictyostelium Discoideum slime mold (right image). Reprinted from (Epstein, I. *PNAS, 103*, p 15727, 2006) with permission from NAS.

coideum slime mold. Through comparison with the BZ reaction, researchers have been able to model the chemical mechanism by which cyclic adenosine monophosphate (cAMP) signaling causes auto-chemotaxis in slime mold. Here, chemotaxis refers to the process by which the slime mold organisms migrate towards high concentrations of cAMP. Since the slime mold organisms emit cAMP, chemotaxis is basically autonomous and results in self-aggregation. Therefore, the study of coupled reaction and diffusion in BZ systems not only elucidates the mechanisms of pattern formation and chemical signaling in biological species, but also clarifies the underlying physical phenomena driving self-aggregation, or auto-chemotaxis, in these organisms. [24,25]

1.2.2 Chemomechanics in biological systems

When oscillatory, chemical dynamics are coupled to other physical attributes, then the overall system behavior becomes even more complex, and may be governed by additional factors and physical constraints such as material mechanics. In muscle tissue, for instance, the chemical energy from ATP drives muscle contraction and motion. [12] Chemical oscillations in the body can also be triggered or altered by external, mechanical stimuli. For example, Huo et al. showed that when a network of individual bone cells (osteocytes) are connected by gap junctions, and a single cell is targeted by applying a mechanical load via nanoindentation, then a chemical signal is triggered in the cell and is self-propagated throughout the cellular network. [29] Cardiac and skin tissue also exhibit the unique capacity to transduce mechanical stimuli into propagating electrical and chemical signals throughout the body. [30] Even plant life can be responsive to environmental stimuli: the *Mimosa Pudica*, also known as the touch-me-not plant, can sense temperature, light, chemistry, and pressure. In response to touch, the *Mimosa* leaves fold together and signal neighboring leaves to enclose, causing a wave of folding

leaves that propagates towards the node.[31–33] At the cellular, tissue, and organism level, chemomechanics plays an important role in biological materials undergoing oscillations.

1.3 Stimuli-responsive materials

In many of the biological examples discussed above, the system or material was responsive to a particular external stimulus. Recently, synthetic materials have been engineered to respond to changes in their external environment. These "stimuli-responsive" materials have become an emerging technology because of their potential application as sensors, transducers, and actuators. In designing such functional materials, researchers aim to develop solutions to problems in drug delivery, energy, analytical detection, and more.[1,2] An example of commercialized, responsive materials are photochromic composites for eyeglass lenses. These materials contain responsive silver halides that react to ultraviolet light. As a result, the eyeglasses darken in sunlight, shielding the wearer from harmful ultraviolet rays.

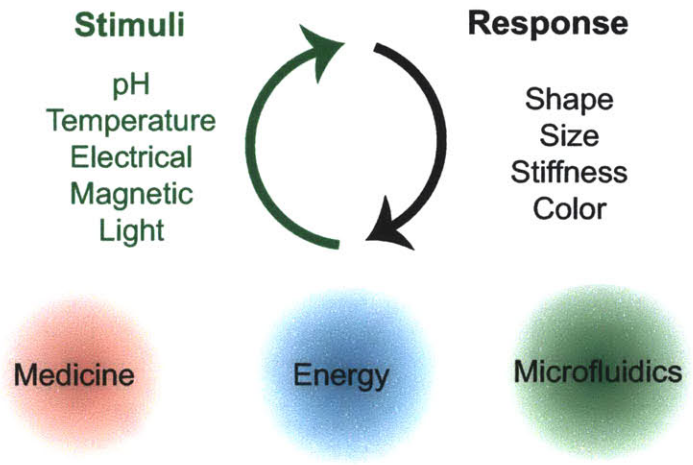

Figure 1-9: Polymer hydrogels are able to respond to various stimuli by exhibiting changes in their physical properties. Such materials have potential applications in medicine, energy, microfluidics, and more.[1,2]

Polymers are an ideal material for designing synthetic systems with stimuli-responsive behavior. One of the unique characteristics of polymers is that they can often exchange energy and material with their external environment. Furthermore, polymers can provide a backbone for composite materials that incorporate responsive particles or structures. When polymer chains are linked by chemical crosslinkers, then a three dimensional material structure is obtained. Either water or solvent can be entrained within the material, resulting in swelling of the polymer network.[10] Because the amount of water absorbed by the material often exceeds the polymer mass,

the crosslinked polymer is referred to as a polymer hydrogel, or just "gel."

Due to the design flexibility of polymer systems, an impressive range of functional polymers has already been demonstrated to change in color, hydrophobicity, conductivity, stiffness, or physical dimensions in response to external stimuli such as pH, temperature, electrical, magnetic, and optical stimuli.[2,10,34–37] Chemomechanical coupling drives stimuli-responsive behavior in some of such materials. For instance, by incorporating cellulose nanofibers in a polymeric material, Capadona et al. demonstrated reversible changes (40x) in tensile modulus, in response to changes in the chemical environment of the material.[38] Schmidt et al. fabricated polymer composite thin films containing Prussian Blue nanoparticles that undergo reversible changes (2x) in the Young's elastic modulus, in response to electrochemical stimuli.[39] And Chia et al. looked at pH induced changes in the reversible swelling of nanotube arrays comprising polyelectrolyte multilayers.[40] In these specific examples, the polymeric materials exhibited tunable mechanical properties in response to different forms of chemical stimuli.

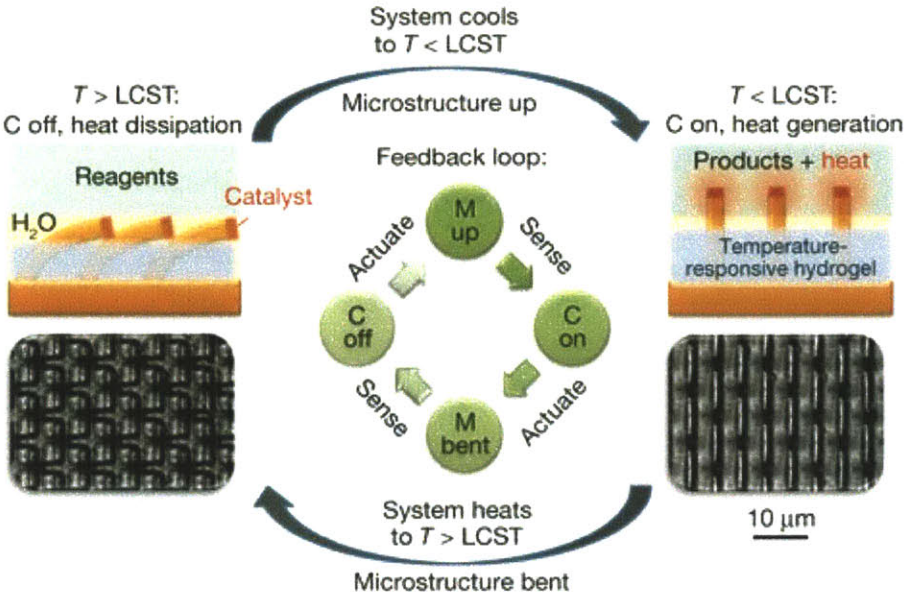

Figure 1-10: Self-regulating material system comprising a thermoresponsive gel undergoing an exothermic reaction. Since the chemistry of the system is coupled to the mechanical properties of the gel, the system is able to cool or heat as necessary in order to maintain homeostasis. Adapted from (He, X. *Nature, 487*, p 214, 2012) with permission from Nature Publishing Group.

One of the current limitations of stimuli-responsive materials is that these systems are often unable to *maintain* responsive behavior, and sustained output requires constant or repeated stimuli. As described previously, biological materials can autonomously regulate a responsive output by exhibiting oscillations. In contrast, synthetic materials typically respond once to an external stimulus and are not able to maintain cyclic or oscillating responses to stimuli for extended durations. In 2012, He et al. fabricated a polymeric system capable of self-regulation. As shown in Figure 1-10, the system is composed

of a thermosensitive hydrogel that supports microstuctures containing chemical catalyst. Due to chemical and mechanical feedback, the system is able to heat or cool itself in order to maintain homeostasis.[41] Thus, hierarchical material systems have quite recently been designed to exhibit autonomous responsive behavior.

1.4 BZ materials

BZ gels are a unique class of stimuli-responsive materials because these gels are capable of undergoing sustained oscillations as a result of the BZ reaction. Most BZ gels confine the transition metal catalyst for the reaction within a polymer backbone, and oscillate when they are submerged in solutions containing MA, BrO_3, and HNO_3. While other BZ media exist, in which the reaction has been incorporated into materials such as membranes and resins (see Table 1.1), BZ gels are unique in that the extent of hydration, or gel swellability, depends on the oscillatory state of the reaction. In 1996, Yoshida et al. invented a BZ gel comprising poly(NIPAAm-co-Ru(bpy)$_3$),[42] and such gels represent the most well studied BZ material. Table 1.1 summarizes some of the experimental research involving these gels and other BZ materials. Note that this list is not fully comprehensive, but covers most of the research groups and some of their studies on the BZ reaction in materials.

Yoshida et al.'s initial studies on BZ gels focused on characterizing the mechanical oscillations of the gel due to the BZ reaction. In those studies, they demonstrated that the overall oxidation state of the covalently bound Ru(bpy)$_3$ catalyst altered the equilibrium swelling - and hydrophilicity - of the polymer network.[42] Because NIPAAm polymer exhibits a lower critical solution temperature (LCST), and becomes partially immiscible at temperatures higher than the LCST, NIPAAm based BZ gels shrink with increasing temperature as the hydrophilicity of the gels decrease. Yoshida et al. showed that the temperature profiles of BZ gels depend on the oxidation state of covalently bound Ru(bpy)$_3$ catalyst, and used these data to demonstrate mechanical swelling and shrinking of a gel undergoing the BZ reaction at constant system temperature (20°C).[42,45]

Later, Yoshida et al. characterized the oscillatory regimes of the BZ reaction for solution and gel phase reactions (see Figure 1-11).[8] They showed that oscillations in BZ solutions generally occur over a larger range of chemical conditions than oscillations in BZ gels. In those studies, oscillations occurring in BZ solutions were measured via potentiometric measurements of redox potential. However, oscillations occuring in BZ gels were measured by quantifying the mean gray value of the gel, since electrodes cannot be easily inserted in a mm-sized BZ gel without disturbing the material. Note that the former method of potentiometry is an established method of accurately measuring redox potential, however the latter method of quantifying gray scale changes may not be accurate at all chemical conditions. A more robust image analysis method of quantifying oscillations in BZ gels would facilitate understanding of the underlying chemical mechanisms that determine oscillatory regimes in BZ gels.

Author	Material	Stimulus	Description
R. Yoshida	NIPAAm gel	Optical	Optical control [43]
	NIPAAm gel	Temperature	Temperature control [44]
	NIPAAm gel	Chemical	Synchronized mechanical oscillation [45]
	NIPAAm gel	Chemical	Ciliary motion [46]
	NIPAAm gel	Chemical	Peristaltic motion [47]
	NIPAAm gel	Chemical	Oscillation in nanogels [48]
	NIPAAm gel	Chemical	Soluble-insoluble oscillation [49]
	NIPAAm gel	Chemical	pH control [50]
	NIPAAm gel	Chemical	Bending-stretching motion [51]
	NIPAAm gel	Chemical	Oscillation w/organic acid [52]
	NIPAAm gel	Chemical	Directional signaling in arrays [53]
	NIPAAm gel	Chemical	Oscillation in viscosity [54]
	NIPAAm gel	Chemical	Flocculating-dispersing microgels [55]
	NIPAAm gel	Chemical	Oscillation with higher LCST [56]
K. Yoshikawa	Resin beads	Chemical	Modes of pattern formation [57]
I.Y. Konotop	PAAm gel	Chemical	Coupled mechanical oscillation [58]
B. Grzybowski	Agarose	Chemical	Modes of pattern formation [59]
R.G. Nuzzo	PAAm gel	Chemical	Oscillation in patterned gels [60]
R.A. Vaia	Gelatin	Chemical	Coupling in patterned gels [61]
K. Suzuki	Membrane	Mechanical	Indentation-induced target wave [62]
V.I. Krinsky	PAAm gel	Mechanical	Stretch-induced vortex drift [63]

Table 1.1: Summary of some of the experimental studies on BZ materials. Corresponding author for the study is listed.

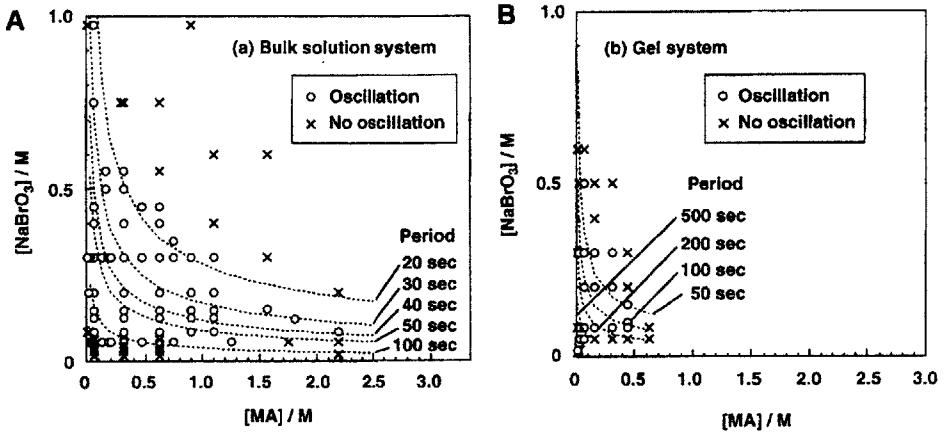

Figure 1-11: Oscillatory regimes of the BZ reaction according to $[NaBrO_3]$ and [MA]. (A) Oscillations in BZ solution occur over a larger range than (B) oscillations in BZ gels. Data correspond to initial concentrations, with constant 0.4 M HNO_3. Adapted with permission from Yoshida et al., *J. Phys. Chem. A, 104*, 43, 1999. Copyright (1999) by American Chemical Society.

As shown in Table 1.1, many of the studies by Yoshida et al. have focused on harnessing chemically driven mechanical actuation to drive macroscopic gel motion, in the form of peristaltic movement, cilia motion, or gel bending and stretching.[46,47,51] BZ gels, therefore, are capable of mimicking basic biological functions such as the conversion of chemical energy into muscle movement, or mechanical motion.

Additionally, many aspects of the BZ gel system have been chemically modified. Led by Yoshida, Hara et al. developed a molecular understanding of polymer chain solubility, by incorporating either a positively charged 3-trimethylammonium propyl methacrylamide chloride (MAPTAC) group,[64] or an acrylamide-2-methylpropanesulfonic acid (AMPS) group in the BZ gel polymer network.[65] Then, by introducing both MAPTAC and AMPS in the BZ gel, Hara et al. showed that BZ oscillations do not require nitric acid, and can occur in the presence of only malonic acid.[52] Synthesis of poly(EMAAm-co-$Ru(bpy)_3$) BZ gels was performed to show that large amplitude self-oscillations of the gel can be achieved at body temperature (37°C).[66] Finally, nanogels[48] and microgels[55] undergoing BZ oscillations have also been reported by the Yoshida group. In the latter system, periodic flocculation was observed due to the alternating colloidal electrostatic repulsion between BZ microgels.[55]

Note that Yoshida et al. have been publishing work on BZ gels for well over a decade now, so it is not surprising that their studies have become increasingly diverse and sophisticated. In addition to studying the BZ reaction, their group looked at pattern formation in polyacrylamide gels undergoing the ferrocyanide-iodate-sulfite (FIS) reaction, which provided visually striking results that observed patterns depend on gel swelling, or the diffusivity of the material.[67] And taking a different perspective on applications involving NIPAAm-co-$Ru(bpy)_3$ gels, Okeyoshi et al. from the Yoshida group

incorporated nanoparticles in the gel to fabricate artificial photosynthetic systems.[68,69]

Taken altogether, it would seem that Yoshida et al.'s pioneering work in the field of BZ gels leaves little room for innovation or contributions from outside research groups. However, it is important to note that nearly all of the BZ gel actuators developed by Yoshida et al. are governed by the same principle of chemically driven mechanical motion. One particular area of unexplored research on BZ gels involves the opposite phenomena in which BZ oscillations are driven by external, mechanical stimuli. Simulations of stimuli-responsive behavior in BZ gels (described next) have predicted that these materials respond to mechanical stimuli.

Overall, theoretical studies concerning BZ gels have been dominated by research groups specializing in computational simulations. Notably, Balazs et al. have developed a computational model for simulating the BZ dynamics in a gel.[70] Their model is based on the FKN model of the BZ reaction (described above by Equations 1.1 - 1.3) in which the polymer volume fraction of the gel is incorporated as a non-reactive species that affects the chemical concentrations of BZ reagents. They modeled the polymer as a network of Hookean springs, and also accounted for interactions between the polymer and BZ solvent using the Flory-Huggins interaction parameter. Lastly, to simulate the BZ gels in three dimensions, the researchers combined finite difference and finite element methodology.[70,71]

Much of the work by Balazs et al. predicts unique behavior in BZ gels, including gel-to-gel "communication" driven by chemical signaling among discrete BZ gels.[72,73] Specifically, signaling occurs when intermediate reaction species are generated within the gel by the BZ reaction, and diffuse through solution toward neighboring BZ gels. Such signaling leads to the development of chemical gradients that allow for macroscopic gel motion and self-aggregation.[72] In 2010 - 2011, the diffusion of BZ intermediate reaction species in BZ droplets was experimentally studied by Fraden et al., and they showed that communication among droplets can lead to synchronization of oscillations.[74,75] However, their system of BZ droplets was unable to exhibit mechanical actuation or movement. In addition, Fraden et al. has not yet explored signal transmission, in which signaling molecules originate from a local source due to an external cue, and then propagate away from the site of origin.

In addition to chemical signaling, the Balazs et al. simulations also predict mechanical responsiveness in BZ gels, toward stimuli such as macroscopic compression, tensile strain, and localized indentation.[5,6,76] While their simulations predict novel responsive behavior in BZ gels, designing actual BZ gel systems that respond to mechanical stimuli is experimentally challenging. Note that Table 1.1 references only a few BZ systems that respond to mechanical stimuli, and so the aforementioned predictions represent an unexplored research area within BZ gels. Since few synthetic materials are able to produce oscillating chemical signals in response to mechanical stimuli, such synthetic material analogues could enable devices that mimic self-healing and pressure sensitive processes where molecular mechanoreceptors enable rapid and localized transmission of chemical signals.[77,78]

1.5 Thesis motivation and strategy

1.5.1 Motivation: understanding chemomechanics in material systems

BZ gels are an ideal material system for studying chemomechanics because the BZ reaction dynamics are constrained by physical confinement within the polymeric material. Indeed, previous studies have already demonstrated the strong chemical and mechanical coupling in BZ gels.[45,58] In this thesis, BZ gels are used as a model system for studying chemomechanics in synthetic gels, and comparisons are made to biological phenomena. One clear advantage of using BZ gels to study generalized chemomechanics is that the state of the gel and reaction dynamics can be readily visualized via color changes and macroscopic size changes of the material. Such colorful responses facilitate interpretation of chemomechanical oscillations that would be relatively difficult to track in biological systems.

1.5.2 Overall objective: engineering novel stimuli-responsive behavior in BZ gels

A strong understanding of chemomechanics in BZ gels enables the design of new material behavior. BZ gels are versatile materials that have demonstrated chemical, temperature, and optical responsiveness. Although numerous studies experimentally demonstrate that BZ gels can convert chemical energy into mechanical motion, few studies have demonstrated material responsiveness toward mechanical cues. The numerous predictions by Balazs et al.,[5,6,76] however, indicate that BZ oscillations can be mechanically induced. Thus, the overall objective of this thesis is to engineer novel stimuli-responsive behavior in BZ gels by devising methods for mechanically triggering oscillations and inducing subsequent signal propagation.

1.5.3 Thesis organization

Chapter 2: At the start of this thesis work, to our knowledge, BZ gels had never been fabricated in the United States. Thus, Chapter 2 describes the organic synthesis of $Ru(bpy)_3$ monomer and incorporation in the polymerization of a NIPAAm polymer, BZ gel. Briefly, characterization of the BZ gel is described, in order to lead into the remainder of the thesis.

Chapter 3: The synthesized gels are characterized according to the BZ dynamics, or the oscillatory characteristics of the gel. Multiple variables and their effects on the BZ oscillations are characterized. These variables include environmental conditions such as reactant concentration and temperature, as well as gel shape and size. In quantifying these variables, the basic chemomechanics underlying chemically driven mechanical oscillations are identified. Qualitative observations, or visual pattern formation in BZ gels, are also characterized according to the shape of the gel.

Chapter 4: This chapter addresses the methods and mechanisms for mechanically triggering BZ oscillations in gels. In developing a protocol for mechanically triggering oscillations using macroscopic gel compression, the chemical phase space for a BZ gel is characterized according to oscillatory and non-oscillatory regimes. Multiple approaches to understanding the mechanism of mechanical triggering, in addition to chemical characterization, are employed. Theoretical considerations are made, and required stresses and strains for triggering oscillations are determined for gels of varying crosslinking density. Last, this chapter introduces a proof-of-concept application using BZ gels as pressure sensors.

Chapter 5: Chemical signal propgation among discrete BZ gel discs is coupled to the mechanical triggering of BZ oscillations. By studying signal propagation over extended distances and complex trajectories, the limitations and robust nature of mechanically induced signaling is explored. Additionally, such experiments further elucidate aspects of chemomechanics in BZ gels.

Chapter 6: Novel results regarding mechanical responsiveness and signal propagation in BZ gels are summarized here. In reviewing the thesis contributions, overall impact on BZ gel theory and applications are discussed. Finally, an overview is given regarding the future directions and potential studies involving BZ gel research.

Chapter 2

BZ catalyst and polymer gel synthesis

We gratefully acknowledge Dr. Ryan Moslin and Dr. Amanda Engler for their expertise and assistance with the Ru(bpy)$_3$ synthesis. We also thank the Institute for Soldier Nanotechnologies at MIT for facility access.

2.1 Overview

In order to fabricate a robust material capable of undergoing the BZ reaction for many hours without degradation, a polymer gel comprising covalently bound transition metal catalyst was synthesized. In this chapter, synthesis protocols for a BZ gel comprising poly(NIPAAm-co-Ru(bpy)$_3$) are described.

The first section describes protocols for synthesizing the transition metal catalyst, or Ru(bpy)$_3$ monomer. These procedures involved several different reactions and separation techniques. While the protocols are based off the synthesis described in references[79] and[80], the reactions are scaled down and the purification steps are described here in more detail. Since several of the materials are explosive, flammable, or highly toxic, safety issues are also considered in this section.

Section 2.2 describes protocols for synthesizing a NIPAAm polymer gel with covalently bound transition metal catalyst. The experimental setup and procedures for both heat initiated and UV initiated polymerization are discussed. The polymer synthesis was originally described in[42], but their equipment was different from ours, so our protocols were adjusted accordingly.

The last section, Section 2.3, describes methods for characterizing the successfully synthesized BZ material. Gels are characterized by quantifying the concentration of covalently bound Ru(bpy)$_3$ in the material, and by measuring the polymer volume fraction or crosslink density of the gel. Since NIPAAm is a thermosensitive polymer that has a lower critical solution temperature, temperature profiles were also measured for the gels.

2.2 Synthesis of $Ru(bpy)_3$ monomer

In order to fabricate a BZ gel comprising covalently bound transition metal BZ catalyst, organic synthesis of a ruthenium transition metal coordination complex with an alkene functional group was required. The synthesis was performed following the procedures of Ghosh et al. and Schultze et al.,[79,80] and experiments were performed at the Institute for Soldier Nanotechnology (ISN) in collaboration with Dr. Ryan Moslin from the Swager laboratory at MIT Department of Chemistry. Importantly, the laboratories at the ISN were appropriately equipped with rotary evaporators, cooling water, and fume hood workstations housing double manifolds that allow for chemical synthesis under inert gas. Do not attempt the following synthesis without the proper equipment or training. The use of a double manifold was essential since some of the chemicals were air-sensitive and explosive.

Specifically, n-butyllithium reacts violently with water. In high concentrations, n-butyllithium will spontaneously ignite in air, and the user may be at risk for skin burns.[81] Phosphorous pentoxide also reacts violently with water to form corrosive phosphoric acid, and the user may be at risk for skin burns.[82] Lastly, the gaseous formaldehye prepared in our experiments was extremely toxic. Formaldehyde is a carcinogen,[83] and inhalation of gaseous formaldehyde was prevented by ensuring tightly sealed gas lines. To mitigate harmful effects and potential dangers, the reactions were scaled down relative to the procedures reported in literature.[79] All flasks were sealed from air, and syringe needles were used to prevent chemical exposure to air. It is extremely important to read the material safety data sheets for all materials prior to attempting the procedures described below, and proper personal protective equipment should be worn at all times. All materials were purchased from Sigma-Aldrich, except for $Ru(bpy)_2Cl_2$ which was purchased from Acros Organics. The materials were used as received unless otherwise noted.

2.2.1 Synthesis of 4-Hydroxyethyl-4'-methyl-2,2'-bipyridine

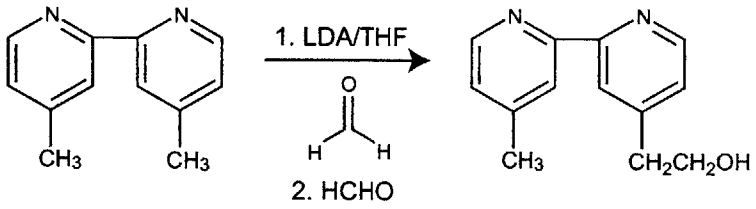

Figure 2-1: Synthesis of 4-Hydroxyethyl-4'-methyl-2,2'-bipyridine from 4,4'-Dimethyl-2,2'-bipyridine. The reaction proceeds once lithium diisopropylamide (LDA) is generated and reacted with the starting compound. A second reaction occurs when paraformaldehyde (HCHO) is added to the mixture.

Shown in Figure 2-1 is an overview of some of the reaction steps involved

in synthesizing the 4-Hydroxyethyl-4'-methyl-2,2'-bipyridine compound, a precursor of the desired $Ru(bpy)_3$ monomer.

Distilled diisopropylamine (0.8 mL, 5.7 mmol)[1] was added to tetrahydrofuran (3 mL) in a vacuum sealed, argon filled flask. Next, 2.5 M n-Butyllithium (2.4 mL, 6 mmol) was added dropwise to the mixture using a syringe pipette, and was stirred for 15 min using a stirplate. Since n-Butyllithium is a strong nucleophile, the compound deprotonates diisopropylamine to form lithium diisopropylamide, a strongly basic compound. Meanwhile, 4,4'-Dimethyl-2,2'-bipyridine (1 g, 5.4 mmol) was dissolved in tetrahydrofuran (25 mL). Using a dropping funnel, the 4,4'-Dimethyl-2,2'-bipyridine solution was added dropwise to the lithium diisopropylamide mixture. The solution was mixed for 2 h to ensure reaction completion. During this time, lithium diisopropylamide deprotonated the methyl group on the 4,4'-Dimethyl-2,2'-bipyridine compound. The color of the mixture turned orange and then dark brown.

Both an inlet and outlet to the flask were quickly added such that exposure to air was limited. The inlet of the flask was connected to tubing with a glass pipette fixed to the end to ensure that the inlet was submerged in the 4,4'-Dimethyl-2,2'-bipyridine mixture. The outlet of the flask was connected to a bubbler to relieve pressure in the flask while maintaining synthesis under inert gas. The inlet tubing was connected to a flask containing dried paraformaldehyde,[2] that was heated in a 180°C oil bath to generate gaseous formaldehyde. A nitrogen inlet was also connected to the paraformaldehyde flask to induce gaseous flow through the tubing. The gaseous formaldehyde was bubbled through the 4,4'-Dimethyl-2,2'-bipyridine mixture. The mixture turned green and then became milky colored before finally turning yellow. After all gaseous formaldehyde was bubbled through the flask, the mixture was stirred for 30 min. During this reaction, the deprotonated 4,4'-Dimethyl-2,2'-bipyridine compound acted as a nucleophile that attacked the carbonyl group of formaldehyde. The reaction was quenched with ice water, and the product was extracted with ether.[3] Ether was then removed from the solid product using a rotary evaporator.

To separate the desired product from unreacted starting material, a silica gel (reverse phase) chromatography column was prepared. Hydrophobic silica was used with a 9:1 ratio of silica to sand. The solid product was dissolved in dichloromethane and poured through the chromatography column. Elution was performed using a mixture of dichloromethane and methanol, and fractions were collected upon elution. A thin layer chromatography plate (TLC) was prepared by rinsing the plate in triethylamine followed by rinsing in 9:1 dichloromethane to methanol. The eluted fractions were tested on the TLC plate to determine which fractions contained starting material versus desired product. Note that the desired product was more polar than the starting material, and was eluted first from the chromatography column. After identifying which fractions contained desired product, these fractions

[1] Diisopropylamine was distilled by Ryan Moslin.

[2] The paraformaldehyde was previously dried in a vacuum for two days with phosphorous pentoxide.

[3] The product was obtained in the viscous ether layer.

were combined and concentrated using the rotary evaporator.

2.2.2 Synthesis of $Ru(bpy)_3$ monomer

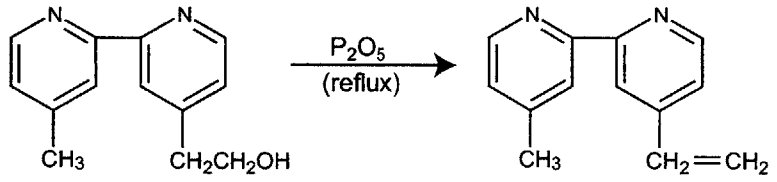

Figure 2-2: Synthesis of 4-Vinyl-4'-methyl-2,2'-bipyridine. The reaction occurs by dehydration of 4-Hydroxyethyl-4'-methyl-2,2'-bipyridine via phosphorous pentoxide (P_2O_5).

The 4-Hydroxyethyl-4'-methyl-2,2'-bipyridine compound (0.78 g, mmol) was dissolved in xylenes (18 mL) and refluxed with phosphorous pentoxide (2.67 g, mmol) for 2 h under inert argon gas. Phosphorous pentoxide is a strong dessicant and dehydrates the 4-Hydroxyethyl-4'-methyl-2,2'-bipyridine compound, eventually converting the alcohol functional group to an alkene (see Figure 2-2). After 2 h, crushed ice was added to cool the mixture and react with excess phosphorous pentoxide. The mixture of xylenes and water was separated using extraction.[4] After removing the xylenes, a large amount of 1 N sodium hydroxide was added to raise the pH to 5 or greater. Further extraction was performed by adding dichloromethane.[5] A rotary evaporator was used to remove the solvent and purify the 4-Vinyl-4'-methyl-2,2'-bipyridine compound.

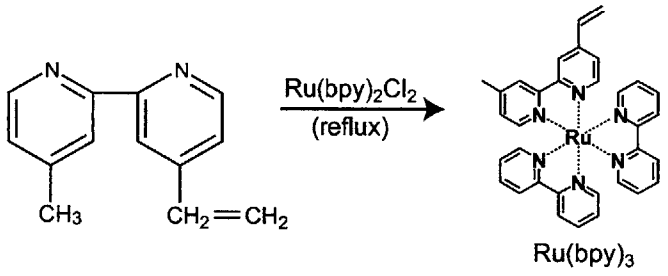

Figure 2-3: Synthesis of $Ru(bpy)_3$ via overnight reflux of 4-Vinyl-4'-methyl-2,2'-bipyridine and $Ru(bpy)_2Cl_2$.

The last step in synthesizing the BZ Ruthenium monomer is another reflux reaction. The 4-Vinyl-4'-methyl-2,2'-bipyridine compound (116.5 mg, 0.59 mmol) and $Ru(bpy)_2Cl_2$ (324 mg, mmol) were dissolved in methanol (6 mL). The mixture was refluxed overnight at 70°C under inert argon gas,

[4]The product was in the bottom, aqueous layer.

[5]The product was obtained in the bottom, dichloromethane layer.

and aluminum foil was used to shield the reaction from light. See Figure 2-3 for a summary of the reaction and the chemical structure of the reactants and product. After $> 10h$, methanol was removed from the product using the rotary evaporator. The resulting solid was orange-brown and was dissolved in water (10 mL). 3 M Ammonium hexafluorophosphate (4 mL) was added to the mixture, and a bright orange-red solid precipitated out of solution. The precipitate was filtered, rinsed with water several times, and dried over the vacuum filter for several minutes. Acetone was used to dissolve the precipitate and collect the desired product. Last, a rotary evaporator was used to remove the acetone from the final product. The resulting product was $Ru(bpy)_3$ monomer, or ruthenium(4-Vinyl-4'-methyl-2,2'-bipyridine)bis(2,2'-bipyridine)Bis(hexafluorophosphate). ^1H NMR (400 MHz, acetone-d6): $\delta = 2.53$ (s, 3H), 5.67 (d, 1H), 6.35 (d, 1H), 6.9 (q, 1H), 7.4 - 8.1 (22H aromatic protons).

Note that the $Ru(bpy)_3$ monomer contains several coordinate covalent bonds in which the bipyridine ligands share electrons with the ruthenium transition metal. Due to the electron repulsion between shared electrons and the spatial arrangement of the orbitals, the energy of the d orbital increases while also splitting into two energy levels. These two energy groups correspond to the $Ru(bpy)_3$ reduced state (+2) and oxidized state (+3), and as electrons transition between these two energy levels, differences in light absorption by the compound result in color change.

2.3 Synthesis of BZ gel

2.3.1 Heat initiated polymerization

A BZ gel comprising poly(NIPAAm-co-$Ru(bpy)_3$) was synthesized by adapting methods by Yoshida et al.[42] (See Figure 2-4 for the polymer components and resulting chemical structure.) Specifically, our polymerization recipe was identical to reference[42], but our polymerization equipment differed. In a typical procedure, $Ru(bpy)_3$ monomer (6.6 mg) was combined with NIPAAm monomer (125 mg), N,N-azobisisobutyronitrile (AIBN) initiator (5.3 mg), and N,N'-methylenebisacrylamide (MBAAm) crosslinker (2-10 mg). The reactants were dissolved in methanol (0.8 mL), and nitrogen was bubbled through the solution in a sealed vial for 5 min (see Fig.2-5B). The polymerization vessel consisted of a crystallizing dish sealed with a rubber stopper. Inside the vessel, a 35 mm Petri dish (Greiner Bio-One) was arranged such that the lid was upside down and placed underneath the dish bottom (see schematic of setup in Fig 2-5C). A long needle was used to fill the vessel with nitrogen gas.[6] Next, using a long syringe needle purged of air with nitrogen gas, the pre-polymer liquid was transfered from the vial to the polymerization vessel. Carefully, the liquid was injected between the Petri dish lid and

[6]If you use a rubber stopper manufactured with two holes, then you can glue small pieces of rubber over the holes. When purging the vessel of air, insert needles through the small pieces of rubber rather than trying to force the needle through the entire rubber stopper. Purging the vessel of air is very important since traces of oxygen prevent free radical polymerization.

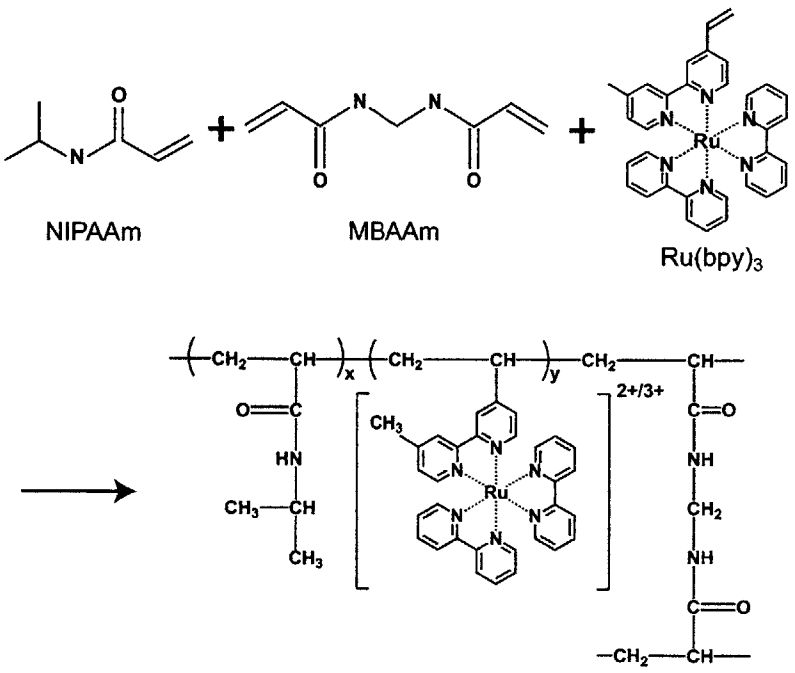

Figure 2-4: Synthesis of poly(NIPAAm-co-Ru(bpy)$_3$ involving NIPAAm monomer, MBAAm crosslinker, and Ru(bpy)$_3$ monomer.

the Petri dish bottom such that the liquid was evenly entrapped between the polystyrene material (see Fig. 2-5D). The entire vessel was placed inside an oven maintained at 60°C, and the reaction was left overnight for 18 h. Other polymerization protocols were tested, including polymerization inside glass vials or polystyrene cups. While the gel successfully polymerizes in these alternative containers, the polymer either irreversibly adheres to the vial, or the polymer is too thick or of uneven thickness. The setup described here represents the most successful and consistent polymerization procedure.

Successfully polymerized gels appeared uniformly yellow or uniformly red, where color depended on the concentration of Ru(bpy)$_3$ monomer. Such uniform gel color indicated that the Ru(bpy)$_3$ monomer was polymerized in its reduced state (+2). Upon removing the polymerization vessel from the oven, the dry polymer gel was tightly adhered to the Petri dish surfaces. A syringe pipette was used to submerge the Petri dish and gel in methanol. The polymer gel gradually absorbed solvent, and excess methanol reduced adhesion between the gel and the Petri dish surfaces. The Petri dish was removed from the vessel when adhesion was no longer affecting the gel. Forcing the Petri dish to separate from the gel before methanol absorption will tear the gel and potentially ruin your material.

Following Yoshida et al.'s procedure,[42] the gel was soaked in methanol for one week, with solvent exchange with fresh methanol was performed each day. This soaking process removed unreacted materials from the system. Used methanol washes were saved for future analysis and determination of Ru(bpy)$_3$ yield. Typically, the first 2 - 4 days of methanol washes were

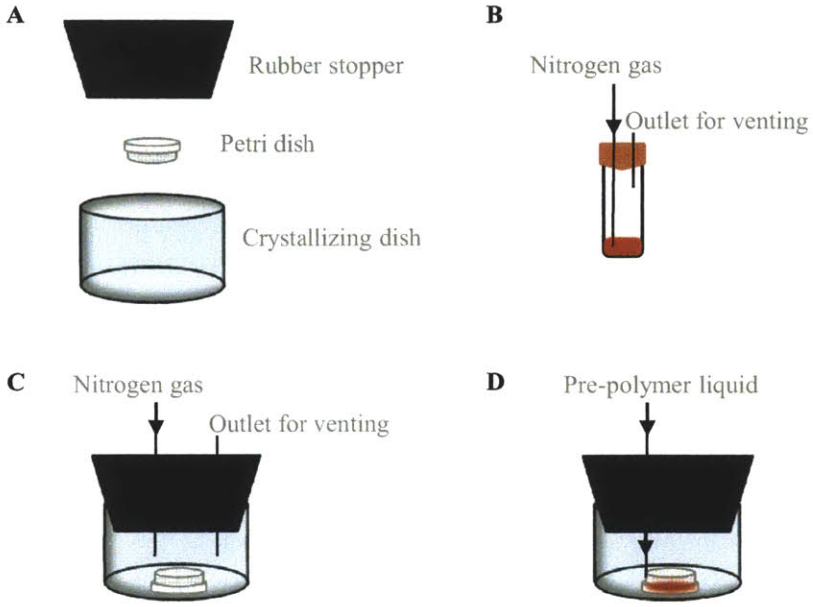

Figure 2-5: Schematic of setup for heat initiated polymerization of BZ gel. (A) Equipment used in polymerization: large rubber stopper, Petri dish, and glass crystallizing dish. (B) Scintillation vial containing pre-polymer liquid, and sealed with a rubber septum. Nitrogen gas was used to purge the liquid of air. (C) Nitrogen gas was used to purge the reaction vessel of air. (D) Pre-polymer liquid was ejected between the lid and bottom of a Petri dish placed inside the purged reaction vessel.

saved, after which time the washes became clear and presumably devoid of detectable $Ru(bpy)_3$ monomer. After one week soaking in methanol, the gel was submerged in a solution of 75% methanol in water for one day. The solvent mixture was exchanged after each day of soaking in increasingly weaker methanol solutions: 50%, 25%, and 0% methanol in water. Soaking the gel in different combinations of methanol and water allows the gel to gradually hydrate.

2.3.2 UV initiated polymerization

Although the heat initiated polymerization protocol was the most consistent procedure, ultraviolet (UV) initiated polymerization was also used to synthesize BZ gels comprising poly(NIPAAm-co-$Ru(bpy)_3$). A Blak-Ray® UV lamp with spot bulb emitting 365 nm UV light (Ted Pella, Inc.) was used to polymerize gels through custom photomasks. The photomasks consisted of a UV-blocking silver emulsion deposited on a film with a 20K dpi resolution (Fineline Imaging, Inc.). In a typical polymerization procedure, $Ru(bpy)_3$ monomer (2-10 mg) was combined with NIPAAm monomer (132 mg), dimethoxy-2-phenylacetophenone photoinitiator (17.5 mg), and N,N'-

methylenebisacrylamide (MBAAm) crosslinker (6-8 mg). The reactants were dissolved in either ethanol or methanol (0.5 mL). Note that gels prepared using ethanol were sometimes more difficult to hydrate. In most experiments, nitrogen gas was bubbled through the pre-polymer liquid for 4 min. Note that purging the polymerization vessel of air was not necessary in the UV initiated polymerization. The photomask with desired pattern was placed inside a 35 mm diameter Petri dish.[7] Next, the pre-polymer liquid was pipetted into an upside down Petri dish lid, and the dish bottom was carefully placed on top of the liquid, effectively sandwiching the pre-polymer liquid. Note that the photomask is not touching the pre-polymer liquid. The dish system was placed under the UV lamp for 1.5 - 3 min, during which time UV protective eyewear was worn, skin was fully covered, and a cardboard box was used to shield any potentially harmful UV rays. Figure 2-6B shows that polymerized gel diameter increased with increasing UV exposure time. The results were graphed according to the maximum, minimum, and average gel diameter for discs polymerized through a photomask comprising an array of circles. As shown in Figure 2-6A, the sizes of the discs were variable during the batch polymerization process. More complex BZ gels, such as the "MIT" letters, were also prepared using UV initiated polymerization (see Fig.2-6C-D for images of the photomask template and resulting BZ gel).

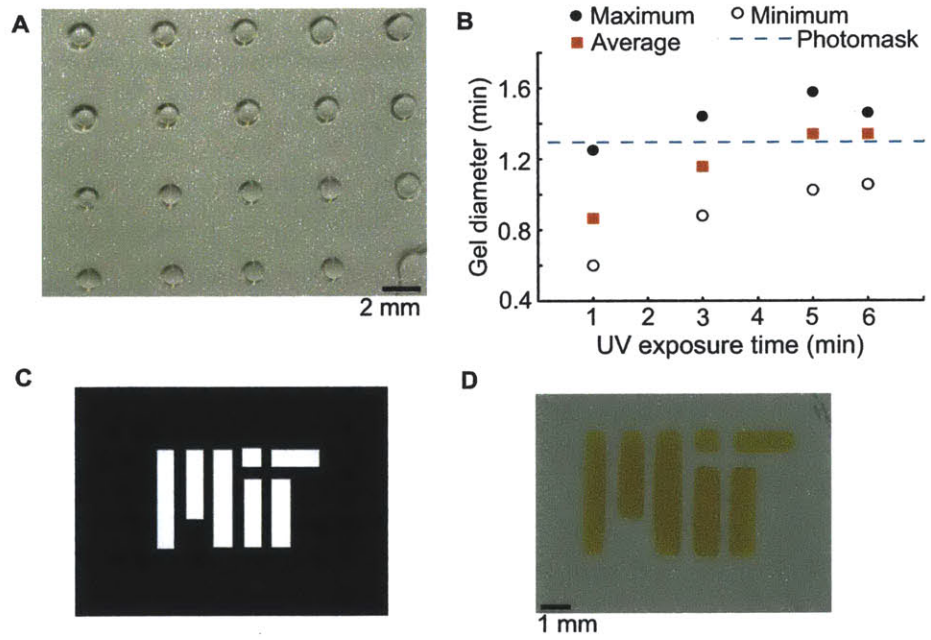

Figure 2-6: UV polymerization through photomasks. (A) Set of NIPAAm gel discs polymerized with 3 min of UV exposure through a photomask comprising 1.3 mm diameter circles. (B) NIPAAm gel diameter versus UV exposure time. (C) Template of "MIT" photomask for UV polymerization. (D) BZ gel polymerized with 1.5 min of UV exposure through "MIT" photomask.

[7]Fineline Imaging (www.fineline-imaging.com) can prepare sheets with multiple photomask patterns. I hand cut the sheets to fit inside the Petri dish.

Several variations on this polymerization protocol were performed due to inconsistent results. Notably, the polymerized BZ gel often irreversibly adhered to the Petri dish. In some experiments, such adhesion was advantageous (see Fig.2-6B where MIT letters are held in place due to adhesion). To prevent adhesion in other experiments, dimethyl sulfoxide (0.1 mL) was added to the pre-polymer liquid. Also note that the pre-polymer liquid was not always purged of air using nitrogen. In fact, when NIPAAm gels were prepared through UV polymerization and contained no $Ru(bpy)_3$ monomer, then gelation occurred consistently in one minute of UV exposure. By contrast, pre-polymer liquids containing $Ru(bpy)_3$ monomer exhibited extremely inconsistent gelation. Most of the time, the liquid failed to polymerize, even when 1 h of UV exposure was allowed. Such inconsistency was attributed to impurities in the $Ru(bpy)_3$ material, however such impurities went unnoticed during heat initiated polymerizations.

Successfully polymerized gels were soaked in methanol and gradually hydrated, as described previously. The resulting gels were typically quite fragile and thin. Also, the yield of $Ru(bpy)_3$ monomer was always less than what was observed for heat initiated polymerizations. For these reasons, experiments on BZ gels comprising poly(NIPAAm-co-$Ru(bpy)_3$) were all prepared using heat initiated polymerization unless otherwise noted in this thesis.

2.4 Characterization of BZ gels

2.4.1 $Ru(bpy)_3$ monomer yield

To calculate the $Ru(bpy)_3$ concentration within the gel, the quantity of unreacted $Ru(bpy)_3$ monomer was subtracted from the total moles of $Ru(bpy)_3$ added to the pre-polymer liquid. Such unreacted $Ru(bpy)_3$ was collected from the gel by soaking the material in methanol. $Ru(bpy)_3$ content in the methanol washes was determined via absorption at λ=457 nm using UV/Vis spectrophotometry. Figure 2-7A shows the UV/Vis calibration curve for absorption of the $Ru(bpy)_3$ monomer in methanol at 457 nm. Figure 2-7B shows typical values of $Ru(bpy)_3$ yield in the gel and corresponding $Ru(bpy)_3$ concentrations. When the amount of initiator and crosslinker are held constant, then the yield of $Ru(bpy)_3$ monomer in the gel increased with increasing $Ru(bpy)_3$ monomer in the pre-polymer liquid.

2.4.2 Polymer volume fraction

The gel was also characterized by determining its polymer volume fraction, $\phi=V_d/V_h$. Here, V_h is the volume of a fully hydrated gel, in which water is entrained by the gel network, and V_d is the volume of the dried gel. The gel dimensions were manually measured, before and after the gel was dried for one day by evaporation. Shown in Figure 2-8 are five different BZ gels polymerized with varying crosslinker (MBAAm). The hydrated gel was more swollen when less crosslinker was used during synthesis (Fig. 2-8Aa). As a result, the polymer volume fraction of the gel, measured when the gels were fully hydrated in water, was smaller for gels containing less crosslinker (Fig.

A

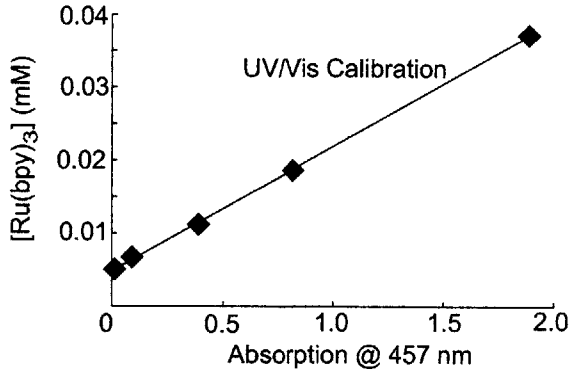

B $[Ru(bpy)_3]$

Pre-polymer liquid (μmol)	MeOH gel wash (μmol)	Gel yield (%)	Gel concentration (mM)
2.22	1.72	77.4	2.15
5.33	4.69	87.8	5.8
7.33	6.66	90.8	8.3

Figure 2-7: UV/Vis calibration curve for $Ru(bpy)_3$ and typical $Ru(bpy)_3$ yields. (A) UV/Vis calibration curve for absorption of $Ru(bpy)_3$ monomer at 457 nm. (B) Tabulated values summarizing amount of $Ru(bpy)_3$ in pre-polymer liquid, unreacted $Ru(bpy)_3$, yield of $Ru(bpy)_3$ in gel, and concentration of $Ru(bpy)_3$ in gel.

2-8B). Also note that the polymer volume fraction of the gels in water was slightly different than the corresponding polymer volume fractions measured in BZ acid.

2.4.3 Temperature characterization

BZ gels were also characterized according to temperature because NIPAAm is a thermosensitive polymer that exhibits a phase transition around 32-33°C.[84] Above this temperature, also known as the lower critical solution temperature (LCST), polymer chains become hydrophobic and insoluble, causing the material to come out of solution. For hydrogel networks comprising NIPAAm, increasing temperature causes the gel to de-swell and eventually collapse above the LCST. The crosslinking density of the gel affects the temperature profile of the gel but does not necessarily change the LCST.[85]

For the BZ gels, the phase transition temperature was characterized by measuring decreasing gel edge length as a function of increasing temperature. Measurements were collected when the gel was fully submerged in 1 mM cerium (III) sulfate or 1 mM cerium (IV) sulfate, corresponding to either the fully reduced or oxidized catalyst states, respectively. The phase transition temperature depended on both the oxidation state of the $Ru(bpy)_3$ catalyst, and the overall $Ru(bpy)_3$ concentration in the material. As shown in Fig. 2-9A, a BZ gel comprising 5.8 mM $Ru(bpy)_3$ collapsed gradually as temperature was gradually increased from 20 to 37°C using a microscope heating stage. Overall, the oxidized gel (black circles in Fig. 2-9A) was more

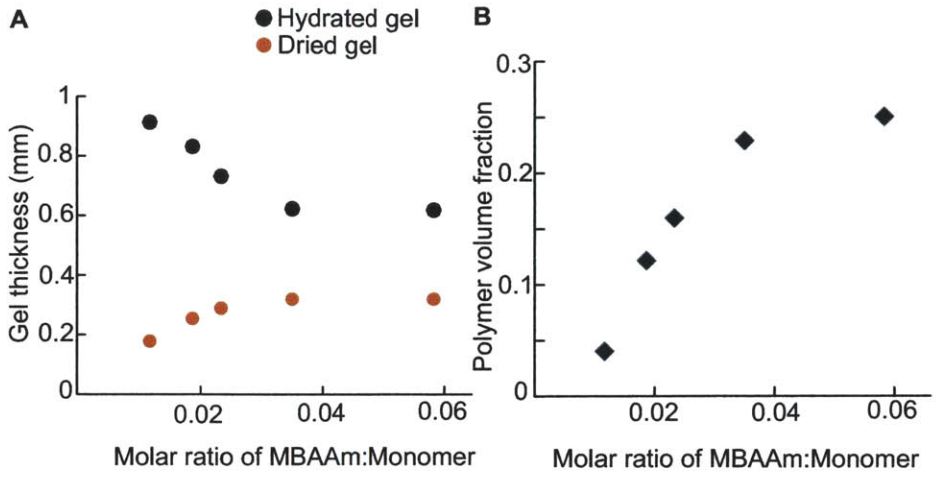

Figure 2-8: Polymer volume fraction of BZ gels in water (A) Hydrated and dried gel thicknesses for gels of varying crosslinking density. The amount of crosslinker (MBAAm) was varied while the amount of total monomer in the system was held constant. (B) Polymer volume fraction of the gels hydrated in water.

swollen than the reduced gel (o data points in Fig. 2-9A). The phase transition appeared to occur around 31-33°C. When the hue (or color) of the gel was characterized according to temperature, the phase transition appeared sharper. (See Chapter 3 for full discussion on hue). For the oxidized gel, the phase transition temperature was approximately 35°C, and for the reduced gel, the phase transition temperature was approximately 28°C (see Fig. 2-9B). These phase transition temperatures shift according to the concentration of $Ru(bpy)_3$ in the material.[86] Physically, oxidized $Ru(bpy)_3$ molecules have a higher charge density than reduced molecules. As a result, the overall charge density and hydrophilicity of the gel is higher when the gel is in a uniformly oxidized state. For this reason, the LCST is observed at a higher temperature in oxidized BZ gels versus reduced BZ gels.

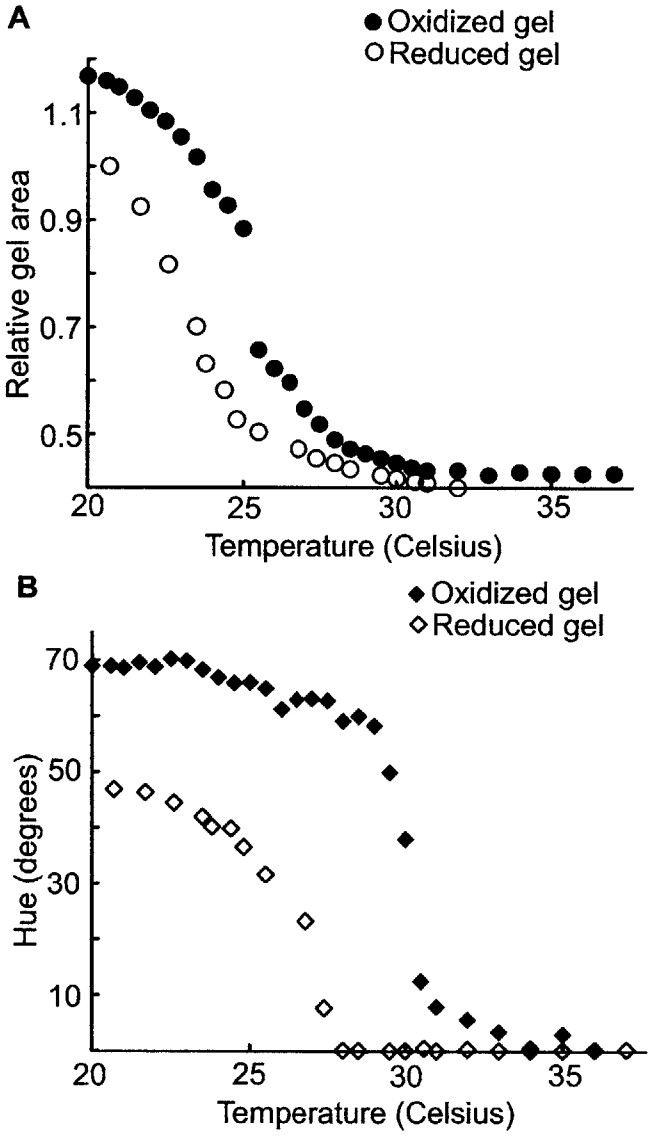

Figure 2-9: Temperature profile for a BZ gel (A) Normalized, projected gel area as a function of temperature for a BZ gel comprising 5.8 mM $Ru(bpy)_3$. Temperature data gathered for uniformly reduced gels (○) and uniformly oxidized gels (black circles). (B) Hue of the gel as a function of temperature. Temperature data gathered for uniformly reduced gels (◇) and uniformly oxidized gels (black diamond).

Chapter 3

Oscillatory characteristics of BZ gels

We acknowledge Dr. John Maloney for contributing to the development of our image analysis methods of gel hue. Portions of this chapter were adapted from Ref.[4] and Ref.[3], and have been reprinted with permission from the Royal Chemical Society and Wiley-VCH.

3.1 Overview

In Chapter 2, the synthesis of a polymer gel comprising covalently bound BZ catalyst was described, and physical properties of the material (independent of the BZ reaction) were characterized. In this chapter, the prepared BZ gels are characterized according to the BZ reaction. In particular, the oscillatory characteristics exhibited by the gels due to the BZ reaction are quantified according to the chemical conditions of the experiment and the physical shape and size of the gel.

Most importantly, this chapter provides a thorough background on BZ gels, and such information is necessary context for both understanding and appreciating the concepts behind both mechanical triggering in BZ gels (Chapter 4) and signaling among BZ gels (Chapter 5).

3.2 Background

For solution phase reactions, BZ oscillations are frequently characterized by period and amplitude of oscillation. Here, period of oscillation represents the duration of time required to complete one BZ cycle, and amplitude of oscillation represents the magnitude of each oscillation. These oscillatory characteristics may change when the reaction is confined within a material. Therefore, when a new BZ material is fabricated, the BZ oscillatory characteristics should be characterized, in addition to basic material properties such as polymer volume fraction.

Thus far, the BZ reaction has been incorporated in membranes, resins, and gels.[42,57,62] Although oscillations in BZ gels have already been characterized for a number of chemical variables,[8] differences in analysis meth-

ods and polymerization procedures necessitate thorough characterization in newly synthesized gels. For BZ gels comprising poly(NIPAAm-co-Ru(bpy)$_3$), certain chemical conditions have resulted in lack of oscillation. Surprisingly, these non-oscillatory chemical conditions have been reported at high malonic acid or sodium bromate concentrations (> 0.5 M).[8] Therefore, in characterizing BZ oscillations across chemical concentrations of reactant species, the oscillatory and non-oscillatory regimes of the gel reaction may be identified.

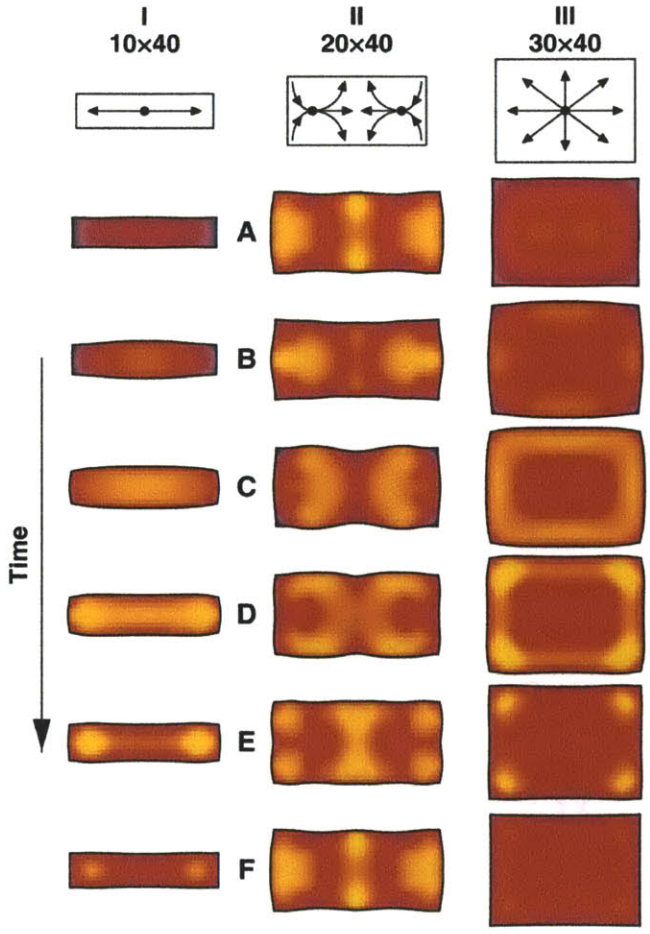

Figure 3-1: Simulated BZ wave patterns in gels of varying aspect ratio. From Yashin, V.V. and Balazs, A.C., *Science, 314*, 2006. Reprinted with permission from AAAS.

In addition to quantifying oscillatory characteristics in BZ materials, pattern formation has also been studied in relation to material shape and size. For instance, Bishop et al. demonstrated that specific chemical compounds (methanol or formaldehyde) can be added to the BZ solution to influence the modes of pattern formation in star shaped, mm-scale, agarose gels. Since methanol and formaldehyde determine whether pattern formation is governed by the dynamics of either the activator or inhibitor BZ species, respectively, then addition of such compounds results in BZ wave initiation

at either the tips of a star (acute angles) or between the star tips (obtuse angles).[59]

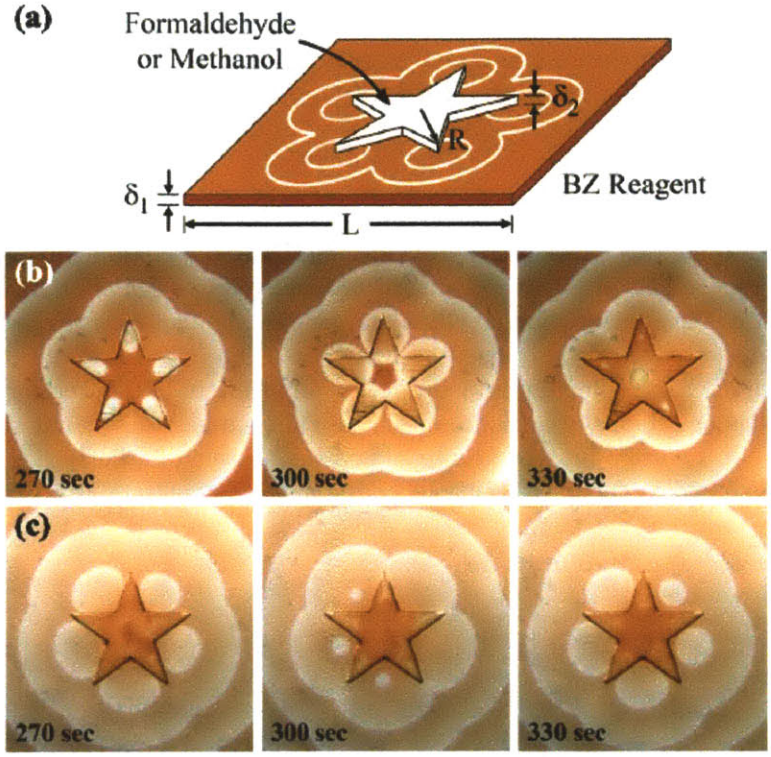

Figure 3-2: Pattern formation in star shaped agarose gels in which pattern formation depends on chemical triggering agents. (a) Schematic of experiment. (b) Observed wave patterns with formaldehyde added to BZ solution. (c) Observed wave patterns with methanol added to BZ solution. Reprinted from Bishop, K.J.M. and Grzybowski, B.A. (Phys. Rev. Lett., 97), http://link.aps.org/doi/10.1103/PhysRevLett.97.128702, 2006, with permission from APS, 2006.

Using the self-oscillating ferrocyanide-iodate-sulfite (FIS) reaction, Yoshida et al. studied pattern formation in polyacrylamide gels. In these materials, pattern formation depended on the diffusivity, or swollen thickness of the hydrogel. In less swollen polyacrylamide gels, the FIS reaction resulted in replicating spot or lamellar patterns, whereas a single spot pattern was observed in more swollen gels.[67] In these studies, the mesh size of the polymer gel network determines the resulting patterns. Overall system size, however, can also influence pattern formation. In resin beads undergoing the BZ reaction, Aihara et al. looked at pattern formation as a function of bead diameter. Specifically, the BZ patterns observed in these beads shifted from travelling, chemical waves to uniform oscillation at a critical bead diameter (0.62 mm).[57] In summary, various studies in BZ materials have demonstrated how material shape, size, and internal structure can influence visual pattern formation.

Few studies have explored pattern formation in BZ gels comprising NIPAAm-co-Ru(bpy)$_3$. However, computational results predict that small changes in aspect ratio influence pattern formation in these gels (see Figure 3-1). Those simulations, performed by Yashin et al., highlighted the strong chemomechanical coupling of BZ gels that drives dynamic shape changes of the material.[87] If such material functionality were experimentally validated, then unique applications comprising BZ gel actuators could be realized.

3.3 Methods

First, we briefly describe the experimental methods and equipment used to monitor oscillations in BZ gels. Using a stereomicroscope (Olympus, SZX7) with an LED light and camera (Olympus, DP25), timelapse imaging of BZ oscillations were recorded in gels (see Figure 3-3A). The BZ gels were cut into their desired shape using either a surgical razor blade to obtain rectangular shaped gels or a biopsy punch to obtain disc shaped gels. As shown in the schematic in Figure 3-3B, the gels rested on the bottom of a Petri dish, and were submerged in chemical solutions containing BZ reactants.

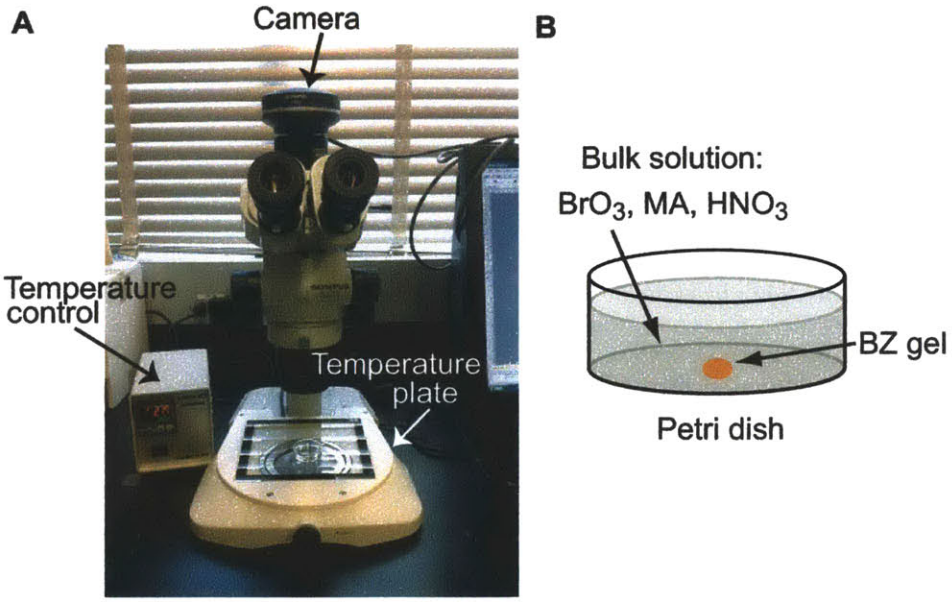

Figure 3-3: (A) Equipment for monitoring BZ oscillations. A stereomicroscope connected to a camera and image acquisition software were used to record oscillations, and a temperature plate with controller were used to set the system temperature. (B) Schematic illustrating BZ gel submerged in a Petri dish containing BZ sclution with soluble MA, BrO_3, and HNO_3.

As mentioned in Chapter 1, previous studies on BZ gels characterized oscillations by quantifying the mean gray value of the material. Note that the mean gray value corresponds to an average of the red, green, and blue values of an image: $(R+G+B)/3$. In our work, we used a more robust method of image analysis to characterize oscillations by analyzing the gel color in

terms of hue,[88] which provides an objective measure of the oxidation state of the $Ru(bpy)_3$ catalyst. In particular, this method was capable of detecting low amplitude oscillations. To calculate hue, red, green, and blue color values were extracted from images of the gel using ImageJ software, and the following equations were used to determine hue:[88]

$$\alpha = R - 0.5(G + B) \qquad \beta = \frac{\sqrt{3}}{2}(G - B) \qquad Hue = atan2(\beta, \alpha) \tag{3.1}$$

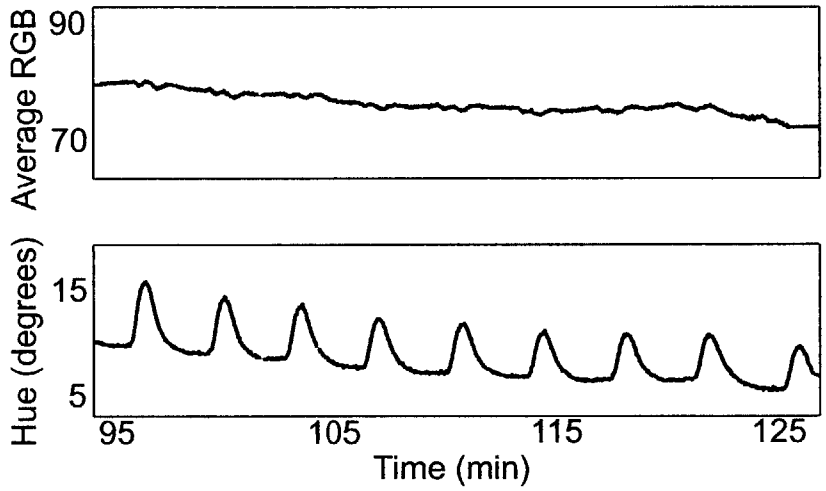

Figure 3-4: Oscillations quantified using average RGB and hue for a BZ gel containing 8.3 mM of catalyst. The external solution contained 0.3 M malonic acid, 0.1 M sodium bromate, and 0.7 M nitric acid.

Shown in Figure 3-4 is a set of data analyzed using both average RGB and hue. When the average RGB was quantified, the gel appeared to be in a non-oscillatory state. However, the gel was actually oscillating, as indicated by the hue of the gel. Thus, a significant amount of information is lost when the average RGB value of the gel is calculated instead of the hue, and plotting oscillations according to gel hue is a more robust method for measuring BZ oscillations.

3.4 Influence of chemical environment

3.4.1 Chemical species present in external, bulk solution

As described previously, the BZ reaction involves several reactants, including $Ru(bpy)_3$, MA, BrO_3, and HNO_3. Here, we describe how the concentrations of individual BZ reactant species affect the oscillatory characteristics of the reaction. To measure oscillations, timelapse imaging of BZ gel discs (approximately 1 mm in diameter and 0.6 mm thick) was recorded for gels fully submerged in 5 mL of BZ solution (see Figure 3-3B).

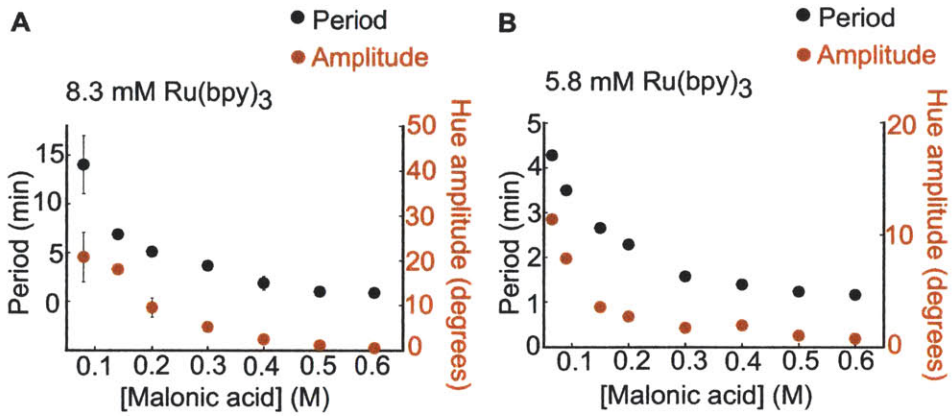

Figure 3-5: Period and amplitude versus MA concentration for spontaneously self-oscillating BZ gels (0.7-0.9 mm diameter) containing (A) 8.3 mM $Ru(bpy)_3$ catalyst, and (B) 5.8 mM $Ru(bpy)_3$ catalyst. Constant 0.1 M BrO_3 and 0.7 M HNO_3.

Figure 3-5 shows the dependence of both period and amplitude on MA concentration. These data were gathered for BZ gels comprising two different $Ru(bpy)_3$ catalyst concentrations: 8.3 mM (Fig. 3-5A) and 5.8 mM (Fig. 3-5B). While both sets of data showed that period and amplitude of oscillation decreased logarithmically with increasing MA concentration, the periods and amplitudes of oscillation were greater when the $Ru(bpy)_3$ catalyst concentration was higher. Since MA is present in the aqueous, external solution and is not confined to the BZ gel, lower MA concentrations result in longer diffusion times. In other words, for low concentrations of MA, the timescale associated with mass transport of MA from the external solution to the gel exceeds the kinetic timescale describing the reaction between MA and $Ru(bpy)_3$. By the same reasoning, the amplitude of oscillation also increased with decreasing MA concentration since amplitude is proportional to the fraction of $Ru(bpy)_3$ molecules undergoing synchronized reduction or oxidation. Therefore, Figure 3-5 illustrates that both period and amplitude increase with decreasing MA concentration.

Note that the waveform was also directly influenced by the concentration of MA in the bulk solution. Low MA concentration resulted in a "rectangular" waveform (Figure 3-6A), whereas relatively high MA concentration resulted in waves that did not exhibit an extended plateau in gel hue (Figure 3-6C). Such observations are attributed to the slow diffusion rate of MA from the external solution to the gel. Gradual reaction with MA did not occur because the oxidation of $Ru(bpy)_3$ by MA is the slowest BZ reaction step (Equation 1.3). As a result, the gel remained green for a longer duration. As MA eventually reacted with the oxidized $Ru(bpy)_3$ molecules, Br^- inhibitor was produced within the gel (see Equation 1.3). Diffusion of Br^- out of the gel must occur before the BZ cycle can repeat itself, and during this time, a large fraction of $Ru(bpy)_3$ molecules in the gel simultaneously exhibited the reduced state. Such observations of a "rectangular" waveform at low MA concentrations have been observed previously in BZ gels.[45] These trends are specific to BZ gels in which the $Ru(bpy)_3$ catalyst is confined to the gel

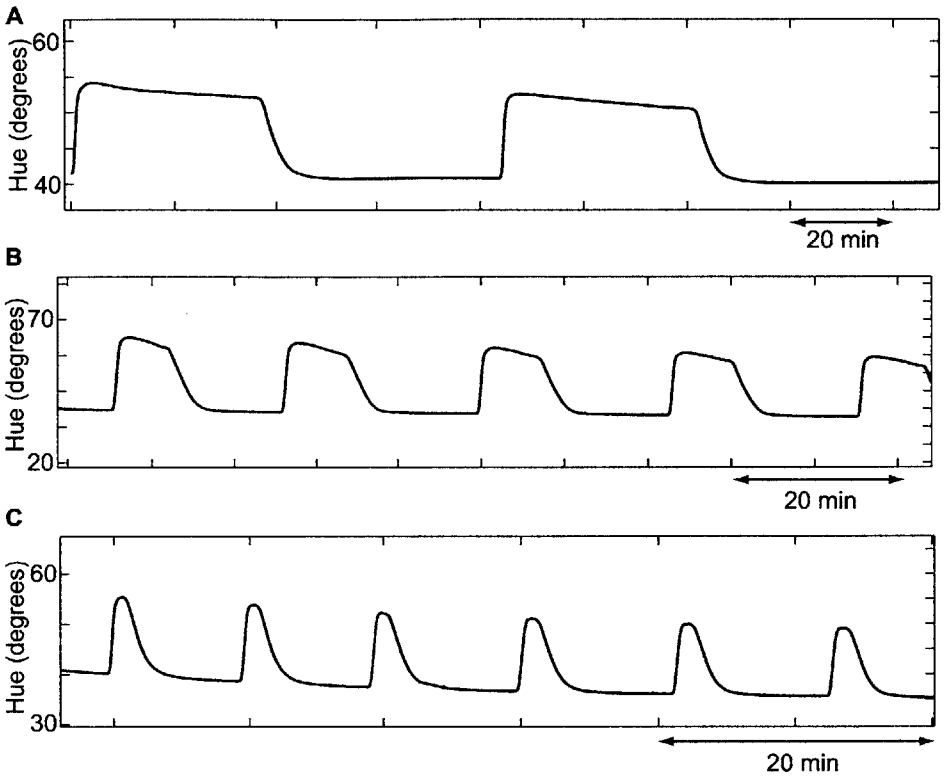

Figure 3-6: Waveform dependence on MA concentration in 8.3 mM BZ gels. (A) 0.01 M MA, (B) 0.05 M MA, and (C) 0.1 M MA. Constant 0.1 M BrO_3 and 0.7 M HNO_3.

phase and mass transport plays a significant role in shaping the oscillatory trends.

While the trends shown in Figure 3-5 are consistent with past observations by other research groups,[45,89] our BZ gels self-oscillated over a relatively wide range of conditions. For example, our gels oscillated at relatively high concentrations of MA (0.6 M), whereas past observations indicated that BZ gels stop oscillating at such high concentrations of MA.[8,89] Such discrepancy may be attributed to different standards in image analysis. Low amplitude oscillations were easily detected by monitoring the hue of the gel, however such oscillations were not visibly discernable, nor were oscillations detectable when average RGB or a blue-filtered gray values were quantified through image analysis.

Next, the concentration of sodium bromate is analyzed with respect to the BZ oscillations. Figure 3-7 shows the dependence of period and amplitude on BrO_3 concentration. These data were gathered for BZ gels comprising two different $Ru(bpy)_3$ catalyst concentrations: 8.3 mM (Fig. 3-7A) and 5.8 mM (Fig. 3-7B). Similar to Figure 3-5, period decreased logarthimically with increasing BrO_3 concentration. Interestingly, the amplitude of oscillation did not follow this logarithmic trend. For the 8.3 mM $Ru(bpy)_3$ gel, the highest amplitude of oscillation was observed at 0.15 M BrO_3, and for the

5.8 $Ru(bpy)_3$ gel, the highest amplitudes of oscillation were observed at 0.1 - 0.3 M BrO_3 (see Figure 3-7).

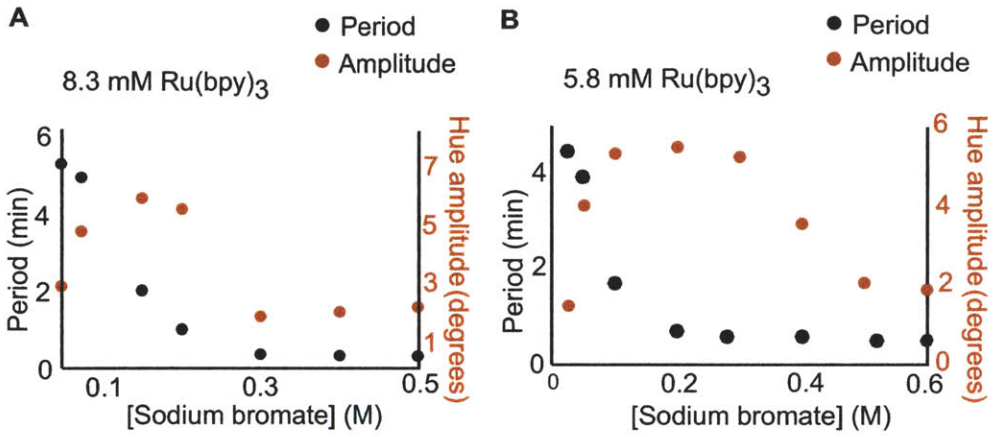

Figure 3-7: Period and amplitude versus BrO_3 concentration for spontaneously self-oscillating BZ gels (0.7-0.9 mm diameter) containing (A) 8.3 mM $Ru(bpy)_3$ catalyst, and (B) 5.8 mM $Ru(bpy)_3$ catalyst. Constant 0.2 M MA and 0.7 M HNO_3.

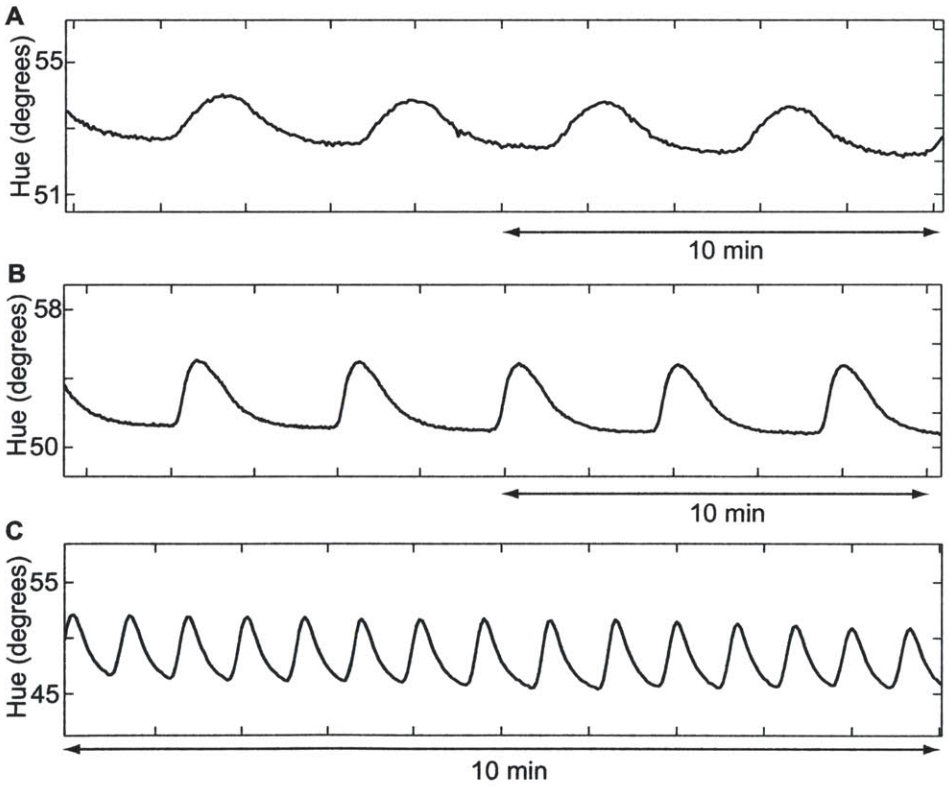

Figure 3-8: Waveform dependence on BrO_3 concentration in 8.3 mM BZ gels. (A) 0.025 M BrO_3, (B) 0.05 M BrO_3, and (C) 0.2 M BrO_3. Constant 0.2 M MA and 0.7 M HNO_3.

BrO_3 concentration also did not strongly influence the BZ waveform. Regardless of $[BrO_3]$, the chemical waveform did not exhibit a rectangular form (see Figure 3-8). The reason why low BrO_3 concentrations did not result in a rectangular waveform are due to the BZ kinetics. While the reduction of $Ru(bpy)_3$ by MA is a relatively slow reaction step, the oxidation of $Ru(bpy)_3$ is quite fast.[20] Fast kinetics allow for gradual oxidation of $Ru(bpy)_3$ by BrO_3. In other words, only a fraction of the total $Ru(bpy)_3$ molecules in the gel undero oxidation at low BrO_3 concentration, and so the amplitude of oscillation is relatively small and lacks a rectangular waveform. Thus, the concentration of BrO_3 affects the period and amplitude of oscillation, but does not influence the oscillatory waveform.

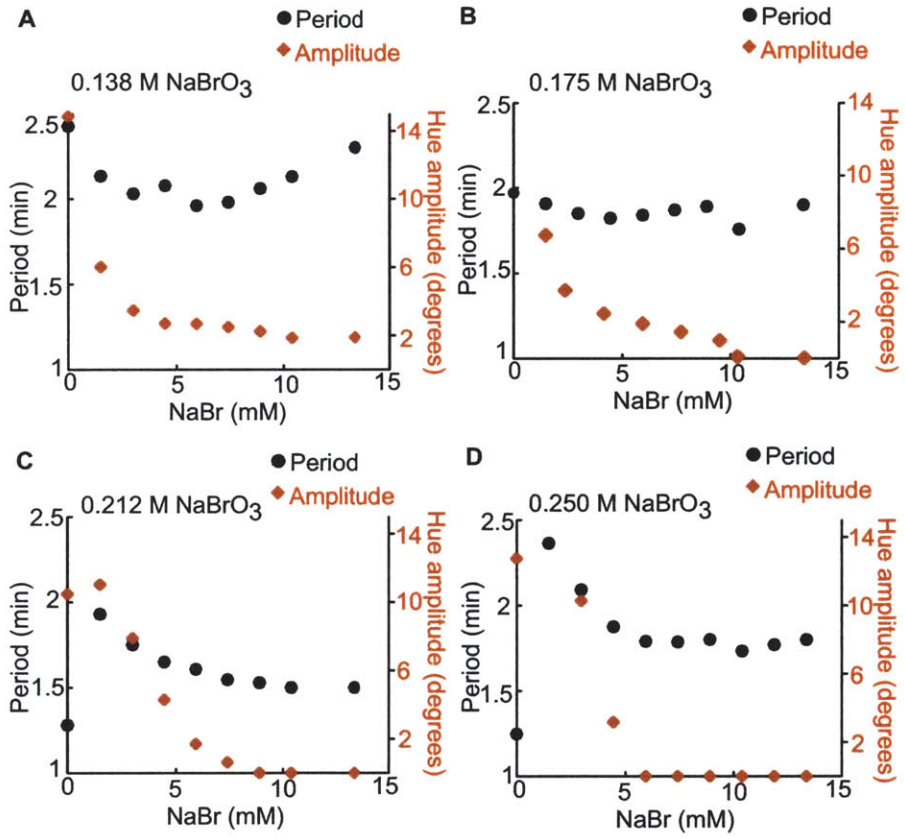

Figure 3-9: Period and amplitude versus Br^- concentration for spontaneously self-oscillating BZ gels (0.7-0.9 mm diameter) containing 8.3 mM $Ru(bpy)_3$ catalyst, and (A) 0.138 M BrO_3, (B) 0.175 M BrO_3, (C) 0.212 M BrO_3, and (D) 0.250 M BrO_3. Constant 0.2 M MA and 0.7 M HNO_3.

Next, we consider Br^- concentration, even though NaBr is not typically added to BZ solutions. For these experiments, BZ oscillations were measured in a gel while small aliquots of NaBr were slowly added to the external solution. Overall, the period and amplitude data shown in Figure 3-9A-D are somewhat difficult to interpret because the trends are variable. The lack of clear trends may be attributed to fluctuations in Br^- concentration, since

Br^- is constantly being generated and consumed throughout the reaction. In general, the amplitude of oscillation decreased with increasing Br^-, while there appeared to be no conclusive trends regarding the period of oscillation. Since Br^- plays an inhibitory role in the BZ reaction, decrease in amplitude with increasing Br^- concentration is expected. Collecting the data shown in Figure 3-9 is important because Br^- is generated within the gel as a product of the BZ reaction (see Equation 1.3), and such data help to elucidate how BZ oscillations may evolve over time as a consequence of Br^- production.

Limited data were acquired regarding HNO_3 effects on BZ oscillations. Overall, the concentration of HNO_3 did not noticeably affect the period of oscillation. In contrast, larger amplitudes of oscillation were observed when BZ gels were submerged in solutions comprising higher HNO_3 concentrations (see Figure 3-10).

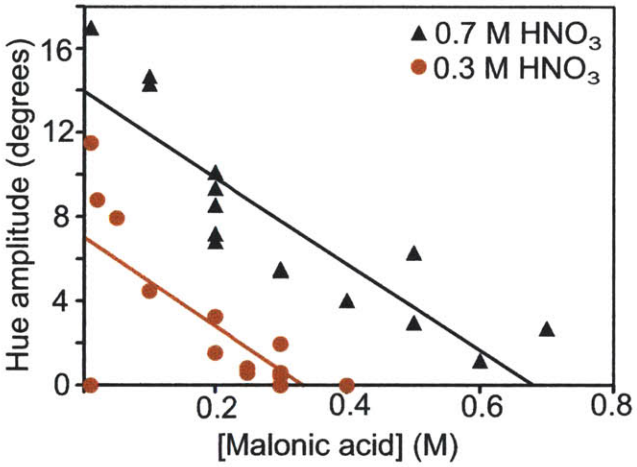

Figure 3-10: Amplitude versus MA and HNO_3 concentration in 8.3 mM $Ru(bpy)_3$ BZ gel (1 mm diameter). Black triangles represent 0.7 M HNO_3, and red circles represent 0.3 M HNO_3. Constant 0.1 M BrO_3.

As described above, $Ru(bpy)_3$, MA, BrO_3, and HNO_3 may be present in variable concentrations and, ultimately, determine the oscillatory state of the material. In theory, when the chemical species have been sufficiently consumed by reaction, oscillations will eventually die out. However, the nature of this dying process depends on the specific chemical conditions of the experiment (see Figure 3-11). Importantly, the absolute concentrations of the individual species, as well as the kinetic synergies between reacting chemical species both need to be considered in order to determine the oscillatory state of the system. Figure 3-11A illustrates an experiment that was prepared with three times the MA concentration as the experiment shown in Figure 3-11B. While oscillations gradually ceased in Figure 3-11A, oscillations abruptly ceased in Figure 3-11B. Decreasing the concentration of MA further, however, does not necessarily guarantee that oscillations will die abruptly. Shown in Figure 3-11C is an experiment with low MA concentration (0.065 M), and the oscillations persisted for at least 24 h. Note that the period of oscillation changed during the course of this experiment.

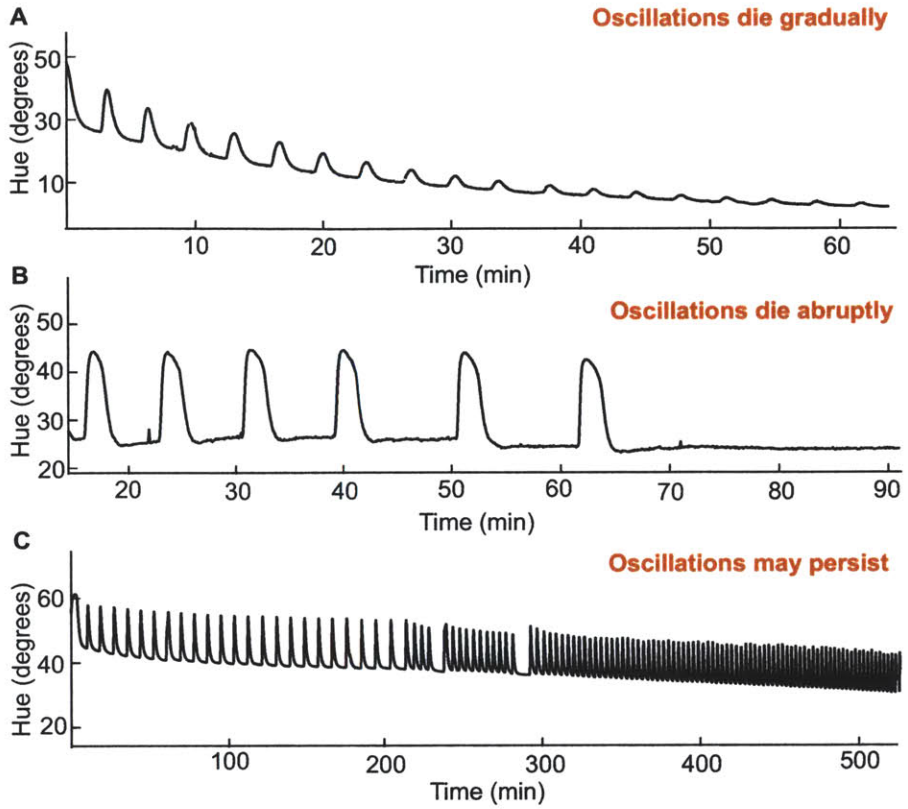

Figure 3-11: (A) 8.3 mM $Ru(bpy)_3$ gel (1 mm diameter) submerged in BZ solution (5 mL) comprising MA (0.3 M), BrO_3 (0.1 M), and HNO_3 (0.7 M). (B) 8.3 mM $Ru(bpy)_3$ gel (0.8 mm diameter) submerged in BZ solution (5 mL) comprising MA (0.08 M), BrO_3 (0.1 M), and HNO_3 (0.7 M). (C) 8.3 mM $Ru(bpy)_3$ gel (3 mm diameter) submerged in BZ solution (3 mL) comprising MA (0.065 M), BrO_3 (0.085 M), and HNO_3 (0.7 M). Oscillations still persisted for at least 24 h.

Such shifts in pattern formation are attributed to changing concentrations of chemical species as reactants are consumed by the BZ reactions.[75]

3.4.2 Influence of gel confined species

In addition to chemical species present in the external BZ solution, gel confined species also influence the oscillatory characteristics of the BZ reaction. Mainly, the concentration of $Ru(bpy)_3$ influences the period, amplitude, and degree of gel swelling. Figure 3-12 shows that as the concentration of $Ru(bpy)_3$ increases, both period and amplitude increase. Because NIPAAm is a thermosensitive polymer, the oxidation state of the covalently bound $Ru(bpy)_3$ catalyst affects the phase transition temperature of the gel (see Chapter 2). Thus, at constant system temperature, the material exhibits periodic changes in hydrophilicity, causing water absorption and desorption as $Ru(bpy)_3$ catalyst is oxidized and reduced, respectively.[90] For high amplitude oscillations, a large fraction of $Ru(bpy)_3$ molecules undergo synchronized oxidation or reduction. As a result, the degree of swelling is larger for

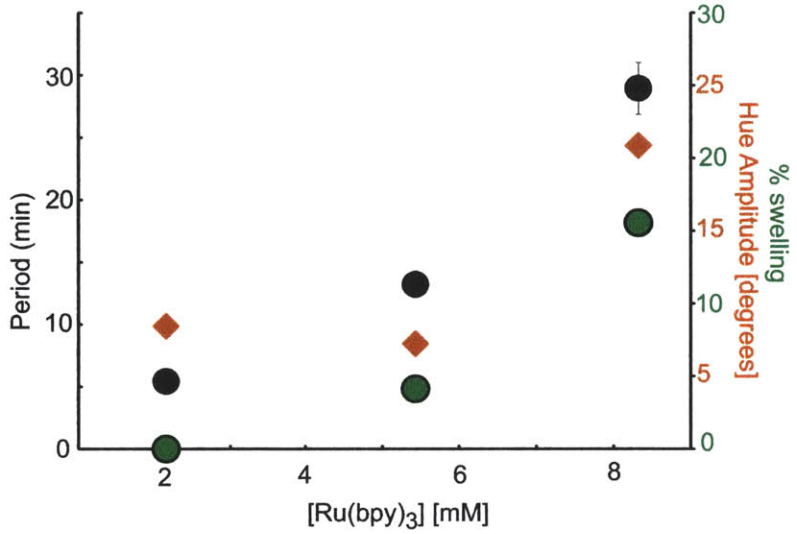

Figure 3-12: Influence of $Ru(bpy)_3$ concentration on oscillatory characteristics. Black circles correspond to period of oscillation (left axis). Red diamonds correspond to hue amplitude (right axis). Green circles correspond to % swelling (right axis). Data was collected using BZ gels comprising 8.3 mM $Ru(bpy)_3$.

such gels undergoing high amplitude oscillations and comprising relatively high concentrations of $Ru(bpy)_3$ (see Figure 3-12). Intuitively, it makes sense that the amplitude of redox oscillation should increase when there is a higher concentration of $Ru(bpy)_3$ capable of undergoing redox changes. Last, Figure 3-12 confirms that hue amplitude scales with volumetric swelling amplitude, demonstrating that hue analysis provides an appropriate method for quantifying redox changes in BZ gels.

3.4.3 Oscillatory and non-oscillatory regimes

In quantifying the BZ oscillations, it was demonstrated that high concentrations of chemical species do not correspond to lack of oscillation. However, oscillatory and non-oscillatory regimes do exist within BZ gels. Figure 3-13A presents a comparison between the period of oscillation and the estimated characteristic diffusion time for BZ gel systems. The period of oscillation was quantified as a function of MA concentration for two BZ gels containing different concentrations of $Ru(bpy)_3$ catalyst: 5.8 mM and 8.3 mM. While similar trends were observed for the different gels, the magnitude of the period differed quantitatively. Specifically, the parameters in a power law fit of the data were dependent on the $Ru(bpy)_3$ concentration. In the absence of any chemical reaction, the diffusion time, τ, for the system can be estimated as:

$$\tau \approx \frac{L^2}{D} \tag{3.2}$$

where L is the characteristic length of the BZ system and D is diffusion coefficient for the system. Here, the characteristic length L is defined by the BZ gel dimensions; the gels for these experiments exhibited diameters ranging from 0.7-0.9 mm and consistent thicknesses of 0.6 mm. As these dimensions are comparable, and as there may be differences between axial and radial diffusion through the gel due to details of the experiments (e.g., the gel rests on a Petri dish), the diffusion time was estimated for a range of length scales (0.6 - 0.9 mm). Accounting for the low polymer volume fraction in our gels (0.08), the diffusivity D of reactant molecules through the BZ gel was similar to that through aqueous solution,[62,87] and the resulting estimated diffusion time for our experiments ranged between 3.3 - 7.5 min (see shaded blue region in Figure 3-13A).

The diffusion time is set by L and D for a given gel, whereas the period of BZ oscillation is related to both L,[4] and the concentration of $Ru(bpy)_3$ and chemical reagents. If the period of oscillation is comparable or less than τ (i.e., below the shaded blue region in Figure 3-13A), then the typical BZ self-oscillatory state is achieved robustly. If instead the period of oscillation exceeds the diffusion time, a quasi-equilibrium distribution of chemical reagents within the gel can be reached and self-oscillation is not assured. Figure 3-13A demonstrates that this quasi-equilibrium can be achieved at sufficiently low concentrations of MA and sufficiently high $Ru(bpy)_3$ concentrations (i.e., within the shaded pink region for gels comprising 8.3 mM $Ru(bpy)_3$). Above some critical MA concentration, gels of this higher $Ru(bpy)_3$ concentration always spontaneously self-oscillated, but below this MA concentration some gels would self-oscillate and others would not.

It is important to emphasize that a strictly non-oscillatory region for these gels comprising 8.3 mM $Ru(bpy)_3$ was not observed. Rather, of the 13 total experiments conducted at 0.08 and 0.14 M MA, only five gels were self-oscillatory at time zero. In contrast, all six experiments conducted above 0.14 M were self-oscillating gels. The behavior observed at lower MA concentrations ($\leqslant$ 0.14 M) for gels comprising 8.3 mM $Ru(bpy)_3$ indicates access to a bistable state, in which the self-oscillatory and steady-states co-exist. Clear demonstration of this coexistence would require a high number of replicate experiments that is beyond the scope of this thesis. In the gel comprising 5.8 mM $Ru(bpy)_3$, we always observed that the gel self-oscillated over the conditions shown in Figure 3-13A, in which the period of oscillation did not exceed 5 min and was thus comparable to or below τ. However, in the gel with 8.3 mM $Ru(bpy)_3$, we observed two regimes that describe oscillations in BZ gels: a robust regime in which self-oscillation is consistently attained, and a chemically sensitive regime in which the sample can either oscillate or attain a steady-state.

While low MA concentrations correspond to ambivalent oscillatory conditions in BZ gels, definite oscillatory and non-oscillatory states can be realized by determining the ratio of BrO_3^- to Br^-.

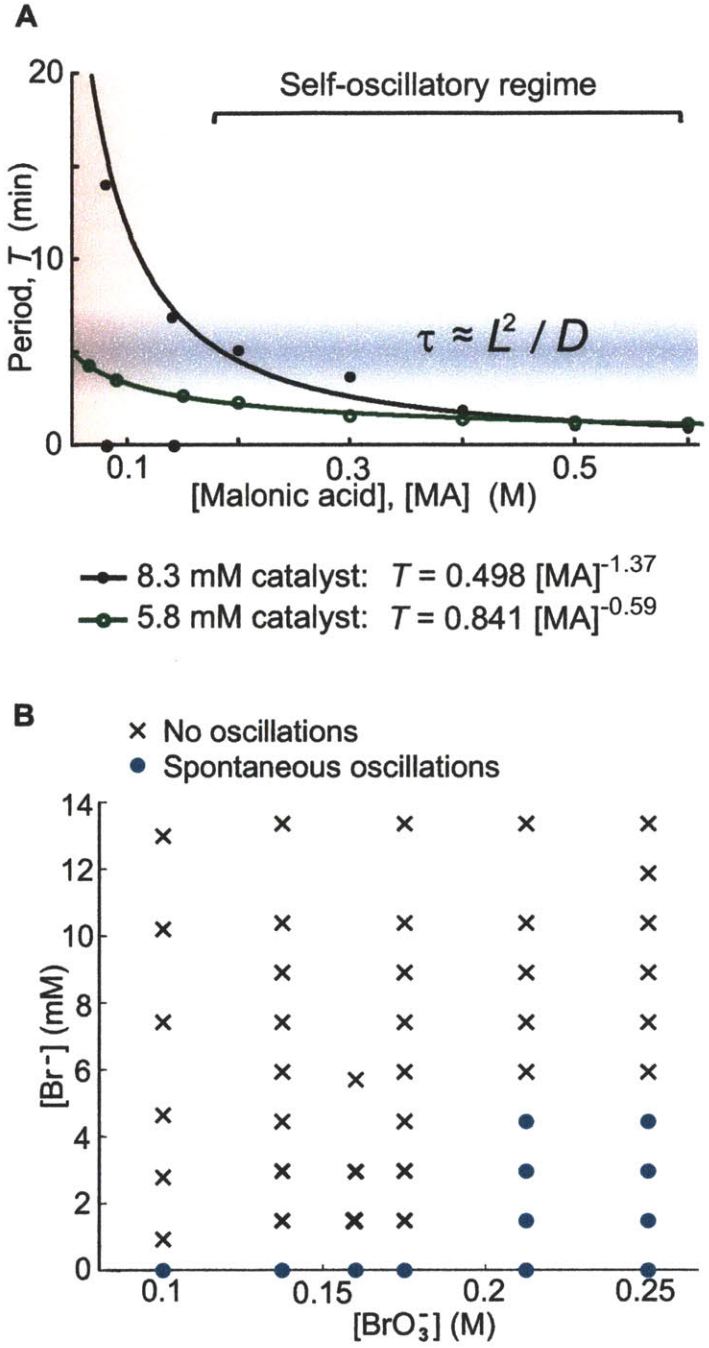

Figure 3-13: Oscillatory regimes in BZ gels. (A) Oscillatory regimes in relation to MA concentration and estimated diffusion time for 0.6 - 0.9 mm sized BZ gels. The blue, shaded region corresponds to the estimated diffusion time τ. When the experimental period of oscillation exceeds the diffusion time, the system becomes sensitive to initial conditions (pink shaded region) and can exhibit either oscillations or a steady-state (note black points on horizontal axis indicating gels that did not self-oscillate). Reproduced from Ref.[3] (B) Oscillatory regimes with respect to BrO_3^- and Br^- concentrations for gels comprising 8.3 mM $Ru(bpy)_3$.

In Figure 3-13B, BZ gels comprising 8.3 mM $Ru(bpy)_3$ were characterized with respect to BrO_3^- and Br^- concentrations. Gel discs of uniform dimensions and catalyst concentration were prepared using a biopsy punch (1.3 mm diameter), and each gel disc was submerged in a solution (5 mL) containing BZ reactants. For the data shown in Figure 3-13B, in which $BrO_3^- \geq$ 0.1 M, spontaneous oscillations were monitored in the absence of Br^-. Subsequently, Br^- was added and well mixed with the bulk BZ solution, and the altered state of the gel was recorded. Further additions of Br^- were performed up to 14 mM Br^-, and the imaging steps were repeated to determine the oscillatory regimes of the gel. Note that data were gathered at constant MA concentrations for simplicity, but more generally, the oscillatory regimes depend also on MA concentration. When the ratio of BrO_3^- to Br^- concentration was high, the BZ gel spontaneously self-oscillated (marked by • in Fig. 3-13B). In contrast, when the BrO_3^- concentration was low, even small amounts of Br^- inhibitor precluded oscillation (marked by × in Fig. 3-13B). Therefore, Figure 3-13B confirms that the oscillatory state of a BZ gel strongly depends on the ratio of BrO_3^- to Br^-.

3.5 Influence of temperature on oscillatory characteristics

In addition to chemical concentrations, system temperature also influences the reaction dynamics. In previous chapters, the gels were characterized by temperature in the absence of BZ reactants. Here, we demonstrate how the gels oscillate under the BZ reaction at different temperatures.

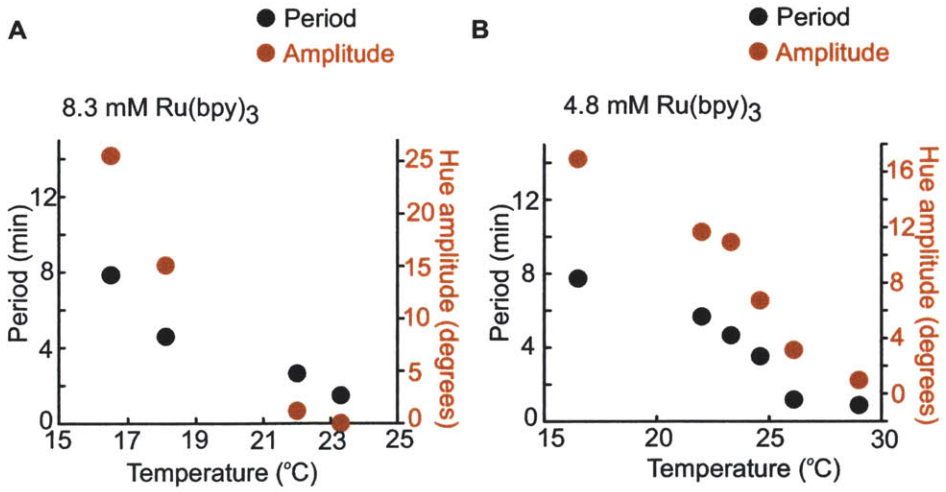

Figure 3-14: Effects of temperature on oscillations in BZ gels. (A) Period and amplitude versus temperature for BZ gels comprising 8.3 mM $Ru(bpy)_3$, and (B) 4.8 mM $Ru(bpy)_3$. For (A-B), constant 0.15 M MA, 0.1 M BrO_3, and 0.7 HNO_3.

Figure 3-14 illustrates the effects of temperature on period and amplitude of oscillation in BZ gels. As the temperature of the system increases, the period and amplitude of oscillations in BZ gels decrease. In other words,

as system temperature increased, the kinetics of the BZ reaction also sped up. These temperature effects were more dramatic for gels comprising 8.3 mM $Ru(bpy)_3$ versus 4.8 mM $Ru(bpy)_3$. In the former case, the gels stopped oscillating above 23°C, while in the latter case, the gels stopped oscillating above 30°C. Most likely, the gels stopped oscillating above a certain temperature because the NIPAAm hydrogels shrink at high temperatures (see discussion of LCST in Chapter 2). By measuring solute diffusivity in thermosensitive BZ gels, Yoshida et al. previously showed that reactant diffusion slows and eventually stops as system temperature increases.[91] Such results were interpreted using the free volume theory of diffusion through polymer networks, and are in agreement with our data in Figure 3-14.

The trends observed in Figure 3-14 are expected because most chemical reactions follow an Arrhenius relationship, in which the reaction rate depends on the system temperature:[20]

$$k = Aexp(-E_a/RT) \tag{3.3}$$

where k is the kinetic constant for the reaction, A is a pre-exponential factor specific to the reaction, E_a is the activation energy, R is the gas constant, and T is the system temperature. While the BZ reaction involves several elementary reaction steps involving many kinetic constants, the overall periodicity of oscillations is proportional to the kinetics of each reaction step, in which an Arrhenius dependence on temperature exists.[20]

3.6 Size threshold of a travelling chemical wave

In addition to species concentration and system temperature, gel size also affects oscillatory characteristics and pattern formation in BZ gels. Figure 3-15 illustrates a set of experiments in which BZ gels were cut into a triangular shape and submerged in BZ solution. For each triangular gel, the three edges were cut to similar length, while the gel thickness was constant in all experiments (0.6 mm). The characteristic length of the system was given by the longest gel edge (x-axis in Figure 3-15). Both period and amplitude of oscillation were affected by the edge length of the gel. The black data points in Figure 3-15 show that period increases with decreasing edge length. The red data points indicate that amplitude also increases with decreasing edge length. Interestingly, pattern formation in the gels were also affected by gel size. Specifically, two different modes of pattern formation were observed: 1) homogeneous color change in which gels exhibited uniform transition from red to green or vice versa, and 2) non-uniform color change characterized by a travelling chemical wave. Such results are indicated in Figure 3-15 (see legend), and are in agreement with past observations in BZ resin beads.[57] Note that the two modes of pattern formation are divided by the dotted line in Figure 3-15. This line represents the theoretical diffusion time given by Equation 3.2. Physically, τ corresponds to the time required for chemical species to diffuse through the BZ gel. When the period of oscillation is longer than τ, then sufficient time for diffusion occurs for chemical species to react with gel-confined reactants. As a result, high amplitude, uniform color

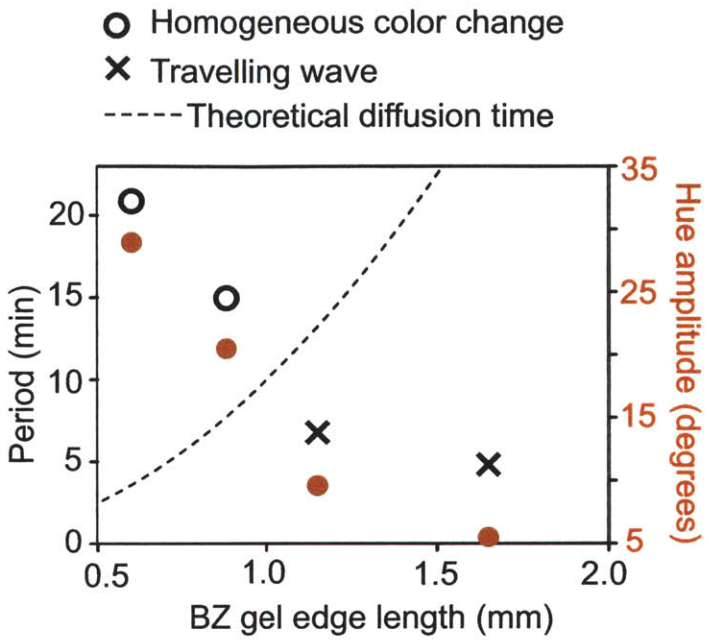

Figure 3-15: Effects of gel size on pattern formation in BZ gels comprising 8.3 mM $Ru(bpy)_3$. Both **O** and **X** represent period of oscillation (left axis), and red circles represent hue amplitude (right axis). Qualitative pattern formation is also indicated on the plot: homogeneous color change in a gel were observed in experiments indicated by **O**, whereas a travelling wave was observed in experiments indicated by **X**. Constant 0.9 M HNO_3, 84 mM BrO_3, and 63 mM MA. Reproduced from Ref.[4].

change occurs in the gel. In contrast, concentration gradients are more likely to exist within large BZ gels, and a travelling chemical wave is observed.

When uniform color change occurs in BZ gels of sufficiently small dimensions, then the chemical oscillations are synchronized with mechanical swelling/shrinking of the material. Figure 3-16 quantitatively confirms such synchronized chemomechanical coupling in BZ gels, as noted extensively for this BZ gel type by Yoshida et al.[45]. Previously, Aihara et al. estimated the critical lengthscale for this reaction to be ~0.6 mm in BZ resins, and showed that the mode of pattern formation changes below this critical size due to a switch in competition between kinetic and transport rates. In particular, traveling chemical waves give way to uniform oscillations in smaller systems.[57] For BZ gels, active mechanical swelling/shrinking is synchronized with chemical oscillations: the gel swells when the catalyst is homogeneously oxidized and shrinks when the catalyst is reduced.[45,92] Figure 3-16 demonstrates this chemomechanical behavior for a gel of ~0.6 mm edge length and 8.3 mM $Ru(bpy)_3$ concentration. The gel synthesized in this work exhibited oscillations every 21.2 ± 2.5 min that lasted >3.5 hours. This chemically induced swelling corresponded to a maximum change in the projected area of the triangular gel of 14.2 ± 2.1%, or a volumetric swelling of 21.9 ± 3.4%.

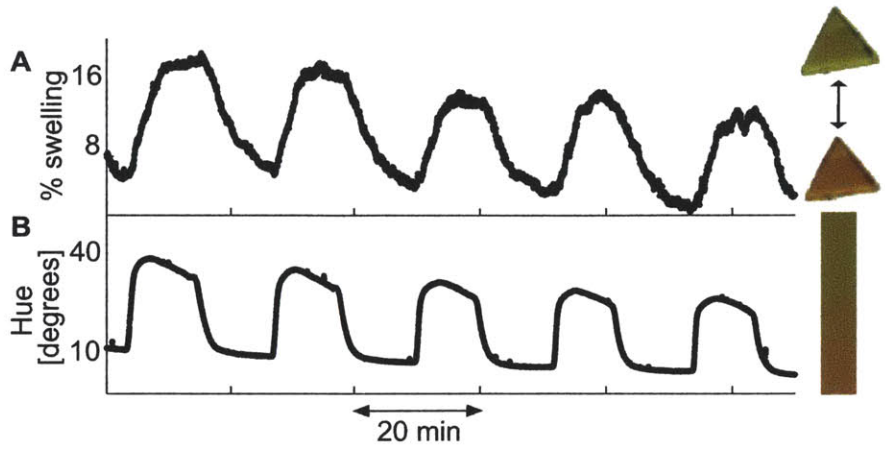

Figure 3-16: Synchronized chemical and mechanical oscillations in poly(NIPAAm-co-Ru(bpy)$_3$) gel of 0.6 mm edge lengths. (A) Swelling and shrinking of the gel are coupled to (B) oscillating change in oxidation state of the Ru(bpy)$_3$ catalyst (8.3 mM), confirming the expected coupling for successfully polymerized BZ gels of sufficiently small dimensions. BZ conditions were 63 mM MA, 84 mM BrO_3, and 0.9 M HNO_3. Reproduced from Ref.[4].

3.7 Influence of gel geometry on pattern formation

In this section, BZ wave patterns are compared at different gel geometries within the mm length scale. Figure 3-17 illustrates that significant confinement of the BZ reaction within a gel can alter the resulting chemical wave patterns. The BZ wave patterns in single phase solutions have been well studied, and spiral and target waves are the major modes of pattern formation.[14,93] Figure 3-17A shows that these chemical waves can be of high visual contrast when ferroin is used as the catalyst: the ferroin color alternates between red (reduced) and blue (oxidized). Figures 3-17B-C show the same BZ reaction, but now confined within two small pieces of polyacrylamide hydrogel that differ in shape and size. To obtain the results shown in Figures 3-17B-C, we synthesized the polyacrylamide-silica gel composite containing electrostatically bound ferroin as described by Konotop et al.[58] Then, the gel was cut into a disc of 7 mm diameter (Figure 3-17B) and a square of 3.6 mm width (Figure 3-17C). These images were obtained at early reaction times, directly after immersion of the catalyst-containing gels in a solution of necessary BZ reactants. Figures 3-17B-C demonstrate that the nature of BZ pattern formation in gels depends on the gel size and shape. Namely, the larger gel disc in Figure 3-17B exhibits spiral waves similar to those observed in solution (Figure 3-17A), whereas in the smaller, square gel (Figure 3-17C), waves originate at the corners and propagate inwards. These waves initiate at the corners and intersect before they can be classified as a full topological spiral or target pattern; here, it is the global geometry-driven nature of the wave fronts that becomes apparent for gels of sufficiently small size. Note that the similarity in pattern formation between BZ solutions and cm-scale BZ polymers was reported previously for various gels and resins

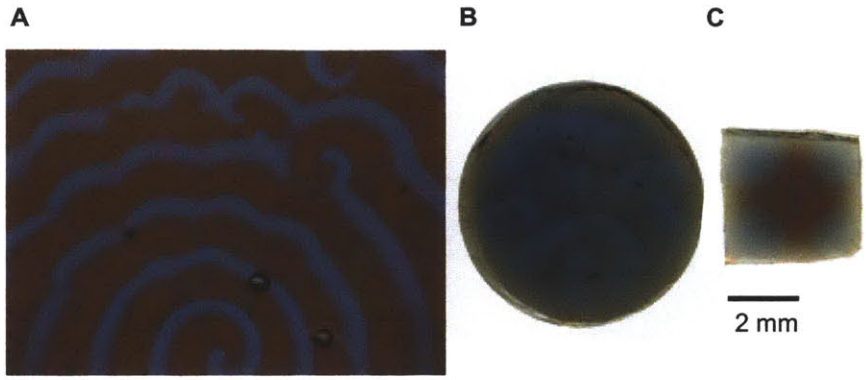

Figure 3-17: BZ reaction with ferroin catalyst (A) BZ reaction in solution, with 5 mM ferroin, 0.3 M sulfuric acid, 0.2 M MA, and 0.3 M BrO_3. (B) BZ reaction in a 7.7 mm-diameter polyacrylamide-silica gel composite disc containing electrostatically bound ferroin, submerged in 0.6 M sulfuric acid, 60 mM MA, and 80 mM BrO_3. (C) BZ reaction in a 3.6 x 3.6 mm square of the same polyacrylamide-silica BZ gel submerged in same conditions as B. Reproduced from Ref. [4].

undergoing the BZ reaction.[94] However, Figure 3-17 shows that modification of BZ gel size and shape can give rise to oscillation patterns that are visually distinct from those observed in solutions.

3.7.1 Pattern formation at early vs. late reaction times

Although the polyacrylamide-ferroin BZ system can be used to study pattern formation (see Figure 3-18A), the gradual desorption of electrostatically bound ferroin from the gel during the BZ reaction limits repeatability of studies over long timescales. See Appendix A for more data and discussion on the polyacrylamide-ferroin BZ system. Thus, to preclude catalyst desorption while observing pattern formation within BZ gels for extended durations, it is advantageous to use a gel system such as the NIPAAm-co-$Ru(bpy)_3$ gel, in which the catalyst is covalently bound to the polymer backbone. Figure 3-18B-D shows how size and shape affect pattern formation in rectangular gels of mm-scale dimensions. Note that these gels provided high color contrast to characterize oscillation patterns, but were of relatively large lateral dimensions and relatively low $Ru(bpy)_3$ concentrations (5.4 mM); thus, concurrent changes in gel size via swelling were negligible.

Gels were immersed in BZ reactants to initiate the BZ reaction at time zero, and the oscillations were monitored via timelapse video microscopy at a constant solution temperature of 20°C. Three different gel aspect ratios, defined as the ratio of the rectangle length divided by width, were considered. Figure 3-18 demonstrates that at early reaction times, pattern formation was sensitive to changes in aspect ratio. In particular, for an aspect ratio of 1, BZ waves penetrated from the corners of the square gel (Figures 3-18A-B). For an aspect ratio of 2, these waves originated from either two points near each gel end or directly at the gel ends (Figure 3-18C). Finally, for an aspect ratio

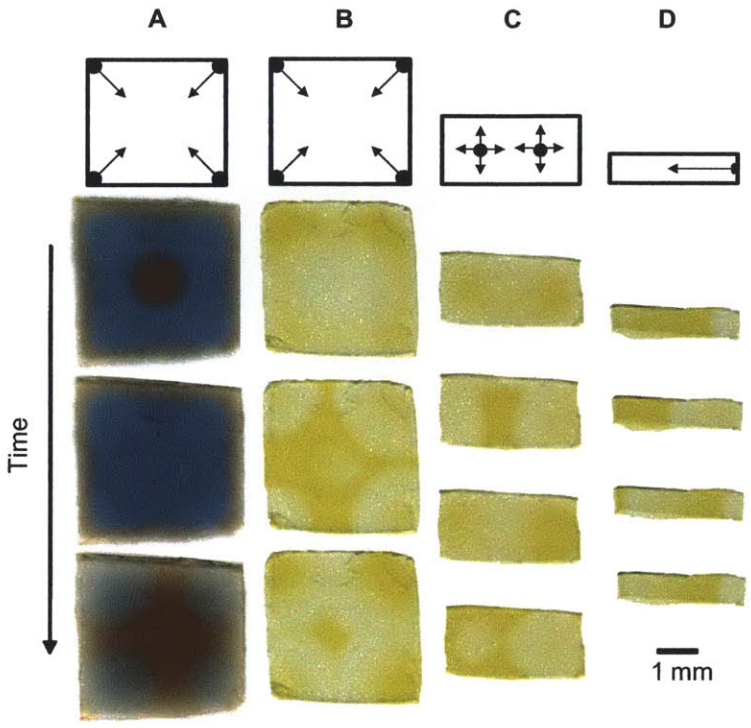

Figure 3-18: BZ pattern formation at early reaction times. (A) 3.6 x 3.6 mm polyacrylamide-silica-ferroin composite; (B-D) poly(NIPAAm-co-Ru(bpy)$_3$) gels comprising 5.4 mM Ru(bpy)$_3$ catalyst and lateral dimensions of (B) 3.3 x 3.3 mm, (C) 3.1 x 1.6 mm, or (D) 3.0 x 0.8 mm. NIPAAm gels were submerged in 63 mM MA, 84 mM BrO_3, and 0.9 M HNO_3. PAAm gels were submerged in 0.6 M sulfuric acid, 60 mM MA, and 80 mM BrO_3. Reproduced from Ref.[4].

of 3.7, the BZ reaction predominantly initiated at both ends of the gel (Figure 3-18D). The induction time of visible oscillations varied insignificantly with gel aspect ratio, and the wave patterns initiated 1-3 minutes after gels were immersed in BZ reactants. Generally, Figure 3-18 illustrates that as the corners of the gel and sites of BZ initiation are in closer spatial proximity, the global pattern transitions from initiation at gel corners to initiation at gel ends. While it has been noted that gel thickness also influences pattern formation,[67,94] the results shown in Figure 3-18 were consistent over a range of gel thickness (0.7 to 1.3 mm). Further, the chemical wavefronts consistently initiated at the same locations in at least 4 replicate samples and experiments for each aspect ratio; Figure 3-18 shows representative images of BZ pattern formation at these early times. Together, these results demonstrate that initial oscillation patterns within BZ gels can be modulated by changes in gel size and shape.

Indeed, shape-dependent pattern formation at early reaction times is anticipated from the nature of the BZ reaction confined within gels. Physically, the BZ reaction initiates only when the solution phase reactants diffuse into the gel to encounter the covalently bound Ru(bpy)$_3$. Initial concentration

gradients within the gel vary according to aspect ratio, resulting in visibly different BZ pattern initiation. It is important to emphasize that the initial pattern formation is affected by imperfections in gel geometry and by boundary conditions such as adhesion to an underlying surface. For example, adhesion of the gel at one end can promote unidirectional wave propagation, a result that resembles the patterns reported by Yoshida et al. for narrow gel strips of aspect ratios up to approximately 20 and fixed at one end.[51,95,96]. While transient patterns have also been recorded for BZ gels containing non-covalently bound ferroin catalyst, previous results[94] were observed in systems too large (>1 cm) for shape and size to influence BZ patterns. Further, those gel and reaction conditions produced highly irregular color oscillations, in contrast to the distinct and robust wave patterns shown in Figure 3-18.

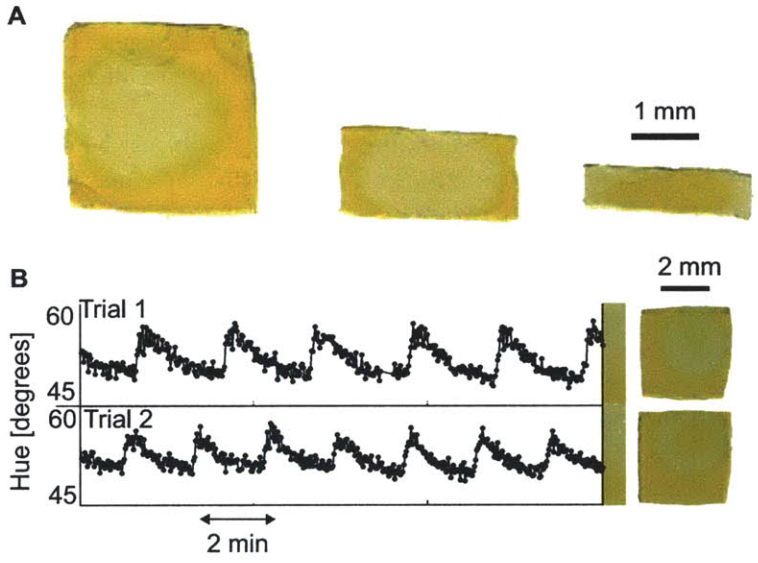

Figure 3-19: BZ pattern formation at late reaction times. (A) poly(NIPAAm-co-$Ru(bpy)_3$) gels comprising 5.4 mM $Ru(bpy)_3$ catalyst and dimensions given in Fig. 3-18. (B) A single gel (3.7 x 3.7 mm) recycled in replicate trials. For both A-B, the chemical conditions are the same as Fig. 3-18. Reproduced from Ref.[4].

For each aspect ratio considered, the self-oscillating patterns changed appreciably after approximately 30 minutes. At longer reaction times (Figure 3-19), oscillation patterns became independent of aspect ratio: BZ waves consistently originated from the gel center and propagated radially toward the gel perimeter. These new patterns were recorded for over 2.5 hours, at which point the experiments were terminated. The radially propogating patterns resemble the typical "target" patterns that are observed in BZ solutions. However, the general nature of pattern formation in BZ solutions does not change with time.[93] In contrast, these results demonstrate clearly that the modes of pattern formation in BZ gels evolve over long timescales.

The physical mechanism underlying pattern change from that observed at early reaction times to that at late reaction times is governed by the changing distribution of BZ reactants within the gel. At late times, there

is a distinct difference between the inner and outer regions of the sample; namely, the intermediate species of the BZ reaction accumulate within the gel network in the presence of the covalently-bound $Ru(bpy)_3$, rather than in the external solution. As a result, the gel center is the most likely point of wave initiation at late oscillation times, as is observed consistently in these experiments. Yamaguchi et al. have also observed temporal evolution of patterns in BZ gels containing ferroin catalyst, noting that patterns became more regular as the chemical concentrations within the gel became more uniform.[94] Further, note that BZ reactions within a single-phase solution also have been reported to undergo a transient regime at the start of the reaction, characterized by inconsistent oscillations and patterns.[14,97,98] Thus, although the change in pattern formation at late reaction times is not unexpected, these results demonstrate the importance of documenting experimental results in such active soft matter over sufficiently long reaction times. Otherwise, it is difficult to distinguish between well-developed, robust oscillation behavior and transient patterns that are affected by initial conditions, including gel shape and size.

Note that an inversion of oscillating patterns was observed at late reaction times for gels of aspect ratio 3.7 in Figure 3-19A: these gels reproducibly exhibited late-time waves of *reduced* catalyst originating from the center of the gel, whereas experiments for gels of lower aspect ratio exhibited waves of *oxidized* catalyst originating from the gel center. The detailed understanding of this pattern inversion in such BZ gels remains unclear and is beyond the scope of this thesis. However, we speculate that this late-time redox pattern inversion is related to conditions under which absolute dimensions of the gel become comparable to diffusion lengthscales of the intermediate reaction species. For gels of aspect ratio ~3.7 in Figure 3-19A, the gel width shrinks to 0.6 mm under the acidic reaction conditions, which corresponds to the critical lengthscale for this reaction. The intermediate species of the BZ reaction are then more likely to diffuse out of the gel network and into the bulk solution, as compared to gels of larger absolute dimensions and similar aspect ratio.

It is important to note that the reported late time patterns, periods of oscillation, and wave velocities for experiments were consistent for both freshly prepared and recycled samples. In fact, Figure 3-19B shows that the same gel sample can undergo the BZ reaction twice without change in pattern formation, duration of the reaction, or period of oscillation. In replicate trials, the reaction was monitored for >2.5 h and exhibited oscillation periods of 2.4 ± 0.2 min and 2.1 ± 0.6 min, respectively. This ability to reuse BZ gels is of particular note, given the highly acidic reaction conditions required to sustain self-oscillation.

3.7.2 Comparison with simulations

Previously, simulated predictions by Yashin et al.[87] were used to explore chemomechanical pattern formation in self-oscillating BZ gels. In our experimental studies of pattern formation, chemomechanical shape changes were not observed. However, theoretical and computational approaches can be

compared to experimental observations to validate model strengths, and to identify model weaknesses. In collaboration with Balazs et al.,[4] the experimental findings shown in Figure 3-19 were compared to simulated predictions based on an Oregonator model for the BZ reaction that accounts for the total concentration of gel confined $Ru(bpy)_3$.[99]

Figure 4-1A illustrates simulated pattern formation in BZ gels of varying aspect ratio. These experimental results generally match those predicted from our BZ gel simulations at late reaction times (Figure 3-19): waves originate in the gel center and migrate radially outwards, regardless of aspect ratio. For the simulation images shown in Figure 4-1, blue and green correspond to a higher and lower concentration of oxidized catalyst, respectively. It is important to note that the behavior is highly robust: simulations for a wide range of system parameters and sample sizes and aspect ratios show that these late-time patterns propagate radially from the sample's center towards its edges. Note that the simulations do not predict the late-time pattern inversion for small gels of aspect ratio 3.7; this is not surprising, in that the BZ reaction model does not explicitly account for intermediate reaction species such as Br^-.

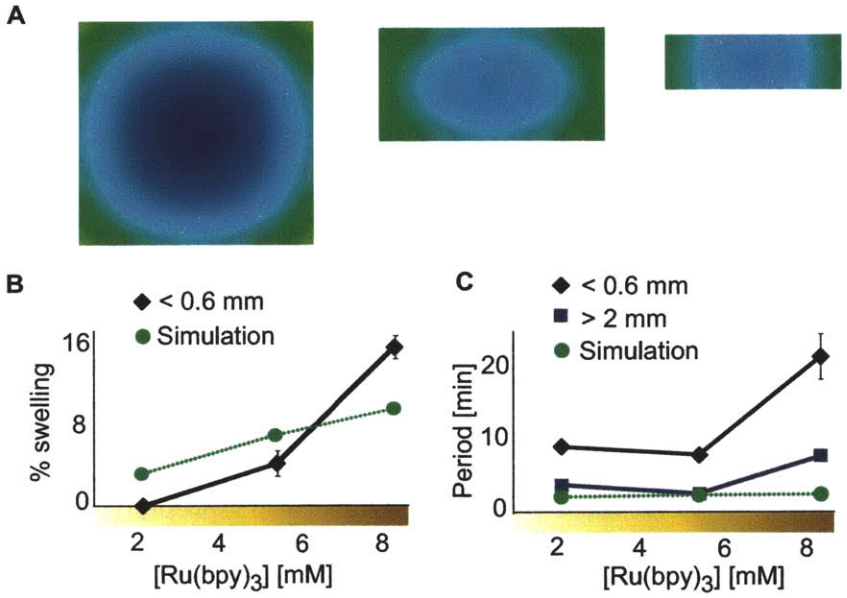

Figure 3-20: (A) Simulated predictions of BZ pattern formation in gels of varying aspect ratio. (B) Experimental and predicted gel swelling as a function of $Ru(bpy)_3$ concentration. (C) Experimental and predicted period of oscillation as a function of $Ru(bpy)_3$ concentration and gel size (see legend). Reproduced from Ref.[4].

In Figure 4-1B, the experimental % swelling and the predicted % swelling are plotted with respect to $Ru(bpy)_3$ concentration. Both experiment and theory confirm that the amplitude of gel swelling increases with increasing $Ru(bpy)_3$ catalyst content, which scales with the color saturation of the gel (Figure 4-1B). Further, the period of oscillation depends both on $Ru(bpy)_3$ content and on physical gel size (Figure 4-1C). Here, the experimental pe-

riods of oscillation were quantified according to hue measured at representative points within the gel. For the gels of aspect ratio 1 and 2, the period of oscillation was 2.1 $\pm$ 0.1 min, and for the gel of aspect ratio 3.7, the period was 11.1 $\pm$ 0.5 min. Thus, both the redox pattern inversion (see Figure 3-19A) and oscillation period observed in gels of aspect ratio 3.7 deviated from gels of aspect ratio 1 and 2. As noted previously, such discrepancy is attributed to the small dimensions (0.6 mm) of the 3.7 aspect ratio gel. This size-dependence of oscillation period has also been noted by Yoshida et al. and Yamaguchi et al., who attributed increased oscillation periods to decreased transport rates in very small or thin gels.[45,94] Furthermore, such results are consistent with Aihara et al.'s observations in which the critical lengthscale of the reaction (0.6 mm) corresponds to a switch from kinetically limited oscillation to transport limited oscillation. When the latter conditions dominate at $\leq$ 0.6 mm, then slow transport rates result in large periods of oscillation.[57]

Figure 4-1C also indicates a slight discrepancy between simulation predictions and experimental results for gels characterized by lateral dimensions $<$ 0.6 mm; this difference may be related to the fact that the simulations do not account explicitly for intermediate reaction species. Further, both the experiments and simulations show that the period depends only mildly on $Ru(bpy)_3$ concentration when gel dimensions exceed this critical lengthscale. Note that the increase in oscillation period with increasing $Ru(bpy)_3$ content exists but is significantly smaller in simulations than in experiments. Through direct comparison between experiments and simulation, we were also able to estimate the strength of the chemomechanical coupling in the BZ gels. In particular, we could extract a realistic value for our model parameter $\chi*$, which relates the mechanical response of the gel to the degree of oxidation of the catalyst. In summary, comparing experimental BZ oscillation with simulated predictions validates the theoretical model for BZ gels developed by Balazs et al. Through comparison, lengthscales at which the model assumptions become invalid were also identified.

3.7.3 Effects of adhesion on pattern formation

Figure 3-21 shows the oscillation behavior for a gel of aspect ratio 3.7 and of lateral dimensions 3.0 x 0.8 mm. Note that these oscillations were recorded prior to establishing image analysis protocols involving hue, so average RGB values are reported. For the first 60 minutes of the reaction, a travelling wave is observed in which waves of oxidized catalyst propagate from one end of the gel to the opposite end (Figure 3-21A). The period of these oscillations is 1.1 $\pm$ 0.1 minutes. After 75 minutes, the pattern formation changes suddenly and oxidized waves penetrate from both ends of the gel, followed by a reduced wave that initiates in the center of the gel and propagates outward (Figure 3-21B). This late time pattern is consistent with the observations made for the 3.7 aspect ratio gel noted in Figure 3-19. In Figure 3-21B, the oscillations occurred every 11.1 $\pm$ 1.0 min.

High aspect ratio gel samples were more sensitive to experimental factors such as adhesion of the gel to the underlying surface (e.g., to the Petri dish).

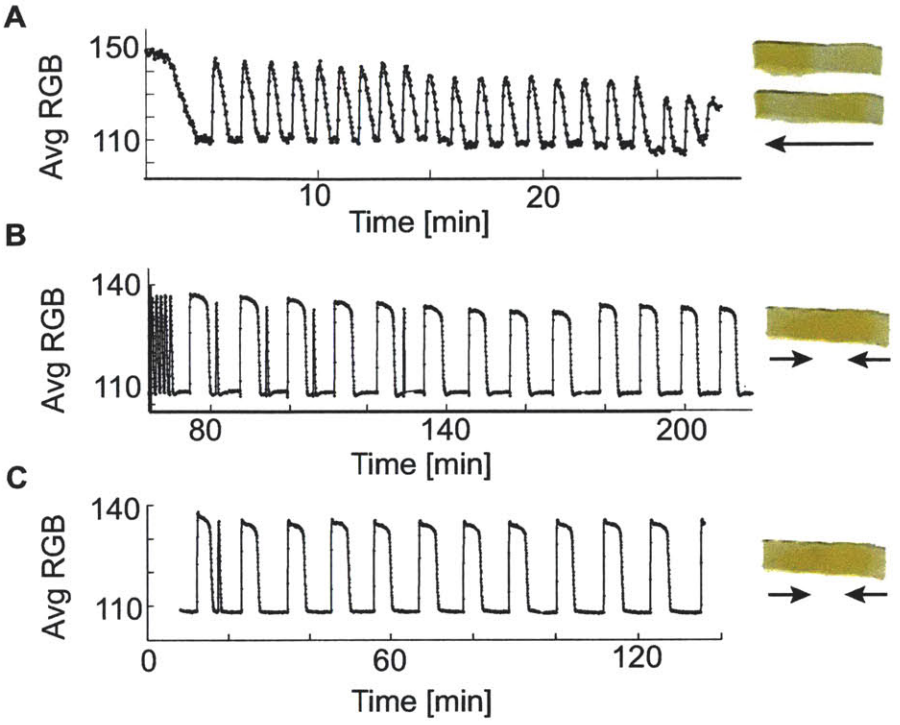

Figure 3-21: Pattern formation in BZ gel of aspect ratio 3.7 and lateral dimensions 3.0 x 0.8 mm. (A) A travelling wave dominates the early time pattern formation. (B) Late time patterns exhibit reduced waves that propagate outward. (C) Pattern formation in a gel for which adhesion was minimized.

We speculate that the early time patterns in Figure 3-21A are dominated by a unidirectional, propagating wave due to non-uniform adhesion of the gel to the Petri dish. Here, adhesion alters the effective boundary conditions at the edges of the gel. Sudden loss of adhesion may explain the abrupt change in pattern formation and period of oscillation after 75 min. In support of these arguments, we repeated the experiment with identical BZ reaction conditions in the same gel but with minimal adhesion (Figure 3-21C). To ensure that the gel did not adhere to the Petri dish, the sample was allowed to drift freely in the solution for 8 min before data acquisition. As shown in Figure 3-21C, the gel did not exhibit a travelling wave; instead, the wave patterns consistently resembled those shown in Figure 3-21B and had a similar period of 11.2 $\pm$ 0.5 min.

Figure 3-22 shows results for a gel of aspect ratio 3.5 and lateral dimensions of 12 x 3.4 mm. In this case for a significantly larger gel (and comparable aspect ratio to that of Figure 3-21), waves of oxidized catalyst initiate from the center of the gel and propagate outwards at late reaction times. Here, the gel size is large enough to accommodate multiple wave fronts. The period of oscillation was 2.1 $\pm$ 0.1 min, which was similar to other gel samples of lateral dimensions greater than 0.6 mm. This experiment demonstrates that the late time pattern observed in the gel of aspect ratio 3.7 (Figure 3-19) deviates from typical late pattern formation because of its absolute

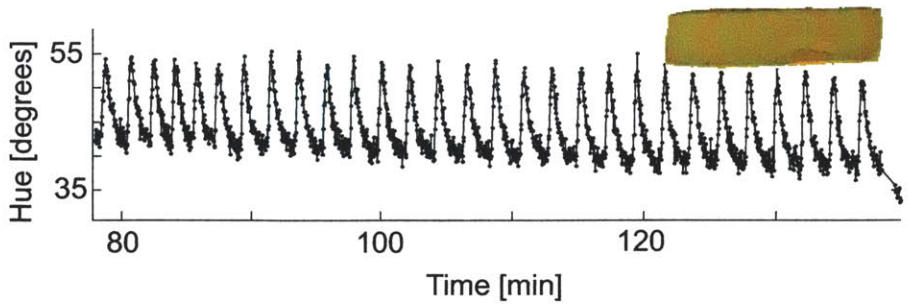

Figure 3-22: Oscillation patterns in a 3.5 aspect ratio gel of lateral dimensions 12 x 3.4 mm.

dimensions, and not necessarily because of gel aspect ratio.

3.8 Conclusions

In this chapter, the oscillatory characteristics of BZ gels were characterized according to period and amplitude. Table 3.1 summarizes the positive and negative effects on period and amplitude for several variables involved in the BZ gel reaction. In quantifying oscillations for a number of system variables, including MA, BrO_3, NaBr, HNO_3, $Ru(bpy)_3$, temperature and gel length, similiarities and discrepancies with existing literature data are identified. Importantly, the non-oscillatory regimes in our BZ gels are not governed by high concentrations of MA or BrO_3. Rather, a sensitive chemical regime is observed at low concentrations of MA, where BZ gels sometimes fail to oscillate. And, a definite non-oscillatory regime is observed when the ratio of BrO_3 to Br^- is sufficiently low.

Variable	Amplitude of Oscillation	Period of Oscillation
[MA]	−	−
$[BrO_3]$	+/−	−
$[Br^-]$	−	+/−
$[HNO_3]$	+	N/A
$[Ru(bpy)_3]$	+	+
Temperature	−	−
Gel length	−	−

Table 3.1: Effects of BZ variables on amplitude and period of oscillation. Positive effect (+) indicates that increasing variable magnitude results in an increase in either amplitude or period. Negative effect (−) indicates that increasing variable magnitude results in a decrease in either amplitude or period. Mixed positive and negative effects (+/−) and no effect (N/A) were observed for certain variables.

In addition, this chapter elucidates how confinement of the BZ reaction within millimeter-sized gels modulates pattern formation and chemomechanical swelling. Experimental demonstration of shape- and size-dependent pat-

tern initiation and evolution provides context for previously reported behavior in self-oscillating gels. Our results show that at early reaction times, pattern formation depends on gel size, shape, and perturbation of initial conditions. At late reaction times, however, pattern formation becomes independent of gel dimensions. Direct comparison between experiments and simulations provides a validation of the theoretical and numerical models of chemomechanical coupling in these complex, active materials. Moreover, we have identified lengthscales at which the simulated reaction model of BZ gels can be further parameterized.

These findings can thus ground future studies that leverage the strong coupling between chemical and mechanical states within these active hydrogels. In Chapter 4, we utilize such information in order to design experiments with the aim of mechanically triggering BZ oscillations in gels. Thus, the results presented in this chapter provide a foundational understanding of chemomechanics in BZ gels, enabling new applications and biological analogues that exhibit self-oscillation.

Chapter 4

Mechanically Triggered BZ Oscillations

Portions of this work have been published in peer-reviewed journals (see Reference[3] and[7]), and are reproduced with permission from John Wiley & Sons and The Royal Chemical Society.

4.1 Introduction

While BZ gels are capable of undergoing mechanical oscillations induced by the alternating chemical redox state of covalently bound $Ru(bpy)_3$ catalyst, there has been limited experimental evidence demonstrating the reverse phenomena in which BZ gels exhibit a chemical response to mechanical stimuli. However, given the strong chemical and mechanical coupling exhibited by BZ gels, it is reasonable to hypothesize that BZ gels are capable of sensing mechanical pressure.

Thus far, results suggesting that BZ media can respond to mechanical stimuli have been limited to membranes and gels containing electrostatically bound ferroin catalyst. Suzuki et al. observed that local compression of an immersed, thin ($\sim$200 μm) BZ Nafion membrane using a glass stick triggered a single target wave in an initially excitable but non-oscillatory system. In their experiment, the membrane did not exhibit self-regulating or sustained BZ oscillations. Rather, additional chemical waves were triggered by repeatedly applying mechanical force to the membrane. Furthermore, the membrane required 30 min of recovery time between waves to restore its mechanical responsiveness.[62] Using a different material system, Munuzuri et al. demonstrated that stretching of BZ polyacrylamide-silica gels at specific frequencies of mechanical loading resulted in vortex drift of BZ spirals.[100] While this mechanical stimulus altered the spatial patterns of the BZ wave, there was no direct conversion of mechanical to chemical energy since the gel stretching failed to initiate the chemical wave. While strong chemomechanical coupling is observed in other BZ systems, such materials have clear limitations in their abilities to convert mechanical energy into robust chemical oscillation.

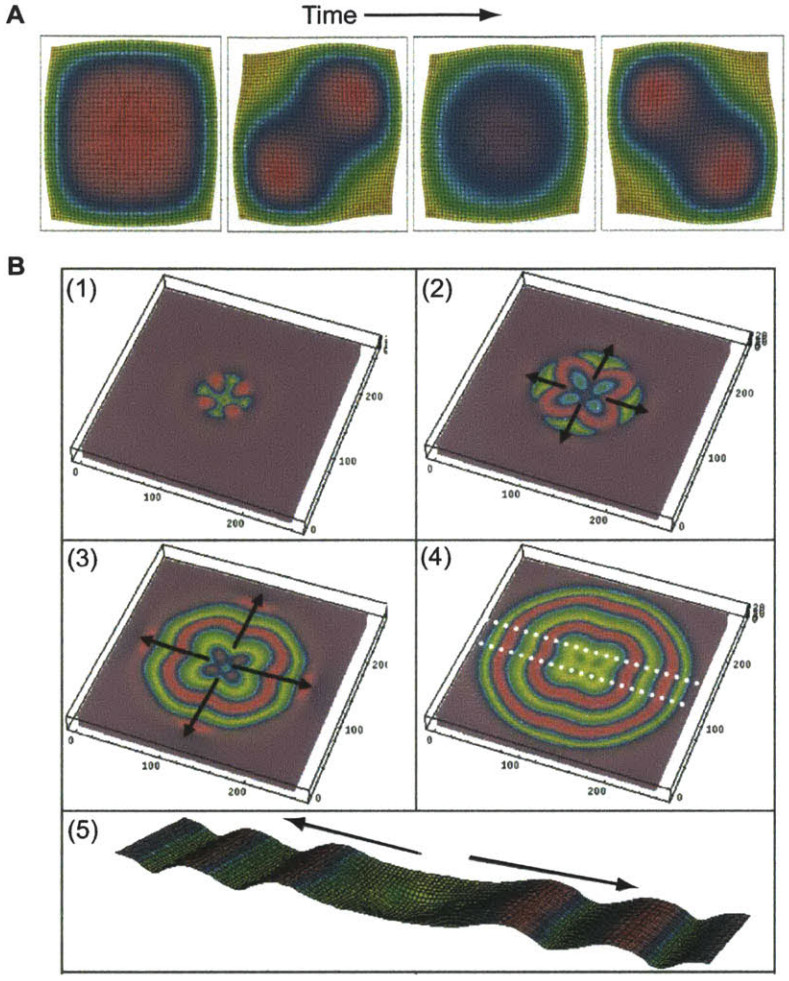

Figure 4-1: Mechanically responsive behavior in simulated predictions of BZ gels. (A) Simulated BZ gel that was induced to oscillate upon macroscopic compression. (B) Snapshots with time (1-4) of BZ gel after localized impact. Side view of gel (5) showing how local swelling affects the gel thickness. See reference [5] and [6] for simulation details and parameters. Both A and B are reprinted from references [5] and [6] - reproduced by permission of The Royal Society of Chemistry.

In contrast, computational simulations have predicted a wide variety of chemical behavior in response to the mechanical deformation of a BZ gel. These mechanical stimuli include macroscopically uniform compression, locally applied pressure, and mechanical strain.[5,6,76] In particular, Kuksenok et al. predicted that mechanical stimuli can trigger sustained chemical oscillations in an initially non-oscillating BZ gel.[5] Figure 4-1A shows simulated predictions illustrating BZ oscillations in a gel after macroscopic compression was applied to the system. Additionally, Figure 4-1B shows computational results in which localized mechanical stimuli induces BZ oscillations at a particular point of impact. Note that the simulations predict localized gel swelling as a result of the travelling chemical wave induced by the BZ oscillations (see Figure 4-1B, 5).[6] Such simulated predictions suggest that BZ

gels can convert mechanical potential into chemical energy, by undergoing transitions between oscillatory and non-oscillatory states.

Prior to the work in this thesis, such computational predictions lacked experimental validation, and there were no studies showing that NIPAAm BZ gels could sense mechanical stimuli. Such demonstration of mechanical sensing, however, affords novel approaches to creating pressure sensors based on BZ gels, since few synthetic materials are able to produce oscillating chemical signals in response to mechanical deformation. In addition, hydrated gel systems would be useful in fabricating devices that mimic the self-healing process of skin in which the initial healing step involves the detection of mechanical impact by mechanoreceptors followed by the transmission of chemical signals throughout the body.[77,78] In this chapter, we report the first experimental evidence showing that non-oscillatory BZ gels respond to mechanical compression by undergoing oscillating color changes. Substantial evidence is provided in order to describe the mechanism of mechanically triggered oscillations, and to further elucidate aspects of chemomechanics in BZ gels.

4.2 Methods

In the following sections, theoretical considerations and chemical conditions required for preparing a mechanically triggerable gel are explained. Here, we briefly describe the experimental setup for inducing macroscopic compression by applying uniaxial stress to fully hydrated poly(NIPAAm-co-Ru(bpy)$_3$) BZ gels.

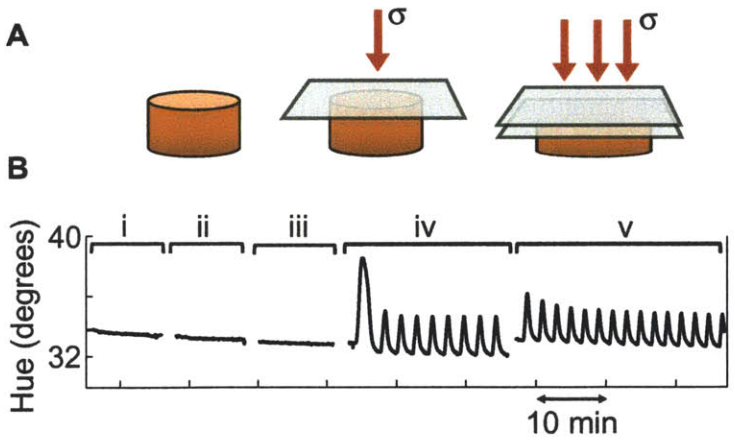

Figure 4-2: Mechanically triggered BZ oscillations. (A) Schematic of a gel being macroscopically compressed. Graphic not to scale. (B) 1.2 mm diameter BZ gel disc (0.6 mm thickness and 8.3 mM Ru(bpy)$_3$ catalyst) in BZ solution with initial composition: MA (0.2 M), $NaBrO_3$ (0.1 M), and HNO_3 (0.7 M). Increasing amounts of stress was applied to the gel throughout the experiment: (i) 0.1 kPa, (ii) 0.3 kPa, (iii) 0.4 kPa, (iv) 1.2 kPa, and (v) 5.6 kPa. Reproduced from Ref.[3].

In all of the mechanical triggering experiments, a BZ gel disc of mm-

scale dimensions and containing covalently bound $Ru(bpy)_3$ catalyst was submerged in solution containing the chemical reactants necessary for oscillations to occur: MA, $NaBrO_3$, and HNO_3. In some cases (noted in the following sections), NaBr was added to the BZ solution. All experiments were conducted at 20°C, which is below the phase transition temperature of NIPAAm, and the temperature of both the external solution and BZ gel varied insignificantly over the course of the experiment. Two methods were employed for obtaining a steady state, uniformly non-oscillatory BZ gel. Both of these methods are explained in this chapter, within the relevant sections. When a non-oscillatory gel state was obtained, the gel was monitored via timelapse microscopy to confirm that the $Ru(bpy)_3$ catalyst was in a uniformly reduced state. Next, increasing amounts of macroscopic, compressive stress was applied to the gel by gently placing glass slides of known mass on top of the disc (see schematic in Figure 4-2A). The gel state was monitored for at least 10 min to determine whether oscillations were triggered. Additional glass slides or heavier slides were added to the stack when oscillations were not observed in order to increase the total applied stress until oscillations were triggered.

For the experiment shown in Figure 4-2, the applied stress was increased every 10 min (see Figure 4-2B, i-v). Increasing amounts of applied stress generally caused the gel to expand laterally and reduce in thickness upon compression, however the axial compression was greater than the lateral expansion of the gel. For the experiment shown in Figure 4-2, the gel remained in a non-oscillatory state when the applied stress was between 0.1 and 0.4 kPa. When the stress was increased to 1.2 kPa, the $Ru(bpy)_3$ catalyst within the gel immediately changed visually from orange to green. The color change was uniform and wave patterns were not observed due to the small dimensions of the BZ gel.[4] The applied stress was held constant for 30 min, during which the catalyst containing gel continued to oscillate with a period of 2.3 ± 0.05 min and an amplitude of 2.6 ± 0.1 degrees. Increasing the applied stress to 5.6 kPa caused the gel to compress by 11 μm but did not qualitatively change the oscillatory characteristics (see Figure 4-2B, v). This experiment demonstrates that chemical oscillations can be mechanically triggered in a BZ gel, and in the following sections, we elucidate the mechanism by which this phenomena occurs.

4.3 Mechanism of Mechanical Triggering

In order to understand the mechanism of mechanical triggering in BZ gels, the required experimental conditions for which such gels become mechanically responsive need to be identified. In this chapter, the chemical phase space that defines access to the "mechanically triggerable state" is quantified. Such results are of critical importance since there is no prior theoretical framework or practical literature protocol for designing triggerable BZ gel systems.

4.3.1 Required Chemical Conditions

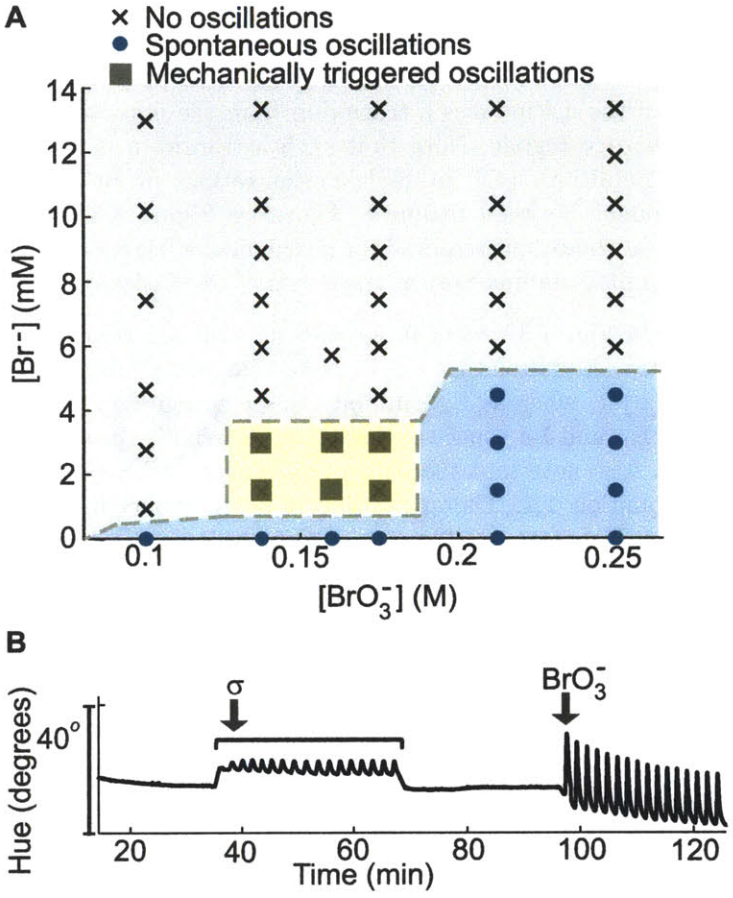

Figure 4-3: Oscillatory regimes for the BZ reaction. (A) Oscillatory regimes in BZ gels with respect to BrO_3^- and Br^- concentrations. Mechanically triggered oscillations (■) were possible at chemical conditions near the oscillatory regime but corresponding to the non-oscillatory regime. (B) BZ gel exhibiting oscillations when compressive stress (σ) is applied to the gel and when BrO_3^- is added to the system.

A subtle prerequisite for any triggering experiment involving BZ gels is that the gel must start off in a non-oscillatory state. In Chapter 2 (Figure 3-13B), the oscillatory regime of a BZ gel comprising 8.3 mM $Ru(bpy)_3$ was characterized with respect to BrO_3^- and Br^- concentrations. As a reminder, there exists a non-oscillatory regime in which the presence of Br^- inhibitor prevents the BZ reaction. For each of the non-oscillatory conditions that were identified in Figure 3-13B, compressive stress was aplied to the gel in an attempt to mechanically trigger oscillations, and the compressed gel was monitored for 30 - 40 min. The stress required to trigger oscillations in these gels was typically <1 kPa due to the relatively high concentrations of $Ru(bpy)_3$, BrO_3^-, MA, and HNO_3. However, up to 7 kPa of stress was applied to the gel, in excess of the required stress, to ensure that oscillations

were triggered whenever possible. As shown in Figure 4-3A, mechanically triggered oscillations were possible for only a small number of conditions tested. Such conditions represented an intermediate ratio of BrO_3^- to Br^- (shaded in yellow and marked by ■). Note that these triggerable conditions existed within the non-oscillatory regime, but near the boundary dividing the oscillatory and non-oscillatory regimes. At these conditions, mechanical compression of the gel induces a transition from the non-oscillatory regime into the oscillatory regime. Note that such a transition is not possible at all chemical conditions (e.g. at high concentrations of Br^-, far from the dividing boundary between regimes). Therefore Figure 4-3A indicates the precise chemical conditions required for mechanically triggerable oscillations, and enables immediate mechanical triggering of oscillations in a BZ gel.

The data in Fig. 4-3A were in agreement with our previous discussion of BZ chemistry (Equations 1.1 - 1.3). Note that BrO_3^- drives oxidation of $Ru(bpy)_3$ catalyst, whereas Br^- inhibits this reaction step (Equation 1.2). Thus, the BrO_3^- and Br^- species compete to determine the oscillatory state of the BZ gel. Also note that the $Ru(bpy)_3$ catalyst and BrO_3^- are both reactants in Equation 1.2. Therefore, increasing the concentration of either reactant drives Equation 1.2 forward. Figure 4-3B demonstrates an experiment in which BZ oscillations were triggered in a gel by first applying a compressive stress, and subsequently by addition of BrO_3^- species. Initially, the gel was in a non-oscillatory, ostensibly quiescent state due to the presence of Br^- species. When 9 kPa of stress was applied to the gel, oscillations were triggered due to the increased $Ru(bpy)_3$ concentration within the gel. Such oscillations ceased upon removal of the applied stress. After an additional 30 min, BrO_3^- was added to the system, again driving Equation 1.2 forward and triggering BZ oscillations.

Note that the addition of MA to this system turned off oscillations, indicating that excess MA plays an inhibitory role in such sensitive systems. Figure 4-4 shows an experiment in which a BZ gel disc was exposed to multiple stimuli. First, the gel was monitored for 1 h to confirm that the gel was in a non-oscillatory, quiescent state. Next, 10 kPa of compressive stress was applied to the gel, triggering oscillations as expected (Figure 4-4A). Oscillations were recorded for 30 min, and the mechanical compression was removed from the gel, at which point the gel reverted back to its non-oscillatory state. After 20 additional minutes, 390 μL of 1 M BrO_3 was added to the solution and mixed well. As a result of the BrO_3 addition, oscillations were chemically triggered, and such oscillations were recorded for 30 min (Figure 4-4B). To observe the effects of MA on the oscillating system, 100 μL of 1 M MA was added to the solution, causing oscillations in the gel to stop (Fig.4-4B). The non-oscillating gel state was recorded, and 300 μL of 1 M BrO_3 was added to the mixture. Again, the addition of BrO_3 chemically triggered oscillations in the gel (Fig.4-4C). In contrast, addition of MA to the aqueous solution forced the oscillating gel into a non-oscillatory regime since MA is involved in the reduction of $Ru(bpy)_3$ catalyst and in the generation of Br^- inhibitor species. Furthermore, MA is not a reactant species in Equation 1.2, so addition of MA does not drive this reaction forward.

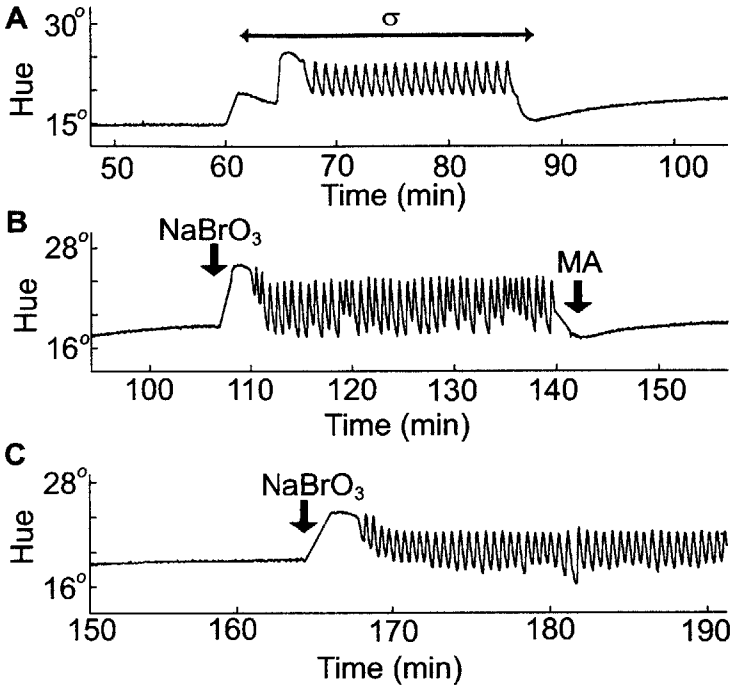

Figure 4-4: Effects of applied stress, addition of BrO_3, and addition of MA (A) BZ gel disc was submerged in 0.2 M MA, 0.1 M BrO_3, and 0.7 M HNO_3. After monitoring the steady-state of the gel for 60 min, macroscopic compression was applied to the gel, triggering oscillations. The compression was removed after 30 min. (B) BrO_3 was added to the external BZ solution at 110 min, triggering oscillations in the gel. While oscillations were occurring in the gel, MA was added to the external BZ solution at 140 min, triggering oscillations off. (C) BrO_3 was added to the external BZ solution at 165 min, again triggering oscillations in the gel.

4.3.2 Theoretical Considerations

In theory, the mechanism for mechanically triggering oscillations in a BZ gel involves an interplay between the deformation of the gel and the chemical dynamics of the BZ reaction.[5] Here, we provide additional background on BZ kinetics and gel dynamics in order to extend current theoretical knowledge of the mechanism for mechanically triggering oscillations in a BZ gel.

When the kinetic equations describing the BZ reaction (Equations 1.1 - 1.3) are transformed into dimensionless variables and represented in terms of dynamic concentrations of chemical species, then the following reaction rate G, which describes the rate of production of oxidized $Ru(bpy)_3$ catalyst, can be formulated as:[6,7]

$$G = (1-\phi)^2 u - (1-\phi) v \tag{4.1}$$

where ϕ is the polymer volume fraction of the gel, u is the dimensionless concentration of $HBrO_2$, and v is the dimensionless concentration of oxidized $Ru(bpy)_3$ catalyst. We have tacitly assumed that the NIPAAm polymer does not react with any chemical species, and only serves to dilute the concentra-

tion of the BZ reactants.

If the gel is in a non-oscillatory state (state 1), then:

$$G_1 = (1 - \phi_1)[(1 - \phi_1)u_1 - v_1] = 0 \tag{4.2}$$

The solution $\phi = 1$ is not physically relevant, since this condition corresponds to the dried, polymer state in which no aqueous solution is absorbed by the gel (and therefore BZ reactants are not present to react with the $Ru(bpy)_3$). The second solution is given by:

$$v_1 = (1 - \phi_1)u_1 \tag{4.3}$$

When macroscopic compressive stress is applied to the gel, the polymer volume fraction changes such that ϕ=ϕ_2. The new reaction rate, G_2 is then given by:

$$G_2 = (1 - \phi_2)[(1 - \phi_2)u_1 - v_1] \tag{4.4}$$

Substituting our expression for v_1 and re-arranging gives:

$$G_2 = (1 - \phi_2)u_1\Delta\phi \tag{4.5}$$

where $\Delta\phi$ is the change in polymer volume fraction of the gel, induced by the applied compressive stress. Equation 4.5 indicates that the instantaneous reaction rate is no longer zero when the gel is compressed, but rather depends on $\Delta\phi$. While Equation 4.5 suggests that the steady-state of the system has been perturbed, this theoretical framework does not indicate the magnitude of strain required to trigger oscillations; it also does not explicitly confirm whether triggering is uniquely defined by an applied stress or applied strain. In the next section, relevant experimental data is provided concerning the stresses and strains for triggering oscillations in BZ gels.

4.3.3 Required Stress and Strain

Figure 4-2 indicated that there exists a critical stress required for triggering oscillations in a BZ gel, in that oscillations are only triggered when increasing increments of applied load reach a specific threshold. However, these data were acquired for specific chemical concentrations and gel properties. To fully understand the interplay between the BZ reaction and the physical properties of the gel, a direct cause and effect relationship needs to be established. In establishing mechanisms of deformation-induced transformations in other material systems, the switch is often found to be triggered or limited by a threshold of stress (normalized load) or of strain (normalized displacement). Even in biological systems such as contractile tissue cells, understanding of mechanotransduction has included consideration of whether cell-generated contraction is limited by the resulting stress or strain[101,102]. Thus, to further elucidate the mechanical triggering mechanism in chemically complex BZ systems, the relationship between gel mechanics and BZ chemistry needs to be quantified.

We hypothesized that the required stress to trigger oscillations in a BZ

gel would depend on the physical properties of the material. Thus, to test the mechanical limitations of the triggering mechanism, three BZ gels of varying polymer volume fraction ϕ were synthesized by adjusting the amount of crosslinker added to the sample during synthesis. When measured in water, the thicknesses of the three gels were 0.6, 0.7, and 0.8 mm, corresponding to $\phi = 0.23$, 0.16, and 0.12, respectively. The hydrated gel was more swollen when less crosslinker was used in the synthesis, as expected. As a result, the polymer volume fraction of the gel, measured when the gels were fully hydrated in water, was smaller for gels containing less crosslinker.

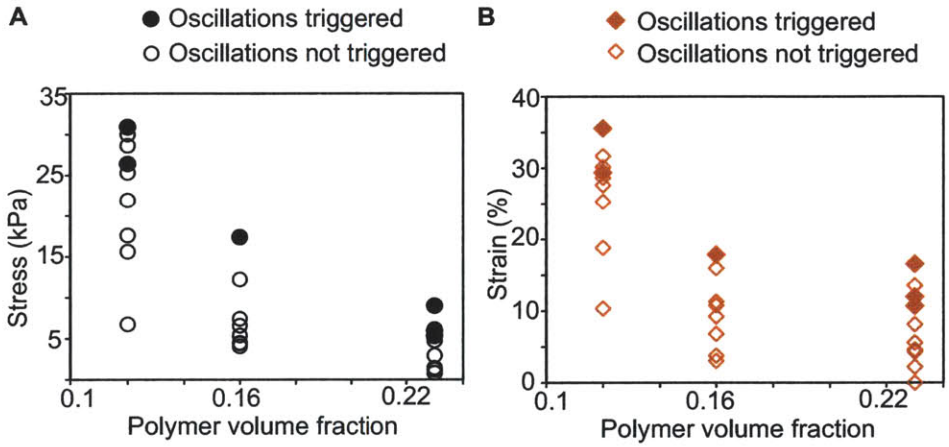

Figure 4-5: Applied stress and strains insufficient to trigger oscillations.

To carefully quantify the variables involved in the triggering mechanism, both the stress applied to the gel and the induced material strain were measured. The $Ru(bpy)_3$ content in the gels was constant (5.0 ± 0.2 mM) and, for each sample, a 1.3 mm biopsy punch was used to prepare uniform gel discs of 1.3 mm diameter, with varying polymer volume fraction and initial thickness. For each experiment, a gel disc was placed in a Petri dish of 3.5 cm diameter and submerged in BZ solution (10 mL) containing MA, BrO_3^-, and HNO_3. Reactant depletion over many hours resulted in an exhuasted, non-oscillating gel, as described in the following section. This exhaustive incubation period was performed to prepare systems requiring relatively large amounts of gel strain to trigger oscillations, so that manual errors in measuring gel dimensions were small in comparison to axial compression. After 23 h of reactant depletion, the gel was monitored for 1 h to confirm that the material was in a uniform, steady-state. The gel dimensions were measured in BZ solution to calculate the polymer volume fraction of the disc while in acidic conditions. Next, the gel was compressed by placing a glass slide of known mass on top of the disc. After monitoring the gel for 10 min, the applied stress was increased in 10 min intervals until oscillations were triggered. See Figure 4-5 for some of the tested applied stresses and induced strains that were insufficient for triggering oscillations in the gels.

We conducted 2-3 replicate experiments at each ϕ, and Figure 4-6A indicates mean and standard deviation of the required stress and strain to

trigger oscillations. Note that the average period of triggered oscillations was 1.8 ± 0.1 min, and the average amplitude of oscillation was 5.0 ± 0.6°. The amplitudes were relatively small because of the low concentrations of reactant species due to reactant depletion, and so the gel discs did not exhibit concurrent, periodic swelling.

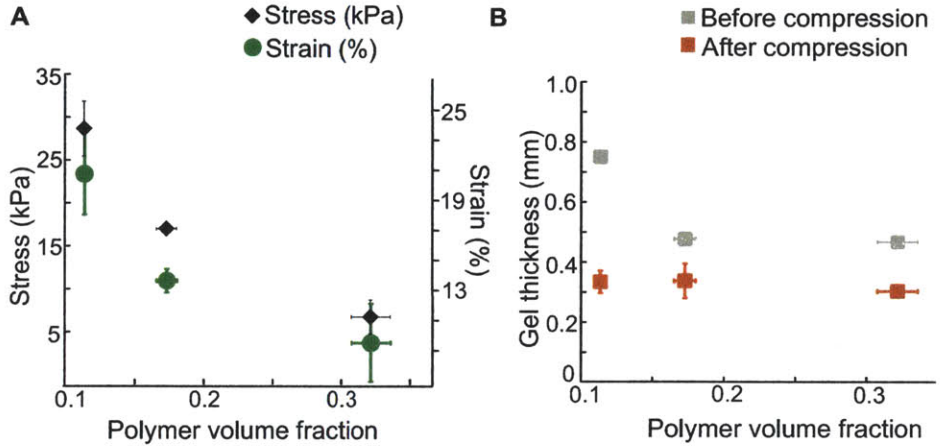

Figure 4-6: Required stress, strain, and gel thickness for mechanically triggered oscillations in BZ gels of varying crosslinking density and thus varying polymer volume fraction, but uniform $Ru(bpy)_3$ concentration. (A) Applied stress (left axis) required to trigger oscillations decreased with increasing polymer volume fraction. Strain required (right axis) to trigger oscillations also decreased with increasing polymer volume fraction. (B) Regardless of initial gel thickness, BZ oscillations were triggered when the gel thickness was approximately 0.3 mm, indicating that oscillations are consistently triggered at a critical gel thickness that corresponds to a critical catalyst concentration. Data points represent averages for 2 - 3 replicate experiments, and error bars represent standard deviation.

As shown in Figure 4-6, the applied stress required to trigger oscillations decreased with increasing polymer volume fraction. Similarly, the corresponding strain decreased with increasing polymer volume fraction. These data indicate that there is a threshold deformation required to trigger oscillations in a given gel, but also that the magnitude of sufficient stress or strain varies according to the physical properties of the gel: if a critical stress was required, one would expect Figure 4-6A to indicate that the required stress does not depend on ϕ, and if a critical strain were required, one would expect Figure 4-6A to indicate that the required strain does not depend on ϕ. Interestingly, oscillations were consistently triggered when the gels reached a thickness of approximately 0.3 mm (Figure 4-6B). The initial thickness of the non-deformed gels in BZ solution ranged between 0.47 - 0.75 mm; thicker gels were more swollen and required relatively large amounts of applied stress and strain to compress the gel to a final thickness of 0.3 mm. Note that the axial compression of the disc was much greater than the induced lateral expansion of the gel (approximately 6.5% increase in radius for 40% decrease in thickness). See Table 4.1 for a summary of the average lateral expansion and axial compression of the gels. Since the $Ru(bpy)_3$

ϕ	Poisson's ratio	Lateral expansion (%)	Axial compression (%)
0.11	0.21	14	56
0.17	0.11	3	29
0.32	0.11	3	35

Table 4.1: Summary of gel dimensions and measured Poisson's ratio for compression experiments.

catalyst was covalently bound to the polymer backbone, and the lateral expansion of the compressed gel was much less than the axial compression of the material, the overall $Ru(bpy)_3$ concentration of the gel disc increased upon compression. When a given gel was compressed to a critical thickness of 0.3 mm, the corresponding $Ru(bpy)_3$ concentration was approximately 11.4 mM, representing more than a doubling of the metal catalyst concentration in the uncompressed gel.

4.4 Mechanical Resuscitation of Oscillations

In this section, we introduce the concept of mechanical "resuscitation" by which mechanical compression triggers oscillations in exhausted BZ gel systems. This technique was used in the previous section to setup experiments for determining the required stress and strains for triggering oscillations. Here, NaBr is not added to the BZ system to prevent oscillation, and mechanical resuscitation is utilized only to restore the oscillatory functionality of the gel after the BZ reaction has died out. This mechanical restoration of oscillation in an exhausted system evokes analogy to resuscitation of a beating heart, though the mechanisms by which BZ oscillations are triggered and restored in a reactant-depleted gel are quite different than the systems-level restoration of blood flow. It is important to note that the mechanism governing mechanical resuscitation in BZ gels is identical to those described earlier in this chapter; however, the experimental setup and material conditioning are unique.

The methods for mechanical resuscitation involve a lengthy protocol involving low concentrations of BZ reactants. In a typical procedure, a BZ gel is immersed in BZ reactants (0.1 M BrO_3, 0.08 - 0.3 M MA, and 0.7 M HNO_3). The gel remained immersed in the BZ solution bath for 20 h. This immersion interval was required in order to achieve a consistent, non-oscillatory state within the gel, regardless of the initial BZ conditions such as acid concentration. During this time, the BZ gel was allowed to spontaneously self-oscillate to the point of exhaustion, meaning that reactant molecules were consumed while inhibitor species (Br^-) were produced until the gel eventually stopped oscillating. After 20 h, the non-oscillatory state of the gel was quantified and confirmed by monitoring the sample hue under an optical microscope in the BZ bath for at least 1 h. Compressive stress was applied to the gel using glass slides of known mass, as described previously. It is important to note that the BZ gel system, prior to compression, attains a steady-state upon depletion of reagents. Macroscopic compression of the gel triggers oscillations

by utilizing unreacted reagents in the aqueous solution. In other words, the BZ reactants are not entirely consumed by the reaction; rather, the presence of generated Br^- relative to the depleted concentration of reactants inhibits the reaction from proceeding. Further note that the concentration of Br^- which inhibits oscillation is very small when the concentration of BrO^- is less than 0.1 M (see Figure 4-3A). At such low concentrations of reactant and inhibitor species, the BZ chemistry becomes very sensitive and difficult to replicate by simply adding NaBr to the initial solution. In summary, we have demonstrated two techniques for preparing a mechanically triggerable BZ gel: the first technique involves adding NaBr to the system in order to attain a triggerable chemical condition according to Figure 4-3A, and the second technique involves exhausting chemical reactants by allowing the gel to oscillate until a quasi steady-state is achieved.

4.4.1 Tunable Oscillations

By varying the initial conditions of the reaction, we found that the oscillatory behavior of a mechanically resuscitated gel was tunable. Specifically, the period and amplitude of oscillation depended on the initial concentration of MA in solution.

A relatively large amplitude (14.4 ± 0.8^o) and longer period (7.3 ± 0.6 min) was observed when the gel was placed in an initial solution containing 0.08 M MA (see Figure 4-7A), as compared with a gel placed in 0.3 M MA that oscillated with an amplitude of 3.7 ± 0.1^o every 0.9 ± 0.04 min (see Figure 4-7B). As noted, catalyst concentration and reaction conditions were maintained as similar as possible among all experiments, in that initial $Ru(bpy)_3$ concentration was verified through correlations with hue prior to the BZ reaction (i.e., in water) and was consistently 0.21 ± 0.01^o. Further, all samples were punched to uniform diameter from a single polymerization batch reaction for which initial $Ru(bpy)_3$ concentration was measured via UV spectroscopy, and the gel thickness was approximately constant at 0.6 mm. In total, four different malonic acid conditions were tested with 2 - 4 replicate samples and experiments at each condition. In all of the experiments, the oscillations were reversibly triggered by adding and removing compressive stress to the gel. These results, summarized in Figure 4-7C, demonstrate that the period and amplitude of the mechanically triggered oscillation can be tuned by changing the composition of the initial BZ reactants.

The error bars shown in Figure 4-7C represent the standard deviation for period and amplitude across replicate experiments in different gel samples. When the initial concentration of malonic acid was > 0.2 M, the triggered oscillations were relatively consistent across replicate experiments in different gel samples. When the initial malonic acid concentration was lower, however, the triggered period and amplitude varied over several minutes and degrees, respectively, across different gel samples. Note that the period and amplitude of triggered oscillations were highly consistent for a given gel sample.

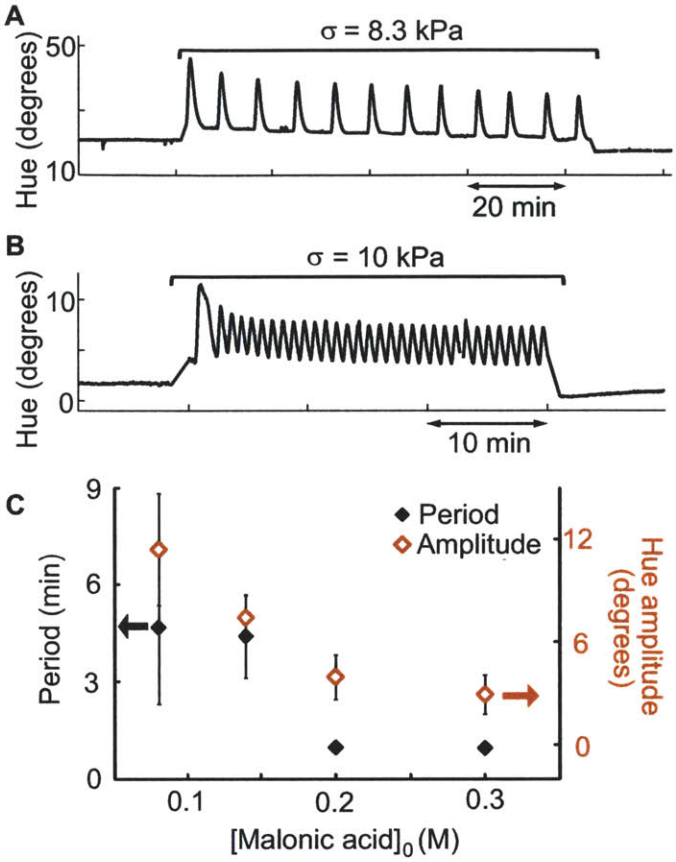

Figure 4-7: Triggered oscillations versus MA concentration in 0.7-0.9 mm diameter BZ gel discs containing 8.3 mM $Ru(bpy)_3$ catalyst. (A) Triggered oscillations in a BZ gel after 20 hrs in a solution containing MA (0.08 M), $NaBrO_3$ (0.1 M), and HNO_3 (0.7 M). (B) Triggered oscillations in a BZ gel after 20 hrs in a solution containing malonic acid (0.3 M), $NaBrO_3$ (0.1 M), and HNO_3 (0.7 M). (C) Triggered period and amplitude of oscillations for gels submerged at time zero in BZ solutions with varying MA. Error bars represent standard deviation for replicate experiments in different gel samples. Reproduced from Ref. [3].

4.4.2 Pressure Sensors

Next, we incorporated our knowledge of chemomechanical transduction in BZ gels to design a pressure sensor. In this experiment, a row of four nearly identical BZ gel discs, spaced >1 mm apart from each other, were placed in a Petri dish containing a BZ solution bath. After 20 h of immersion, self-oscillations in all four discs were exhausted and a non-oscillatory state was achieved. After monitoring the non-oscillatory state for 1 h, disc 1 was mechanically compressed, triggering oscillations in only that disc. Forty minutes later, discs 3 and 4 were simultaneously compressed. Again, the applied stress triggered oscillations in both discs, although the induction time elapsed between the application of stress and the observation of oscillations varied due to slight differences in disc thickness. Disc 2 was a control region that was uncompressed and remained in the non-oscillatory state (see Figure 4-

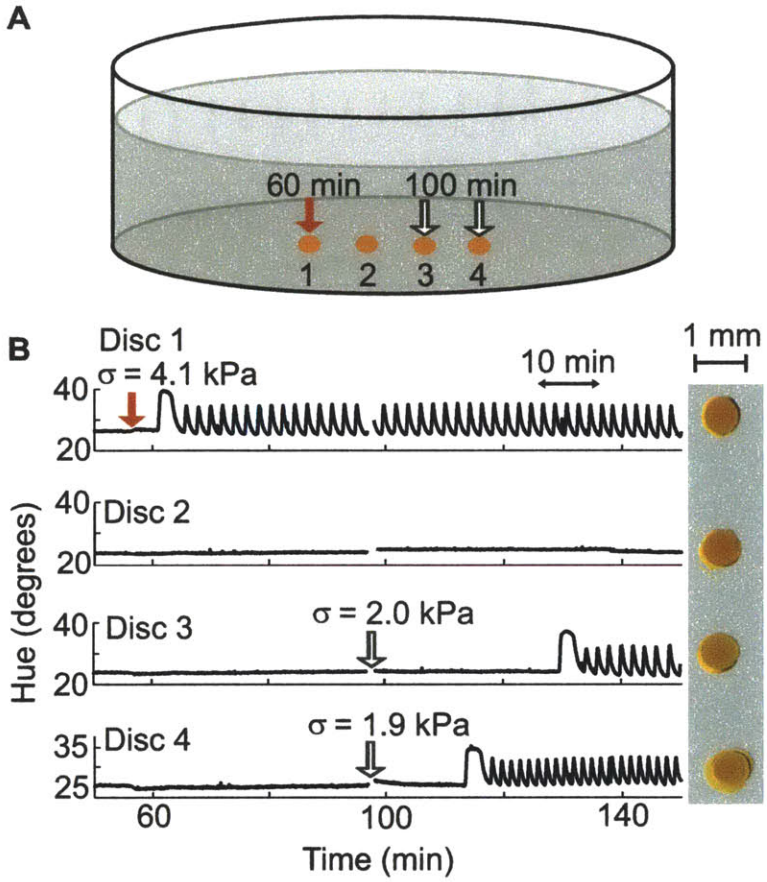

Figure 4-8: BZ gel discs as a pressure sensor. (A) Schematic of experiment indicating the times at which discs 1,3, and 4 were mechanically compressed (not to scale). (B) Hue of discs 1-4, indicating discs 1, 3, and 4 were mechanically triggered. BZ gel discs were 0.7-0.8 mm in diameter (0.6 mm thickness and 8.3 mM $Ru(bpy)_3$ catalyst) in BZ solution with initial composition: MA (0.08 M), BrO_3 (0.1 M), and HNO_3 (0.7 M). The gap distances between discs were 1.8 mm (disc 1 and 2), 1.3 mm (disc 2 and 3), and 1.5 mm (disc 3 and 4). Reproduced from Ref. [3].

8). The periods of oscillation for discs 1, 3, and 4 were approximately 2.1, 2.0, and 1.5 min, respectively. The amplitudes were 10.0, 9.4, and 6.9°, respectively. Thus, we have demonstrated an application in which the BZ gel discs function as a touch-sensitive material, oscillating only when each disc is mechanically triggered.

In a separate experiment (see Figure 4-9, we demonstrated that the gel discs can communicate with each other via chemical diffusion, after only one gel is mechanically triggered to oscillate. Figure 4-9 shows two BZ gel discs, with an edge-edge spacing (gap distance) of 0.23 mm as measured while submerged in BZ solution. Again, the gels were submerged in a BZ solution bath for 20 h to achieve non-oscillatory states. Disc 1 was mechanically compressed, triggering oscillations, as expected. Interestingly, despite remaining uncompressed, disc 2 also began to oscillate. This result indicates that in-

termediate, activator species that were generated by the BZ reaction in disc 1 diffused across the gap within seconds, triggering an oscillatory response in disc 2. At these experimental conditions, the gels oscillated at low amplitudes such that the gap distance of 0.23 mm was constant. Although the discs exhibited similar hues in water (0.2^o), the steady-state hue of the gels prior to compression differed. As noted previously, the steady-state hue of the gel does not affect the magnitude of the triggered period or amplitude. The period of oscillation for disc 1 was 1.5 min with an amplitude in hue of 8.9^o, while the period of oscillation for disc 2 was 1.8 min with an amplitude of 6.7^o. Physically, these results indicate that there is a critical gap distance between discs for communicative chemical diffusion to occur. As noted by Tateyama et al. and Fukuda et al., the critical gap length between chemically communicating BZ oscillators depends on the detailed conditions of the experiment.[53,103] At these specific chemical conditions, a gap distance of 0.31 mm was too large, and the uncompressed gel did not oscillate. In summary, our experiment demonstrates that the BZ gel can sense mechanical impact and transmit oscillating, chemical signals away from the affected area.

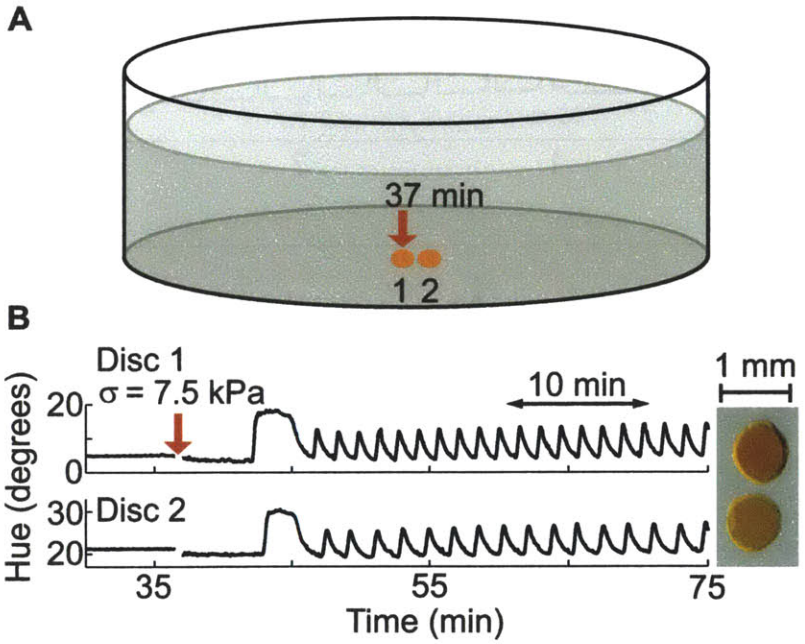

Figure 4-9: BZ gel discs as a pressure sensor with signaling ability. (A) Schematic of experiment indicating the times at which only disc 1 was mechanically compressed (not to scale). (B) Hue of discs 1 and 2, indicating that both discs oscillate in response to mechanical triggering of disc 1. BZ gel discs were 0.7 mm in diameter (0.6 mm thickness and 8.3 mM $Ru(bpy)_3$ catalyst) in BZ solution with initial composition: MA (0.08 M), BrO_3 (0.1 M), and HNO_3 (0.7 M). The gap distances between discs was 0.23 mm. Reproduced from Ref.[3].

4.5 Additional Aspects of Mechanical Triggering

Experiment time affects triggered oscillatory characteristics

In the above sections, mechanical triggering of oscillations was demonstrated in non-oscillating systems. Either NaBr was added to the BZ solution to inhibit oscillations, or oscillations were allowed to naturally die out before compression was applied to the gel. Oscillations may also be mechanically triggered in the absence of inhibitory NaBr and without chemical conditioning in which reactants are depleted over time.

At specific chemical concentrations that are sensitive to initial conditions, a steady-state may be achieved immediately within the BZ gel, even when NaBr is not added to the system. Chapter 3 discussed such sensitive conditions in which the self-oscillatory and steady states appeared to coexist. Specifically, for BZ gels comprising 8.3 mM $Ru(bpy)_3$ and exposed to $\leqslant$ 0.14 M MA, spontaneous oscillations in the gel are not guaranteed. When oscillations are not immediately observed at these chemical conditions, then macroscopic compression can be used to mechanically trigger oscillations.

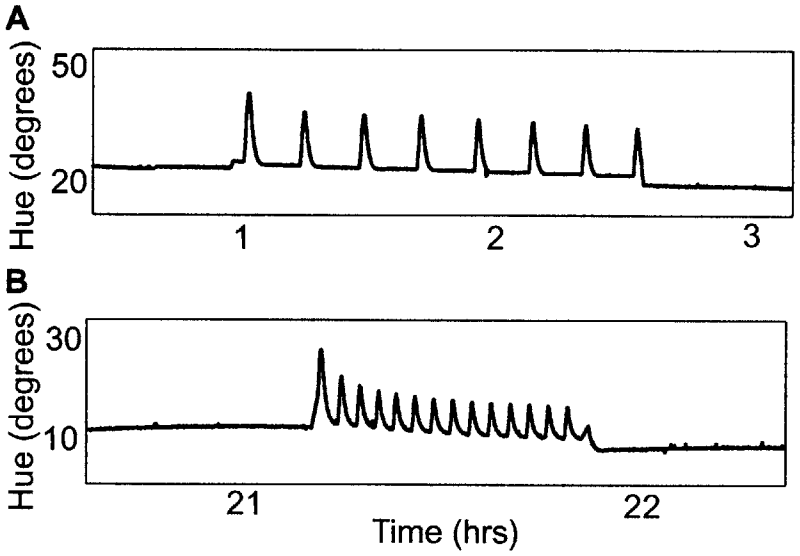

Figure 4-10: Mechanically triggered BZ oscillations at 2 different time points in a 0.8 mm gel. (A) Oscillations triggered after 1 h. (B) Oscillations triggered after 21 h.

Figure 4-10 corresponds to an experiment in which an 0.8 mm diameter gel was submerged in a BZ solution containing 0.14 M MA, 0.1 M $NaBrO_3$, and 0.7 M HNO_3. The gel did not spontaneously self-oscillate and the non-oscillatory state of the gel was recorded for 1 h. After 1 hr, 8.7 kPa of stress was applied to the gel, triggering oscillations every 13.1±0.7 min with an amplitude of 13.3±0.7 degrees. Compression was removed and the gel remained submerged in BZ solution. Approximately 21 h later, the gel was mechanically compressed again (8.7 kPa of stress), and the triggered oscillations were recorded. This time, the gel oscillated every 2.9±0.4 min with an

amplitude of 6.7±0.2 degrees. The decrease in both period and amplitude with increasing immersion time in BZ acid (e.g., 1 h vs 21 h) suggests that the distribution of chemical reactants in solution changed. In other words, the chemical species present in solution continued to react for 21 h even though such reactions did not affect the oscillatory state of the submerged BZ gel. Therefore, the mechanically triggered oscillatory characteristics were affected by the total experiment time for which the BZ gel was submerged in BZ solution.

Gel swelling affects required stress and strain for mechanical resuscitation

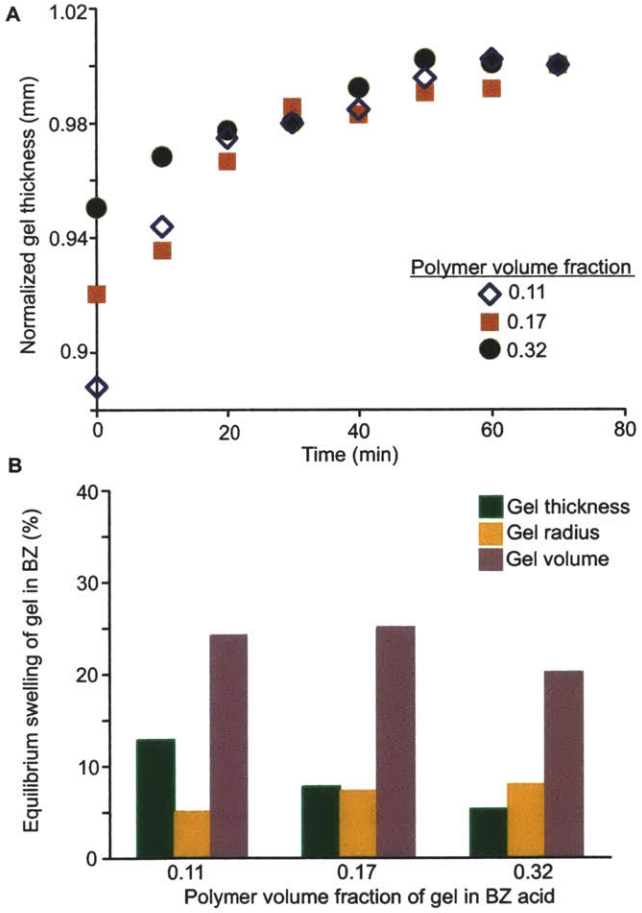

Figure 4-11: Gel swelling in BZ solution after overnight reactant depletion. The disc shaped gels (5 mM $Ru(bpy)_3$) were initially submerged in 10 mL of 0.08 M MA, 0.1 M $NaBrO_3$, and 0.7 M HNO_3. After 21 h of reactant depletion in an enclosed Petri dish, the dish lid was removed from the system. (A) Gel thickness measurements were recorded as a function of time until a plateau in swelling was observed. (B) Equilibrium swelling for gel thickness, radius, and overall gel volume.

Another aspect affecting mechanically triggered oscillations is gel swelling due to chemical concentrations. Whenever oscillations were mechanically re-

suscitated, incubation of gels in BZ acid was performed overnight in a closed Petri dish. Small amounts of bromide species were entrapped in the Petri dish due to this overnight incubation. When the Petri dish lid was removed, then evaporation of small amounts of bromine occurred. As a result, the gel exhibited gradual swelling after the bromine was released from the system. Approximately 1 h after the lid was removed, an equilibrium gel thickness was reached (see Figure 4-11A). Figure 4-11B shows the equilibrium swelling values corresponding to gel thickness, gel radius, and gel volume for gels of varying polymer volume fraction.

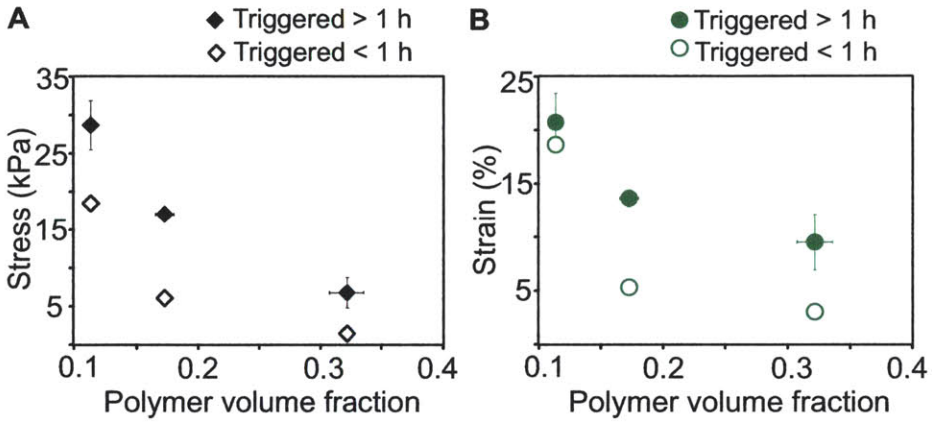

Figure 4-12: Required stress and strain at different time points for mechanically triggered oscillations in BZ gels of varying crosslinking density. (A) Applied stress required to trigger oscillations, measured prior to equilibrium gel swelling (< 1 h) and after equilibrium gel swelling (> 1 h). (B) Induced strain required to trigger oscillations, measured prior to equilibrium gel swelling (< 1 h) and after equilibrium gel swelling (> 1 h).

Because the gradual gel swelling due to bromine release affected the overall gel volume, the required stress and strains for inducing oscillations in the gels also depended on experiment time. Figure 4-12 contains the same data as Figure 4-6 in which the required stress and strain were measured for gels of varying polymer volume fraction. As described previously, the gels were monitored for 1 h prior to applying compression to the gels. Sufficient time (> 1 h) had elapsed in those experiments to ensure that equilibrium swelling of the gel was achieved (see Figure 4-11A). For each polymer volume fraction, a mechanical triggering experiment was performed in which macroscopic compression was applied to the gel < 1 h after removing the Petri dish lid, and equilibrium swelling was not attained. In these experiments, the required stress and induced strain to trigger oscillations was consistently less than the stresses and strains required for triggering oscillations in fully equilibrated gels (see open data points in Figure 4-12). Physically, the gels had not reached their equilibrium thickness, and so, less stress was required to reach the critical thickness of 0.3 mm. These data support the conclusion that triggered BZ oscillations require neither a critical stress nor strain that is independent of ϕ.

Gel modulus in BZ gels of varying polymer volume fraction

The modulus of BZ gels hydrated in water should theoretically increase with crosslinking density and increasing polymer volume fraction.[104] However, the actual modulus of gels submerged in BZ acid varied insignificantly with crosslinking density.

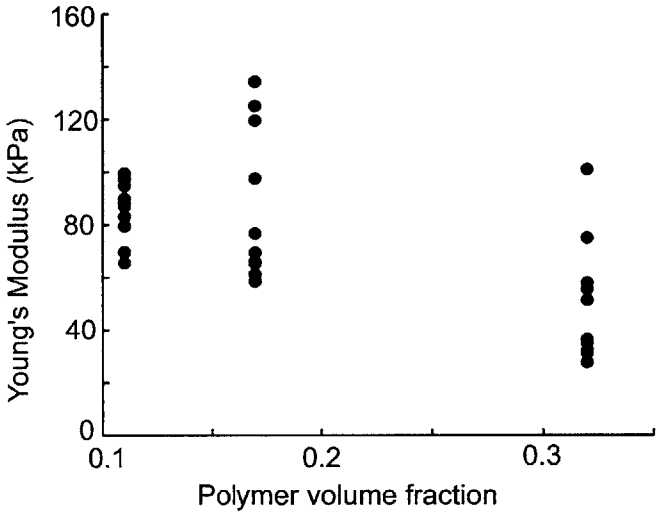

Figure 4-13: Young's elastic modulus measured from triggering experiments. The Young's elastic moduli E of the gels were calculated and compared to their respective polymer volume fractions, measured in BZ acid. The Young's moduli were calculated by quantifying the applied stress divided by the induced strain of the gel.

Figure 4-13 shows the Young's modulus E of the gels measured during the compressive, triggering experiments. The data shows that the gels exhibited similar Young's moduli even though they were synthesized with varying amounts of crosslinker. The Young's modulus was also measured for each gel sample using Atomic Force Microscopy (AFM) indentation. For the polymer volume fractions of 0.11, 0.17, and 0.32, the Young's moduli measured by AFM-enabled nanoindentation were 67.5 $\pm$ 2.9 kPa, 168 $\pm$ 61 kPa, and 46.5 $\pm$ 0.9 kPa, respectively. These values were the averages and standard deviations measured for 10 indentations performed at 3 different areas on each gel sample. The AFM indentations were performed in BZ acid, using a tetrahedral Si probe (OMCL-AC240TS, Olympus), and the spring constant of the cantilever was 2.17 N/m (calibrated prior to indentation experiments). Note that the BZ acid caused partial dissolution of the probe, and the effects of the geometric degradation on the accuracy of the measured Young's modulus was not known. We do not believe the AFM measurements to be accurate for this reason, and note that the findings via this method are also counter-intuitive in that one would expect an increase in gel stiffness with increasing polymer volume fraction. However, it is possible that the gel properties were altered significantly by the acidic conditions of the BZ experiment. Indeed, the gels initially shrink when submerged in BZ solution, which immediately

affects the mechanical properties of the hydrated material. As the actual magnitude of gel Young's modulus was interesting but not critical for understanding the critical conditions of mechanical triggering in BZ gels, the experimental analysis of E was not further refined.

BZ gels cannot be recycled in mechanically triggered experiments

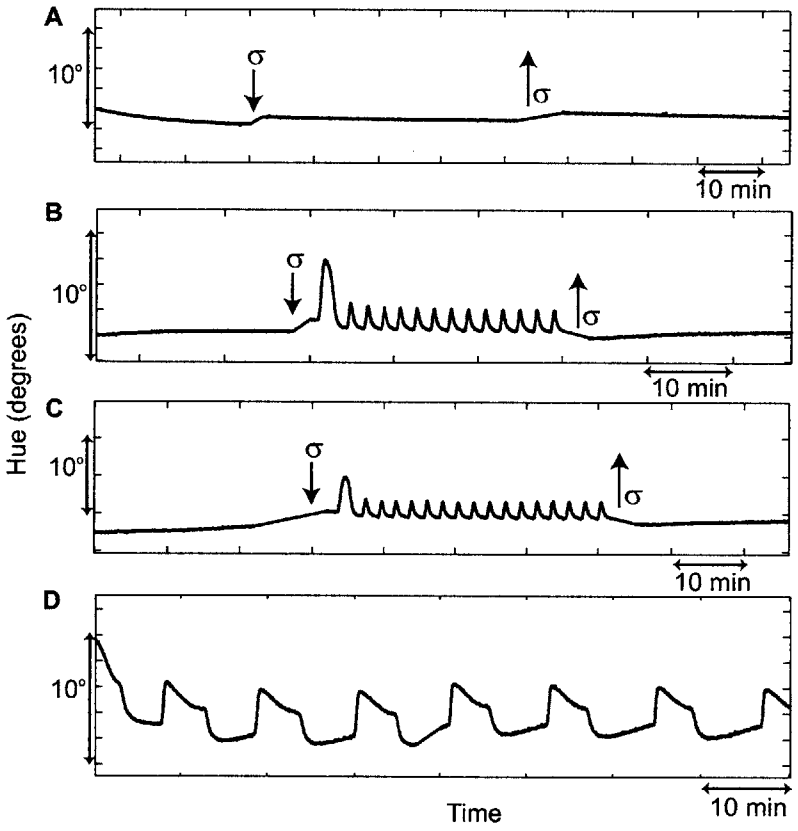

Figure 4-14: Multiple triggering experiments performed on a single BZ gel. (A) Freshly cut BZ gel submerged in 0.2 M MA, 0.1 M $NaBrO_3$, and 0.5 M HNO_3. The gel was compressed with 5 kPa of stress yet failed to oscillate. After the experiment, the gel was submerged in 0.3 M MA, 0.3 M $NaBrO_3$, and 0.9 M HNO_3 for 1 h. (B) After rinsing in water, the gel was submerged in 0.2 M MA, 0.1 M $NaBrO_3$, and 0.5 M HNO_3. Oscillations were triggered when 5 kPa of stress was applied to the gel. (C) After rinsing in water, the experiment in part (B) was repeated. (D) After rinsing in water, the gel was again submerged in the conditions stated in part (B). The gel spontaneously self-oscillated and exhibited an unusual waveform.

In all of the experiments in this chapter, fresh BZ gels were used. Although BZ gels can often be recycled, prolonged exposure to the BZ acidic conditions changes the material composition. Since mechanically triggered experiments are sensitive to chemical conditions, recycled BZ gels may lead to ambiguous experimental results. Shown in Figure 4-14 are a set of multiple experiments performed on the same BZ gels. The data in Figure 4-14A-D

represent experiments in which the same BZ conditions were employed, yet the oscillatory behavior of the gel was often quite different. In part A (first BZ acid exposure), the gel did not oscillate and could not be mechanically triggered to oscillate. Next, the gel was exposed to strong BZ conditions (2nd exposure, see caption for concentrations) to force oscillations (data not recorded). Then, in part B and C (3rd and 4th exposures), the gel did not oscillate but could be mechanically triggered to oscillate. And in part D (5th exposure), the gel spontaneously oscillated while exhibiting an unusual waveform. Between each exposure to BZ acid conditions, the gel was thoroughly rinsed in water at least two times. These results indicate that the oscillatory nature of the BZ gel is permanently affected by prior exposure to BZ solution.

Induction time depends on concentration of NaBr

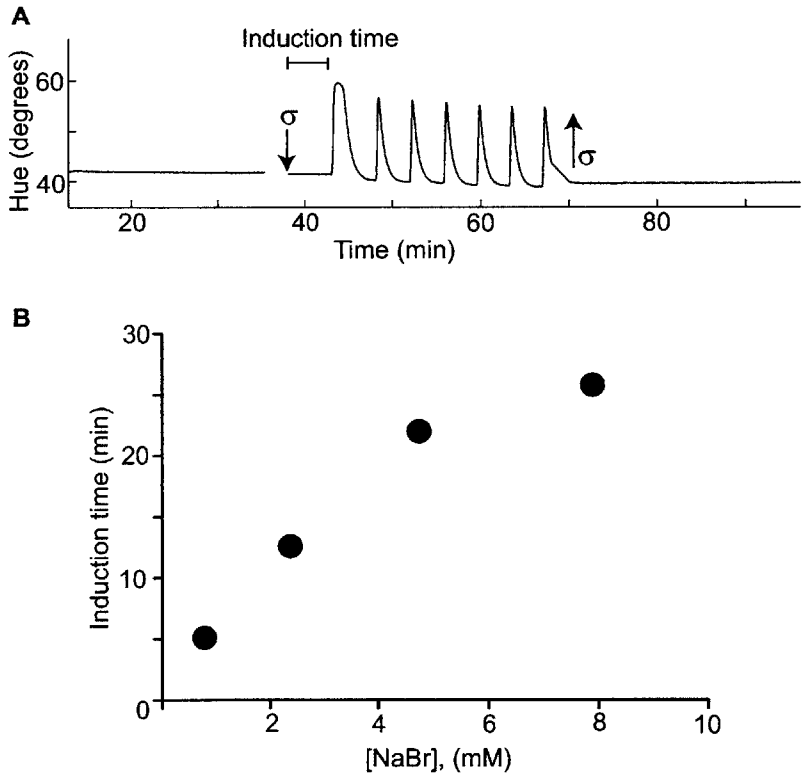

Figure 4-15: Induction time as a function of NaBr concentration for a BZ gel comprising 5 mM $Ru(bpy)_3$. (A) Mechanically triggered oscillations corresponding to [NaBr]=0.8 mM. Induction time is the time elapsed between application of compressive stress (σ) and initiation of hue oscillation. (B) Induction time vs NaBr concentration in mechanically triggered experiments. BZ solution contained MA (0.11 M), $NaBrO_3$ (0.16 M), and HNO_3 (0.7 M)

Induction time is another aspect of mechanically triggered experiments that is affected by the chemical conditions of the system. Here, induction time is defined as the time elapsed between exposure to chemical or mechan-

ical stimuli and the time at which oscillation first begins (see label in Figure 4-15A). In general, as the concentration of NaBr increases, then the induction time for BZ oscillation also increases. Such knowledge of induction time is critical for planning triggering experiments with sufficient timescales regarding the monitoring of oscillations. Additionally, constant NaBr concentration across different experiments ensures expected outcomes and consistent induction times. Note that the data in Figure 4-15 was acquired for a 5 mM $Ru(bpy)_3$ gel, which exhibited different regimes of mechanical responsiness than Figure 4-3.

Pre-compression gel hue does not affect the overall hue amplitude of oscillations

For the mechanically triggered experiments, the hue values of BZ gels were quantified before exposure to BZ acid by analyzing an image of the gel in water. The gel hue was consistently 0.2 degrees. However, note that the hue of the gel in the non-oscillating steady-state, attained after exposure of each gel sample to BZ acid reagents for 20 h, was not identical in separate experiments. This may be related to slight differences in sample diameter and defects at the sample perimeter. The hue after exhausting the BZ self-oscillations was considered a small perturbation, in that while variable hue prior to compression affected the minimum hue (orange color, +2 state) observed in a particular experiment, there was no correlation between minimum hue and the magnitude of the triggered period or amplitude.

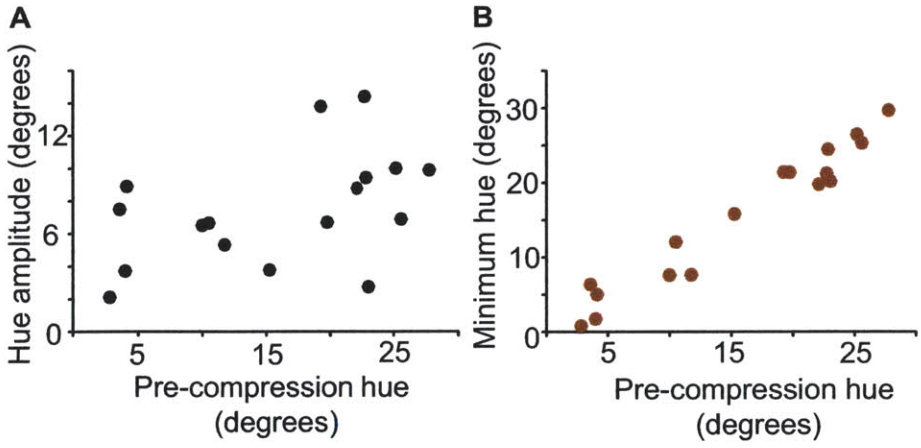

Figure 4-16: Analysis of hue in mechanically triggered BZ oscillations. The minimum hue corresponds to the oscillation trough when the gel is uniformly orange. The pre-compression hue corresponds to the hue of the gel while in BZ acid, before compressive stress is applied to the material, and while the gel is uniformly orange and in a non-oscillatory state.

Figure 4-16A shows that the pre-compression hue varies greatly (0.8 26 degrees), but does not correlate with the mechanically triggered period or amplitude. There was a slight trend with MA concentration because the gels shrink more in higher acid concentrations. As shown in Figure 4-16B, the

minimum hue observed during oscillations is related to pre-compression hue. Therefore the mechanically triggered oscillations are shifted with respect to hue, but the magnitude of oscillations are not not affected by the pre-compression hue.

Conclusions

In summary, these studies have demonstrated that visible chemical reactions within a non-oscillating BZ gel can be mechanically triggered. Due to the design flexibility of polymer systems, the responsive behavior of mechanically triggered oscillations in BZ gels can be tuned in various ways (see Figure 4-17). For instance, the polymer volume fraction the gel can be altered in order to adjust the threshold of stress or strain required to trigger an oscillatory response in the material. This ability to engineer BZ gel systems enables the design of tunable pressure sensors that are triggered at specified stresses. Also shown in Figure 4-17, both mechanically triggered period and amplitude of oscillation may be tuned by adjusting the chemical concentration of malonic acid. Thus, BZ gels can act as tunable pressure sensors that are simultaneously capable of detecting the concentration of MA within a certain range of concentrations.

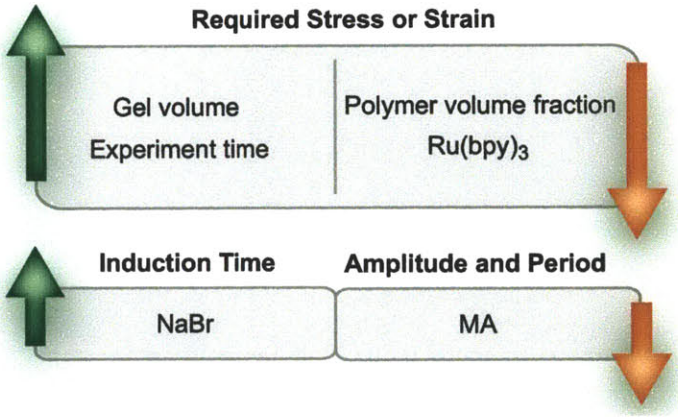

Figure 4-17: Graphic summary of variables affecting the mechanism of mechanically triggered oscillations. The required stress and strain for triggering oscillations increase with increasing gel volume and experiment time, whereas stress and strain decrease with increasing polymer volume fraction and $Ru(bpy)_3$. Induction time increases with increasing NaBr concentration. Amplitude and period of oscillation decrease with increasing MA concentration.

Prior to these results, studies on NIPAAm BZ gels focused on chemically driven mechanical actuation. Thus, our studies on BZ gels represent the first hydrogel system capable of sensing mechanical stimuli and transducing such input into self-regulated chemical oscillations. Such findings motivate future studies that determine how BZ gels react to other forms of mechanical stimuli such as tensile strain or localized impact. Additionally, outside researchers interested in mechanical sensing in polymer gels now have a the-

oretical and practical foundation for studying aspects of mechanical sensing in BZ gels. Very recently, for instance, Shiota et al. determined that compression of self-oscillating NIPAAm BZ gels altered the period of oscillation and actually suppressed oscillation.[105] There, they applied compression to an oscillating gel, whereas we have always applied compression to a non-oscillating gel. Thus, our studies of mechanically triggered oscillations in BZ gels have introduced a new area of potential research on self-oscillating hydrogels.

Since BZ oscillations can be mechanically triggered after extensive depletion of chemical reagents, our findings also have important implications for restoring the functionality and, thus, extending the lifetime of devices that exploit BZ gels. To demonstrate the useful functionality of these gels, we designed BZ gel sensors that detect the location of mechanical impact and have the capacity to transmit chemical signals away from the area of deformation. Note here that the nature of mechanically induced signal propagation in BZ gels was not fully understood. In the next chapter, aspects regarding the mechanism of chemical signaling and the robustness of signal transmission are evaluated. Altogether, these proof-of-principle demonstrations confirm novel functionality and versatility of BZ gels, and we foresee a wide range of new applications with additional heterostructured and compositional complexities that are able to sense mechanical stimuli and respond chemically.

Chapter 5

Chemical Signaling in BZ Gels

Portions of this work are currently under review in PNAS.

5.1 Introduction

Living systems exhibit the hallmark capacity to sense environmental stimuli and transduce such cues into propagating signals. In particular, mechanotransduction – the conversion of mechanical cues to biochemical signals – enables responsive behavior in organisms from touch-me-not plants[31] to nematodes[106], to tissues such as cardiac muscle[30], and to single cells that respond to mechanical deformation via transmission of molecules that propagate biochemical signals to neighboring cells.[107,108] While sensing and signaling are ubiquitous in nature, synthetic materials rarely exhibit complex behaviors such as mechanotransduction coupled to self-regulating signaling networks.[28,109] However, design of such sensing and signaling systems in aqueous environments can enable unique applications that detect mechanical stimuli and simultaneously transmit chemical information that cannot be captured using traditional electrical and audio signaling methods.[110]

The ability to control chemical signaling, or information transport, would enable design of communicative and potentially reconfigurable materials comprising BZ gels. In fact, computational simulations by Kuksenok et al. predict that such synthetic communication among BZ gels may result in coordinated motion, and eventual aggregation of multiple, discrete gels (see Figure 5-1).[7] Such artifical chemotaxis would resemble natural chemotaxis in biological materials such as slime mold, whose individual cells sense cyclic adenosine monophosphate (cAMP) signaling molecules and gradually migrate towards high cAMP concentrations.[111] While synthetic chemotaxis in BZ gels may enable interesting applications, research on chemical signaling among BZ gels is currently lacking.

Although wave propagation among BZ gels has been previously studied, such studies have focused on chemically triggered propagation alone. For instance, Tatyema et al. determined that gel shape can influence the direction of BZ wave propagation in a series of discrete BZ gels. In their study, rows

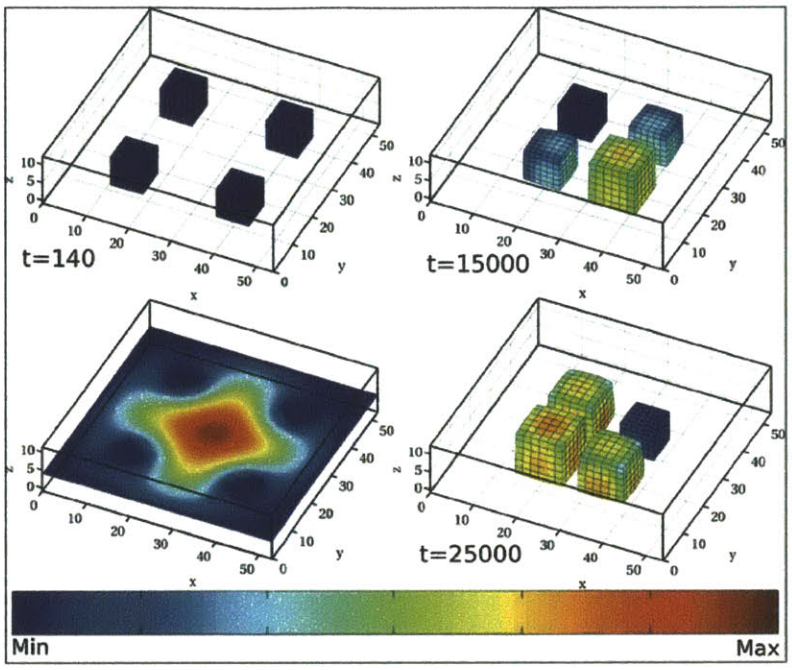

Figure 5-1: Artificial chemotaxis in four discrete BZ gel cubes. Snapshots of the gel cubes are shown at different simulated time points. Color map of the system illustrates accumulation of $HBrO_2$ species at the center of the system. Red corresponds to maximum $HBrO_2$ concentration, and blue corresponds to minimum $HBrO_2$. Adapted from Ref.[7], with permission from The Royal Chemical Society. See reference for simulation details and parameters used.

of either triangular or pentagonal BZ gels were synthesized. Due to an increased likelihood of wave initiation at gel corners (acute angles), directional BZ waves develop according to the geometrical arrangement of the gels.[53] It is important to note that each of the BZ gels in their experiment was exposed to chemical conditions corresponding to spontaneous self-oscillation. If signaling molecules are generally defined as compounds that affect a network of cells or gels in a manner that is distinct from the behavior of the individual unit,[112] then the directional wave propagation observed by Tateyama et al. is not necessarily due to direct chemical signaling. In other words, their system is globally uniform: each BZ gel is fully responsive and capable of generating diffusive, intermediate species via self-oscillation, so the signal amplitude should be retained throughout their system. In this chapter, we aim to understand mechanically induced signaling in locally triggered systems comprising gel discs that are not capable of oscillating unless perturbed or induced to do so.

Recently, synchronization and locally induced coupling in BZ systems have been explored by Seth Fraden at Brandeis University.[74,75] In 2011, Delgado et al. applied local illumination to 100 μm diameter BZ droplets in order to trigger BZ oscillations in specific droplets. Diffusion of Br^- species between discrete droplets then resulted in oscillatory coupling between the

droplets.[75] While such studies are similar to the local triggering we apply to BZ gels in this chapter, several differences exist between their system and ours. These differences include: (1) The system composition and lengthscales are different, (2) The underlying triggering mechanisms are not comparable, and (3) The ultimate goals differ. All of these points of differentiation will be discussed below.

In the previous chapter, chemical signaling was demonstrated between two BZ gel discs that were placed < 1 mm apart. When one of the gel discs was mechanically compressed, chemical signals diffused through aqueous solution and triggered oscillations in the neighboring BZ gel. In the experiment, the BZ gels utilized intermediate reaction species to "communicate" by transmitting information about the chemical and mechanical state of the compressed gel. In this chapter, we elucidate the mechanisms of mechanical triggered chemical signaling in BZ gels and the modes of accessible signal propagation in order to enable design of robust, artificial signaling systems. To our knowledge, this is the first demonstration of synthetic mechanotransductive media capable of spatiotemporal signal propagation.

5.2 Methods

Previously, a pressure sensor with signaling ability was demonstrated in an exhausted BZ gel system. Here, we describe methods for inducing mechanically triggered signal propagation in BZ gel systems that have not undergone reactant depletion over many hours. While such methods are described using an illustrative example in which the BZ gels are cut into the shape of a smile, the experiment protocol is nearly identical for all other mechanically induced signaling experiments described in this chapter.

Figure 5-2A illustrates the experimental setup and components involved in mechanically triggered oscillations and subsequent signal transmission in BZ gels. In this experiment, three BZ gel pieces of mm-scale dimensions were cut from a single larger gel to resemble a smiling face in which the mouth and two eyes were not touching. The gels rested on the bottom of a Petri dish, and were submerged in BZ solution containing chemical reactants (0.1 M MA, 0.16 M BrO_3^-, 0.7 M HNO_3) and inhibitor species (3 mM Br^-). Due to the presence of bromide inhibitor, the gels initially exhibited a non-oscillating steady-state condition in which the color of each gel piece remained uniformly orange-red. After 25 min of monitoring the gels in the non-oscillating state, a macroscopic, compressive stress (4.3 kPa) was applied to the mouth piece by placing a glass slide of known mass on top of the gel, triggering oscillations in the mechanically loaded gel (the smiling mouth). Here, the period of oscillation was 3.6 ± 0.1 min, and the amplitude was $14.3 \pm 0.4°$. Note that reactant depletion was not a prerequisite for observing mechanically triggered oscillations or subsequent chemical signal transmission in this BZ gel system.

When the eye pieces were placed 0.6 mm away from the gel mouth, the uncompressed gels remained in the non-oscillatory state while the compressed gel mouth continued to oscillate (see Figure 5-3). However, when the

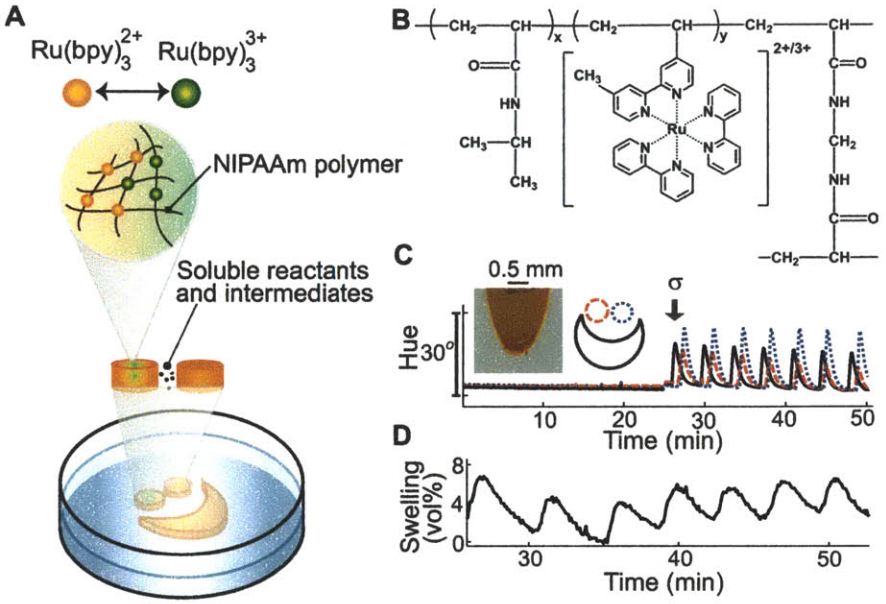

Figure 5-2: Mechanical sensing and signaling in a smiley BZ gel. (A) Schematic illustrating the components involved in mechanical sensing and signaling in BZ gel systems. Not to scale. (B) BZ gel polymer structure comprising N-isopropylacrylamide (NIPAAm), $Ru(bpy)_3$, and MBAAm crosslinker. (C) BZ oscillations in three discrete gels comprising 8.3 mM $Ru(bpy)_3$. After 25 min of monitoring the gels in the uncompressed, non-oscillatory state, compressive stress (σ) was applied to the gel shaped as a smile, inducing oscillations in this gel (solid, black line). The chemical signal propagated next to the left eye (red dashed line) and then the right eye (blue dotted line). (D) Volumetric swelling and shrinking was monitored in the right eye to demonstrate that signal transmission from the mechanically triggered gel (the smile) resulted in mechanical actuation in an adjacent gel (the eye).

gap distances between the mouth and left or right eye were 0.1 mm or 0.2 mm, respectively, oscillations occurred in the mechanically triggered mouth as well as both eyes (see Figure 5-2C). This experiment indicates that activator species produced by BZ oscillations in the mouth piece diffused across the gaps, and induced oscillations in the eye pieces. In other words, the activator species functioned as signaling molecules that altered the behavior of non-deformed gels. Note that the gap distance between the left and right eye was approximately 50 μm, and the right eye was of slightly smaller diameter than the left eye. Since oscillatory amplitude decreases with increasing gel size,[4] the right eye exhibited a larger change in hue than the left eye. We recorded the reversible mechanical swelling of the right eye, and measured an average volumetric swelling of 3.7 $\pm$ 0.5% (see Figure 5-2C). Thus, the mechanical stimulus was sensed and transmitted by one BZ gel and caused mechanical oscillation in the neighboring gels of sufficiently close proximity. This simple design demonstrates that BZ oscillations can be mechanically triggered in metallopolymers, and also that gel-to-gel communication occurs via chemical diffusion through the aqueous media.

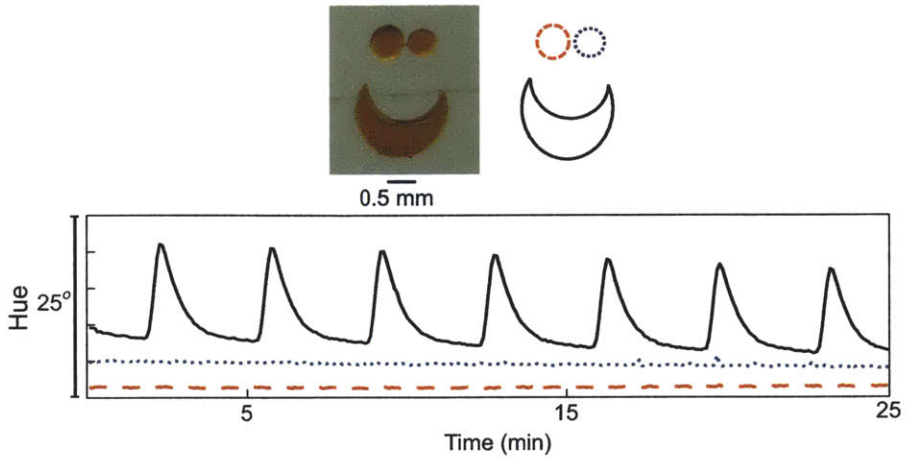

Figure 5-3: BZ gels comprising 8.3 mM $Ru(bpy)_3$. Compressive stress was applied to the gel shaped as a smile, triggering oscillations in this gel (solid, black line). Oscillations did not occur in the left eye (red dashed line) or the right eye (blue dotted line), when the eye pieces were placed 0.6 mm from the mouth piece.

5.3 Critical gap distance in communicating BZ gels

Since the activator species for the BZ reaction ($HBrO_2$) is not a stable chemical species in solution, there exists a critical gap beyond which chemical signaling is not possible. In the experiments described by Figure 5-2, the critical gap distance was approximately 0.2 mm. Since gel shape, specifically gel curvature, has been observed to influence chemical gradients and local accumulation of chemical species,[59] we initially hypothesized that curvature would affect the critical gap distance.

Experiments involving a 1 mm disc gel placed near a larger, crescent shaped BZ gel were performed to determine if curvature influences the critical gap distance (see bottom right image in Figure 5-4). In the experiment, the crescent gel was mechanically compressed, while the small disc was not mechanically stimulated. The critical gap distance was measured by moving the small disc gel increasingly further away from the crescent shaped gel, until oscillations were no longer observed in the disc. To compare the critical gap distances with a similar experiment lacking curvature, the crescent shaped gel was replaced with a similar sized semi-circle gel (image not shown), and the measurements were repeated while the semi-circle gel was mechanically compressed. All gap distances were measured in constant BZ conditions: 0.1 M MA, 0.16 M BrO_3^-, 0.7 M HNO_3, and 3 mM Br^-. We found that curvature had no influence over the critical gap distance. For both the crescent shaped gel and the semi-circle shaped gel, the critical gap distances were around 0.2 mm.

We also tested whether gel size influences the critical gap distance required for BZ gel communication. Here, we hypothesized that the critical gap distance would increase if larger BZ gels were used. In an experiment, a 3 mm diameter BZ gel disc was placed 2 mm away from a 0.7 mm BZ

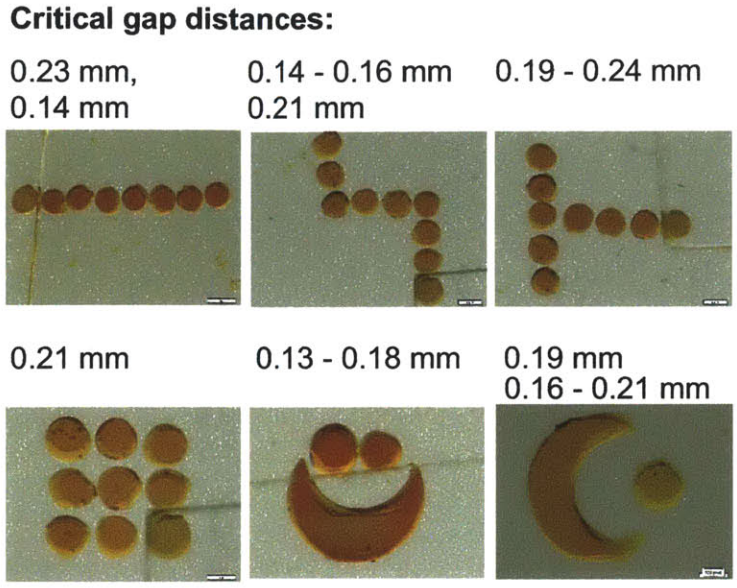

Figure 5-4: Critical gap distances measured for different BZ gel systems of varying geometry and sizes. Note that the scale bars vary in these experiments, but the disc shaped gels are all approximately 1 mm in diameter. All gap distances were measured in constant BZ conditions: 0.1 M MA, 0.16 M BrO_3^-, 0.7 M HNO_3, and 3 mM Br^-.

gel disc (image not shown). The 3 mm diameter disc was mechanically compressed, triggering oscillations, and the smaller gel disc was moved closer to the larger gel, until oscillations were observed in both gels. Again, all gap distances were measured in constant BZ conditions: 0.1 M MA, 0.16 M BrO_3^-, 0.7 M HNO_3, and 3 mM Br^-. We measured a critical gap distance of 0.16 mm, suggesting that gel size does not influence the critical gap distance. Note that chemical concentrations have previously been shown to influence critical gap distances,[53] and so the chemical concentrations in our experiments were held constant. Figure 5-4 summarizes some of the critical gap distances measured in mechanically triggered BZ signaling experiments. Altogether, the critical gap distances were consistently around 0.2 mm, and did not change according to gel size or gel shape.

5.4 Mechanically induced directionality in a series of BZ discs

While diffusion-mediated coupling of independent *self-oscillators* has been explored by Delgado et al.[75] and Tateyama et al.[53] in systems triggered by light or chemistry, coupling between mechanical stimuli and chemical oscillations has not been extensively explored in BZ gel systems. One could hypothesize that the mechanically induced signal would attenuate with increasing distance from the site of triggering: as noted previously, the BZ

reaction generates both an activator ($HBrO_2$) and inhibitor (Br^-). Since $HBrO_2$ dissociates in acidic liquid[113], it is plausible that the concentration of this activator species would decrease too readily with distance from the triggered site to sustain high-amplitude signal propagation. Shown in Figure 5-5 are two possible scenarios in which $HBrO_2$ is generated within the mechanically triggered gel and then diffuses (dotted lines) towards neighboring gels. Shown in Figure 5-5A is a schematic representation of $HBrO_2$ diffusing towards neighboring gels and activating $HBrO_2$ generation within those gel discs. Shown in Figure 5-5B is a schematic representation of an alternative mechanism in which the concentration of $HBrO_2$ decreases with increasing distance from the site of mechanical triggering. In this latter mechanism, signal attenuation would be expected.

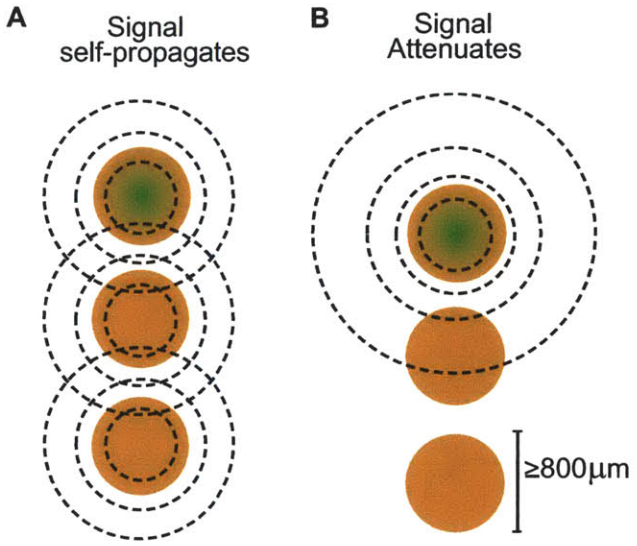

Figure 5-5: Schematic of two possible mechanisms for mechanically induced signal transmission in BZ gels. $HBrO_2$ (dotted lines) is generated in the mechanically triggered disc, and (A) activates $HBrO_2$ generation in neighboring gels, or (B) $HBrO_2$ concentration (and signal amplitude) attenuates with increasing distance from the site of triggering.

To test both hypotheses, we arranged eight BZ gel discs in a straight line. The diameter of each disc d_{gel} was 0.8 - 0.9 mm, and the shortest distance between two neighboring gel discs was given by x_{gap} (see schematic in Figure 5-6A). Discs were submerged in a solution containing BZ reactants and inhibitor species. After monitoring the discs to ensure that each gel was in a non-oscillatory state, disc 1 was compressed, triggering oscillations in this deformed gel. As expected, the mechanically triggered signal was transmitted from disc 1 to disc 2, inducing oscillations in the non-deformed, neighboring gel. As mentioned previously, both Br^- species and $HBrO_2$ species were generated within the gel by the BZ reaction. Due to the inhibitory nature of Br^-, chemical signaling between neighboring BZ gels must have occured via diffusion of $HBrO_2$.

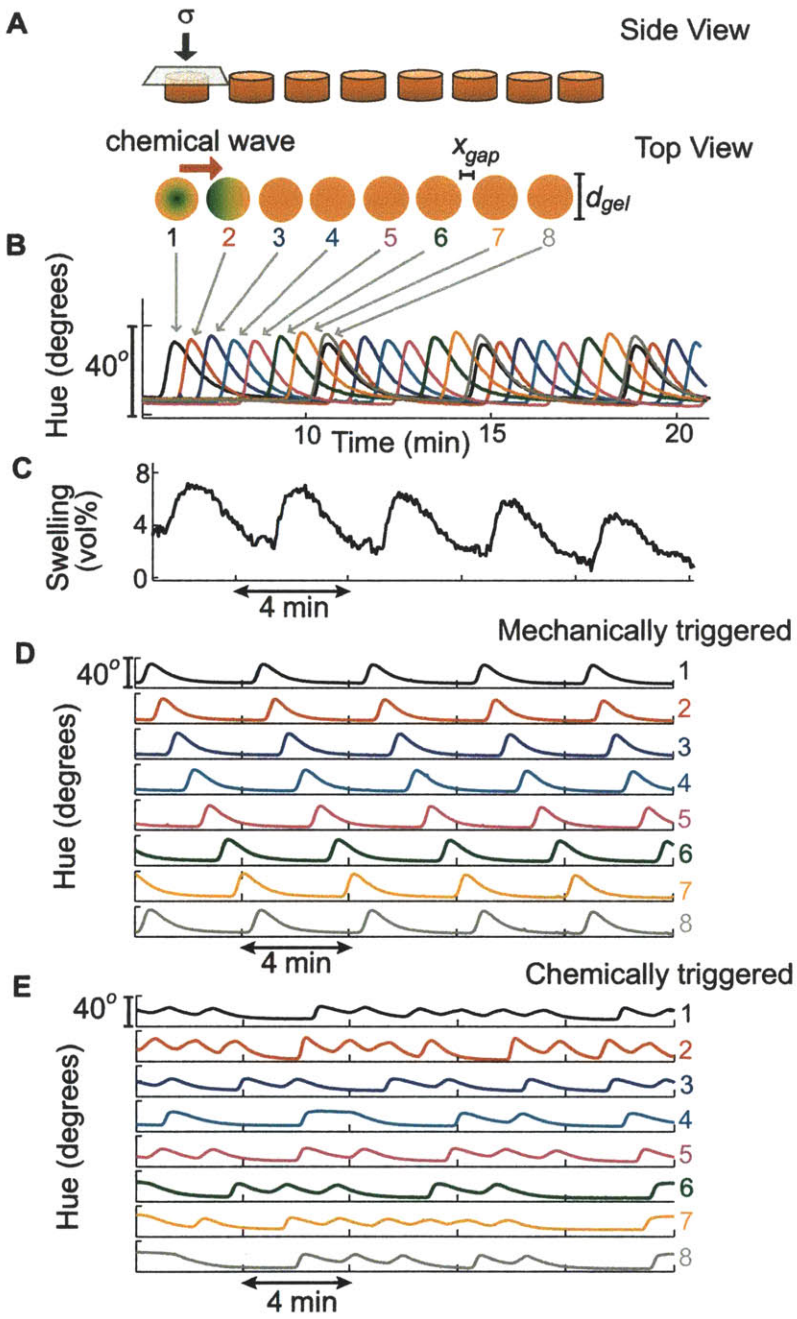

Figure 5-6: Gel to gel signaling in a row of eight BZ gel discs. (A) Schematic of experiment showing the side view and top view of 8 BZ gel discs when stress (σ) is applied to gel 1. (B) Hue of gels 1-8, indicating that all 8 discs oscillate while gel 1 is compressed. Note that the signal amplitude does not decay along the row of discs. (C) Swelling and shrinking measured in disc 3 while disc 1 is compressed. (D) Hue of gels 1-8 while disc 1 is compressed, demonstrating that the chemical signal travels in a consistent direction from disc 1 to disc 8. (E) Hue of eight discrete BZ gels, measured while all discs exhibited spontaneous oscillation in the absence of mechanical triggering.

Interestingly, the amplitude of oscillation in disc 1 (24°) was comparable to the amplitude of disc 8 (25°), indicating that the signal amplitude was not sensitive to distance travelled away from the triggered site. (see Figure 5-6B). Thus, the signaling molecules ($HBrO_2$) generated and released by the mechanically triggered gel (disc 1) not only activated oscillations in the nearest-neighbor (disc 2), but also induced $HBrO_2$ generation and sequential activation of BZ oscillations along the entire array.

Such positive feedback is analogous to biological signaling in which release of Ca^{2+} results in pulsatile signaling among cells.[114] For the experiment shown in Figure 5-6B, signal transmission was conveyed by both periodic changes in color and in gel volume, which both correlate directly with the redox state of the metal catalyst. In other words, the external mechanical cue applied to disc 1 induced oscillatory mechanical swelling in neighboring discs. As shown in Fig.5-6C, the average volumetric swelling in disc 3 was $3.5 \pm 0.4\%$. In the previous chapter, signal transmission in BZ gel pressure sensors resulted in lower amplitude oscillations ($< 10°$), and thus the gels were not capable of undergoing periodic swelling and deswelling.[3] In constrast, relatively high reactant concentrations were employed in Figures 5-2 and 5-6, corresponding to relatively large amplitudes of oscillation and periodic gel swelling. For the above conditions, the gap distance between discs varied from 54 - 136 μm, and gap distances beyond 200 μm were too large for signal propagation. Thus, the inhibitory chemical conditions prohibited typical BZ self-oscillation in all gel discs, and oscillation was only achieved in gel discs 2 - 8 due to the unique transmission of $HBrO_2$ signaling molecules that carried information about the mechanical and chemical state of disc 1.

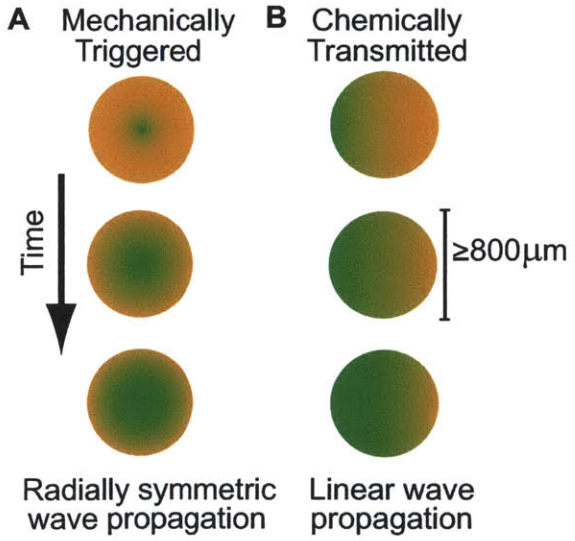

Figure 5-7: Schematic of wave propagation in BZ gels. (A) Mechanically triggered waves are characterized by wave initiation at the center of the gel. (B) Oscillations resulting from chemical signaling are characterized by wave propagation that starts on one side of the gel, and travels to the opposite side.

Figure 5-6D shows hue as a function of time for each individual BZ gel

disc, to illustrate that the direction of the induced chemical wave proceeded from left to right (disc 1 to disc 8). Within the linear array, only one gel disc reached its peak hue at a given instant, and peak oscillation was consistently observed in disc i following peak oscillation observed in disc i-1. Visually, the chemical wave triggered in disc 1 originated at the center of the disc and propagated outward to the edges of the gel (see Figure 5-7A). In contrast, the chemical waves in discs 2 - 8 began at the left side of the gel and travelled to the right side of the gel (see Figure 5-7B). Therefore it is possible to differentiate between mechanically triggered BZ gels and signal activated BZ gels, by comparing the individual BZ gel wave patterns.

It is important to note that wave direction can also be predetermined by the shape of the gel. Specifically, the likelihood of wave initiation is greater at gel corners characterized by acute angles versus obtuse angles, and asymmetric shape effects may result in directional bias.[53] In contrast, the BZ gels shown in Figure 5-6 were radially symmetric, and the gel shape did not influence the direction of wave propagation. Figure 5-6E illustrates a control experiment in which compressive stress was not used to trigger oscillations. In that experiment, the sizes and arrangement of the gels were consistent with those in the mechanically triggered array of Figure 5-6A-D. However, in order to observe BZ waves in the absence of mechanical triggering, the gel discs were submerged in a solution containing BZ reactants and lacking Br^- inhibitor, and such conditions corresponded to chemical triggering of spontaneous oscillations. The results shown in Fig. 5-6E indicate no temporal order to the chemically triggered oscillations in a linear array of gels, and the chemical waves did not propagate in a consistent direction. Peak hue was observed in more than one gel at a given moment in time, and any one of the eight gels exhibited chemical waves that originated at the disc center and propagated outwards. Similarly, any one of the eight gels exhibited chemical waves that travelled either from left to right or right to left; there was neither spatiotemporal order nor synchronization in oscillations among these gels. Therefore, the combination of a chemical inhibitor species and a mechanical stimulus induced directionality of signal propagation in a series of BZ gels that would otherwise lack directional specificity.

The results presented in Figure 5-6 share similarities with Delgado et al.'s work on 1-D arrays of BZ droplets.[75] However, several important differences exist between our system of BZ gels and their system of BZ droplets. The first main difference between Delgado et al.'s system and ours is that the former consists of BZ droplets rather than BZ gels, and one cannot assume that liquid-liquid systems behave the same as solid-liquid systems. Furthermore, the scale of our system is 5-10X larger than Delgado et al.'s droplet system. Certainly, such disparity in lengthscales would affect diffusion of intermediate species, and overall system behavior. Perhaps the most important difference between Delgado et al.'s system and ours is that the underlying triggering mechanisms are different: oscillations in their system were initiated using illumination rather than localized, mechanical compression. And while photochemical coupling between light and BZ oscillations may be well understood in BZ solutions and now droplets,[75] mechanochemical coupling between mechanical stimuli and oscillatory signaling has not

been extensively explored in BZ systems. In other physical systems, light and mechanics are treated quite separately, and it is not acceptable to assume that illumination and compressive stress affect materials with comparable underlying mechanisms. Finally, the goals of Delgado et al.'s studies were to determine conditions resulting in attractors.[75] Simply put, their published work did not demonstrate signal turning, splitting, or annihilation. In contrast, our studies focus on signal propagation over long ranges and complex trajectories. In our system, a single (mechanically compressed) gel acts as the stationary "source of the signal, while the neighboring gels remain uncompressed.

5.5 Signal transmission over complex trajectories

5.5.1 Signaling around bends

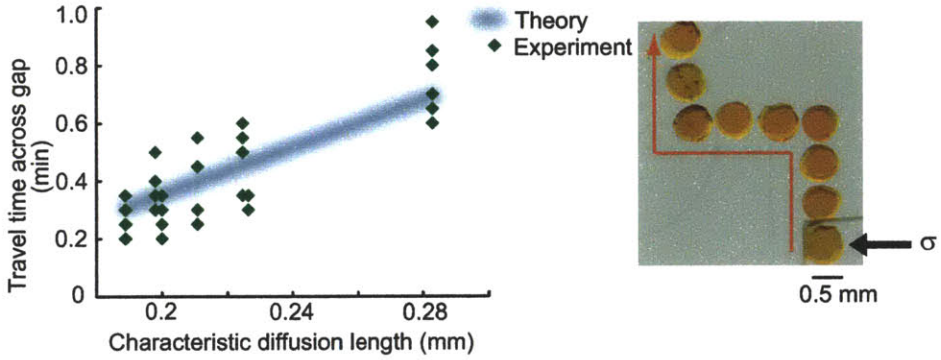

Figure 5-8: Theoretical and experimental diffusion times between BZ gel discs arranged with 2 bends (left). There was no time delay when the BZ signal changed directions after bends. Snapshot of experiment (right).

To investigate signal transmission along complex trajectories, we designed BZ systems capable of signaling around bends. Here, we hypothesized that signal amplitude would not decay, but would experience a time delay associated with switching directions. Note that past observations of nonlinear signal propagation were performed in simulations and architectureless BZ substrates in solution, in which bending and splitting was achieved at locations of illumination impurities,[115,116] and thus lacked mechanotransduction capabilities. As shown in Figure 5-8, nine BZ gels were configured to form two right-angle bends. The gel discs were spaced no more than 140 μm apart, and were submerged in BZ reactants and inhibitors, as described previously. The bottom gel was mechanically triggered to induce oscillations, and the signal travelled upwards along the linear array, as expected. At the bend in the series, the signal changed directions and subsequently travelled from right to left. At the second bend in the series, the signal again changed directions and travelled upwards. Similar to the response of the linear array shown in Figure 5-6B, there was no apparent decay in the signal amplitude as the chemical wave travelled away from the site of mechanical triggering.

Presumably, diffusion of $HBrO_2$ from the gel occurred uniformly and in all directions, allowing for signal transmission around bends.

In order to determine whether time delays resulted from travelling around bends, we compared the theoretical and experimental diffusion time of $HBrO_2$ across gap distances (see Figure 5-8). First, we calculated the theoretical diffusion time (defined earlier by Eqn. 3.1: $\tau = L^2/D$). Previously, we determined the theoretical diffusion time of reactant species through the BZ gel. Here, we were interested in calculating the theoretical diffusion time of chemical species through aqueous solution. Thus, the characteristic diffusion length, L, representing Figure 5-8, was given by the average linear distance between gel edges, and D was the diffusion coefficient for $HBrO_2$. We calculated a range of diffusion times by employing the actual gap distances and gel diameters from the experiment, and we assumed that the diffusion coefficient of $HBrO_2$ was that for small molecules through aqueous solution (1.8 - 2.0 x 10^{-5} cm^2/sec).[117]

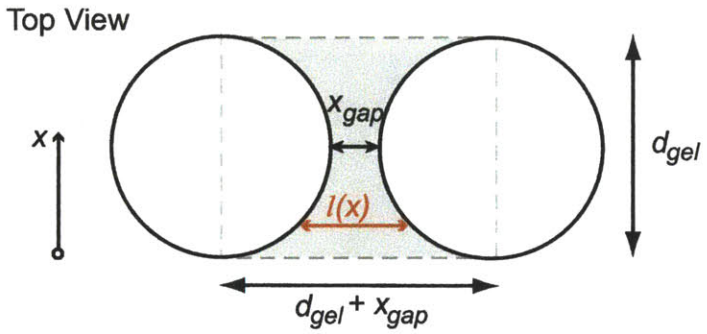

Figure 5-9: Diagram of two neighboring BZ gel discs.

For BZ gels cut in a disc shape, the average linear distance between gels (L) is given by the following equation (also see Figure 5-9):

$$L = \frac{1}{d_{gel}} \int_0^d l(x)dx \tag{5.1}$$

where l depends on the x-axis location, and is indicated by the red line in Figure 5-9. To simplify the calculation, the shaded area in Figure 5-9 can be determined using geometric relationships. Let us call the shaded area A, and the area of the rectangle bounded by the dashed line B. Assuming that the two discs are of the same diameter, then

$$A = B - \pi(\frac{d_{gel}}{2})^2 \tag{5.2}$$

$$L = \frac{(d_{gel} + x_{gap})d_{gel} - \pi(\frac{d_{gel}}{2})^2}{d_{gel}} \tag{5.3}$$

$$L = d_{gel} + x_{gap} - \frac{\pi}{4}d_{gel} \tag{5.4}$$

To quantify the observed travel times across gaps, we quantified the time elapsed between color change in a given gel and subsequent color change in its receiving, neighboring gel. There were eight gaps between the nine gel discs, and we measured travel times across each of these gaps for six distinct chemical waves. We observed no apparent time delay associated with travelling around bends, and the experimental diffusion times were comparable to the theoretical diffusion times (Figure 5-8). Discrepancies between theory and experiment were attributed to imperfect disc geometry and manual error in measuring d_{gel} and x_{gap}, and the apparent width in the theoretical response is due to the uncertainty in the value of the diffusion coefficient for small molecules through aqueous solution. As expected, signals took longer to travel across large gaps versus short gaps. Such results quantitatively confirm that the mechanism of gel to gel communication is governed by diffusion of $HBrO_2$ species, and Figure 5-8 illustrates that there was no time delay associated with signal transmission around bends.

5.5.2 Signal splitting

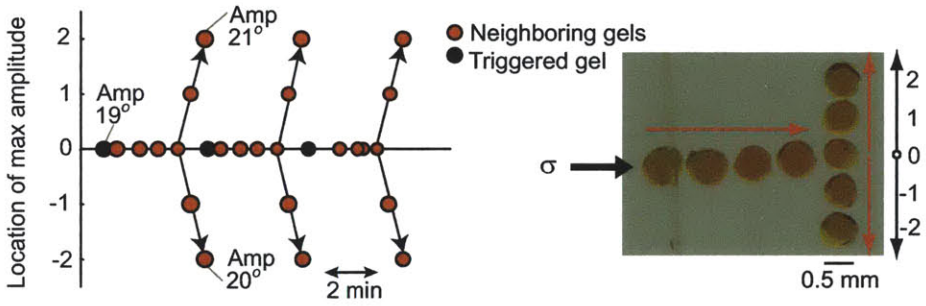

Figure 5-10: Bubble diagram for a BZ system exhibiting signal splitting. The location of the maximum amplitude is graphed as a function of time, with relative bubble diameter corresponding to the hue amplitude. The BZ signal can split into two opposite directions and that signal amplitude was unaffected by splitting. Snapshot of the experiment and relevant coordinates (right).

Next, we determined whether mechanically triggered BZ waves could split into two signals travelling in opposite directions. Shown in Figure 5-10, we arranged nine BZ gel discs in the shape of a T. Again, the gels were submerged in BZ reactants and inhibitors. As shown in the image, the y-axis was defined such that stress was applied to the leftmost gel at y=0. The chemical signal travelled along y=0 until it reached the fifth gel. At this point, the signal could have travelled in the positive y-direction, in the negative y-direction, or the signal could have split and travelled in both positive and negative y-directions. We observed that the signal did indeed split, and travelled in both the positive and negative y-directions.

These results were quantified by plotting the y-axis location of the maximum amplitude versus time (Figure 5-10). Here, the size of each data point indicates the relative hue amplitude of oscillation. Prior to running the ex-

periment, we hypothesized that the signal amplitude would divide in half after signal splitting. Physically, if half of the $HBrO_2$ molecules diffuse in the direction of one branch, and the remaining $HBrO_2$ molecules diffuse in the direction of the opposite branch, then the signal amplitudes might be 50% of the starting amplitude. Interestingly, signal amplitude was not affected by signal splitting, and the amplitudes at y=±2 were comparable to the amplitude of oscillation observed in the triggered gel. By engineering two branches of BZ gels connected at a BZ gel node, the signal output was essentially doubled in this experiment. These observations suggest that the threshold of total $HBrO_2$ molecules required for sequential activation of oscillations in neighboring BZ gels is much lower than what was achieved at our experimental conditions. In summary, we have demonstrated the robustness of signaling in BZ gels by showing that a chemical signal that is initiated at one distant site can propagate and split into two opposite directions without loss of signal amplitude.

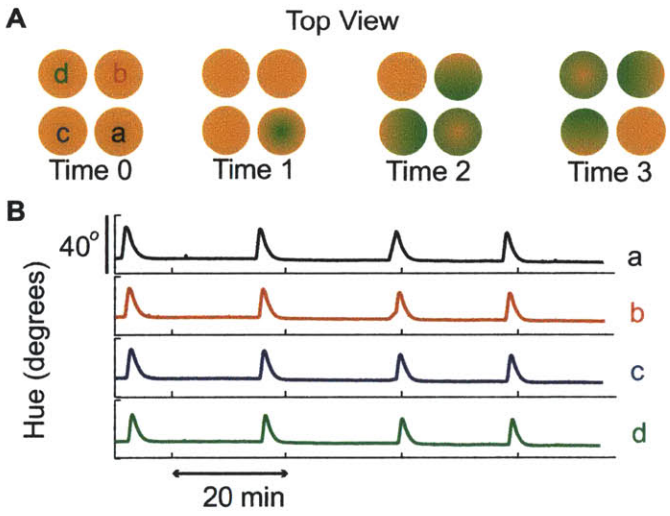

Figure 5-11: Mechanically triggered oscillations and signal propagation in BZ gels. (A) Schematic of experiment indicating sequential order of wave propagation (shown in green) in gels a-d. Indicated times are unit less and do not reflect the actual period of oscillation or wave velocity. (B) Hue of gels a-d, demonstrating actual wave propagation in gels. Due to the long period of oscillation, it is difficult to see that gel a did indeed oscillate first, followed seconds later by gels b and c. Gel d oscillated seconds after gels b and c.

Note that the signal output can be immediately doubled by mechanically triggering a "node" BZ gel that has two neighboring gels. Figure 5-11 shows that when gels are placed next to a mechanically triggered gel, wave propagation occurs in all of the neighboring discs, provided that the discs are within the critical gap distance. Here, four gel discs (of 0.7-0.8 mm diameter) were arranged in a 2 x 2 matrix with nearest-neighbor edge spacing <0.2 mm. As described previously, macroscopic compression was applied to only one BZ gel to observe wave propagation in neighboring gels. All 4 discs exhibited BZ oscillations in a temporally delayed fashion that depended on distance

from the compressed gel. Color change was sequential, occurring first in the triggered gel (labeled a), and then followed by propagation to the bottom left and top right gels (b and c, the nearest neighbors), and then finally ending with propagation to the top left gel (d, the next-nearest neighbor). This sequential propagation shows that the signaling did not occur directly across the 0.52 mm distance between gels a and d. A 3 x 3 matrix of gels were also tested (see image in Figure 5-4), and similar results were obtained.

5.5.3 Signal collision

Finally, we analyzed and observed the outcomes of engineered signal collision in a single BZ gel. Here, we cut a BZ gel into the shape of a ring (see Figure 5-12 for snapshot and relevant coordinates).[1] The gel was submerged in BZ reactants and inhibitors as described previously. Mechanical stress was applied to the gel at a specific site on the ring, designated by the coordinates of $\pm 180°$, as indicated in the image (Figure 5-12). The mechanically induced chemical wave travelled both clockwise (cw) and counterclockwise (ccw), away from the site of triggering. As expected, the signals travelled at similar velocities and collided at 0°. At this point, the signals may have potentially annhilated one other, passed through each other without attenuation, or combined to produce an amplified signal. We observed that the signals did not pass through each other and did not continue to propagate after collision. Instead, the signals terminated at 0°, which was consistent with some of the past observations of signal propagation in BZ systems.[115,116]

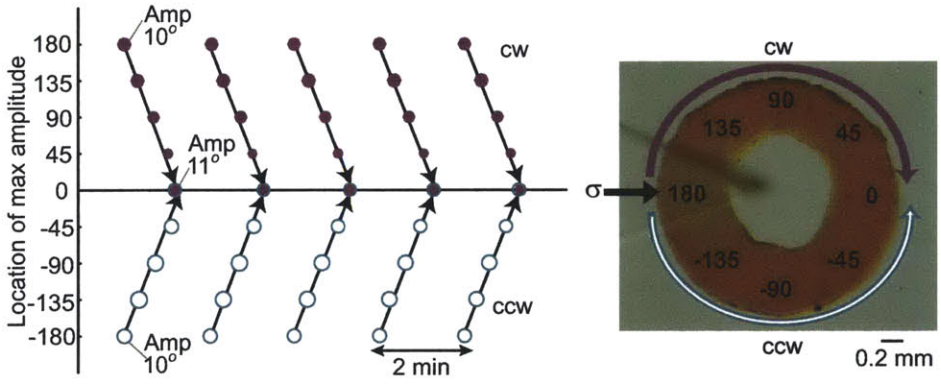

Figure 5-12: Bubble diagram for a BZ gel ring demonstrating signal collision. The location of the maximum amplitude is graphed as a function of time, with relative bubble diameter corresponding to the hue amplitude. The BZ signal amplitude did not significantly decay or amplify at the location of signal collision. Note that the collision point was the location of signal termination. Snapshot of the experiment and relevant coordinates (right).

To quantify our results, we graphed the location of the maximum hue

[1] A line of five BZ discs was also prepared to study signal collision when the end gels were mechanically triggered. It was too difficult to coordinate gap spacing and gel size such that wave collision was consistent in the third gel. Thus, a BZ gel ring was prepared instead.

amplitude versus time. Again, the size of each data point indicates the relative amplitude of oscillation. As shown in Figure 5-12, the amplitude of oscillation at 0° was comparable to the amplitude of the signal originating at ±180°. Note that the amplitude of oscillation was limited by the total amount of $Ru(bpy)_3$ molecules in the gel. As noted in previous chapters, a high amplitude of oscillation is observed when a relatively large number of $Ru(bpy)_3$ molecules oscillate simultaneously. For this type of BZ gel comprising 8.3 mM of $Ru(bpy)_3$ catalyst, the largest amplitude of oscillation previously reported was 29°.[4] In contrast, the amplitude of oscillation at ±180° in the present experiment was only 10°. Such disparity suggested that only a fraction of the total $Ru(bpy)_3$ catalyst molecules were oscillating in Figure 5-12. We initially hypothesized that increased amounts of $HBrO_2$ diffusing through the gel from both clockwise and counterclockwise directions would result in an amplified signal at 0°, in which a higher fraction of $Ru(bpy)_3$ catalyst molecules become oxidized. However, it was clear that signal amplification did not occur, indicating that the system was limited by inhibitory chemical conditions.

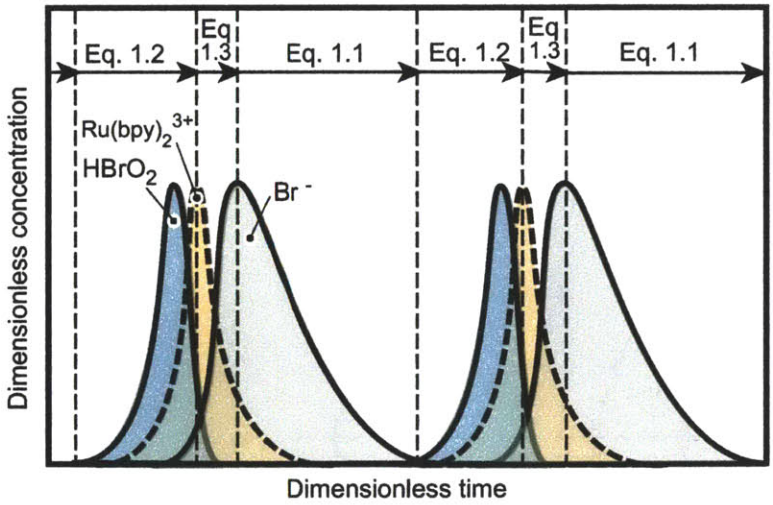

Figure 5-13: Predicted concentration profiles for $HBrO_2$, $Ru(bpy)_3$, and Br^-. Adapted with permission from Ref.[8]. Copyright 1999, American Chemical Society. See reference for model parameters and details.

The results from Figure 5-12 may be understood by reviewing the BZ chemistry within the context of reaction-diffusion systems. Figure 5-13 shows the theoretical concentration profiles for $HBrO_2$, Br^-, and $Ru(bpy)_3$, and illustrates how these profiles are related to the three main reaction steps given by Equations 1.1 - 1.3. Recall that oxidation of $Ru(bpy)_3$ occurs according to Equation 1.2. Following peak concentration of oxidized $Ru(bpy)_3$, Equation 1.3 proceeds, in which $Ru(bpy)_3$ is reduced and Br^- is produced. Subsequent oscillation (Equation 1.2) cannot proceed until the concentration of Br^- decreases (see Figure 5-13). Although the BZ gel ring in Figure 5-12 is uniformly exposed to 3 mM Br^-, the $HBrO_2$ generated within the gel by the BZ reaction (Equation 1.2) is produced in concentrations sufficient to over-

come Br^- present in the surrounding aqueous solution. However, because additional Br^- molecules are produced inside the gel as a consequence of $Ru(bpy)_3$ catalyst reduction (Equation 1.3), it is plausible that the cumulative Br^- concentration precluded further signal propagation (see Figure 5-13), until sufficient time elapsed for the diffusion of exiting Br^- molecules from the gel. For these reasons, the BZ signals were unable to cross paths, and collision resulted in signal annihilation.

The observations from Figure 5-12 are not in agreement with the steady-state approximation that $d[Br^-]/dt \approx 0$, which is an assumption often made in BZ theory.[5,118] In particular, we observed that the inhibitor Br^- species appears to play a significant role in the mechanism of gel signaling and mechanical triggering. Furthermore, it is evident that the concentration of Br^- oscillates with a period comparable to the period of oscillation describing $Ru(bpy)_3$ concentration. The concentration of metal catalyst is not neglected when modeling BZ oscillations and, by the same token, the concentration of Br^- should also not be disregarded. Therefore, analytical or numerical predictions that include a steady-state approximation which neglects $d[Br^-]/dt$ would not be expected to predict our findings of signal extinction upon collision of propagating BZ waves within a BZ gel.

5.6 BZ signaling does not lead to auto-chemotaxis

Last, we test hypotheses regarding artifical chemotaxis in BZ gels. Such hypotheses were presented in the beginning of this chapter (see Figure 5-1). As a reminder, computational simulations predicted that oscillating BZ gels would self-aggregate as discrete gels migrate towards the highest concentration of BZ activator species ($HBrO_2$). The computational predictions assume that motion of the gel would be caused by the cyclic swelling and de-swelling of the gels due to the BZ reaction, and that $HBrO_2$ species would accumulate in high concentrations at regions between discrete gels. Such hypotheses were tested by cutting either cubic or disc shaped BZ gels (see images in Figure 5-14A-B), and submerging four of these gels in BZ solution. Five experiments using either gel discs or gel rectangles were performed, and timelapse microscopy was used to record the oscillations of each BZ gel and any motion or communication among the gels.

Figure 5-14C shows that the BZ reaction induced high amplitude oscillations, causing the gels to swell and shrink periodically (swelling data not shown). While the gels were capable of motion, we found that the individual pieces did not migrate towards each other, or exhibit any semblance of auto-chemotaxis. To quantify the results, the gap distances separating two gel pieces were manually measured throughout the experiments, and Figure 5-14D-E shows the gap distances for an experiment comprising four rectangular gels arranged as in Figure 5-14B. In Figure 5-14D, the gap distances separating the two lower gels are shown in red, and the gap distances separating the two upper gels are shown in black. For both sets of data, the closed data points represent gap distances measured while the gels were in the reduced, shrunken states, and the open data points represent gap distances

measured while the gels were in the oxidized, swollen states.

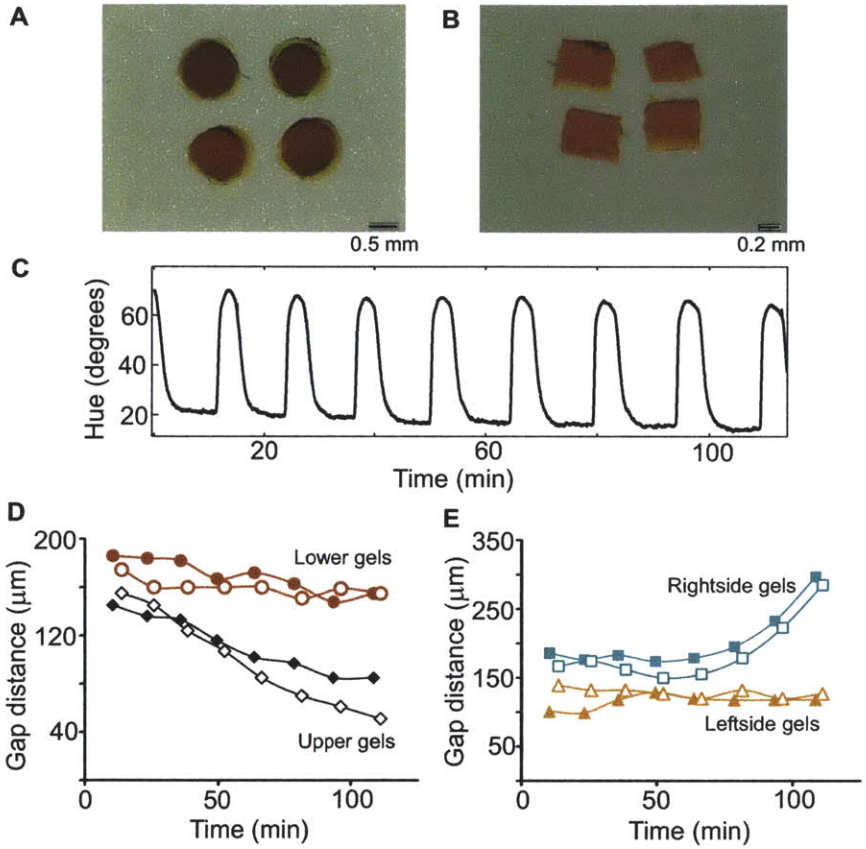

Figure 5-14: (A) Image of an experiment comprising four BZ gel discs of 1 mm diameter. (B) Image of an experiment comprising four rectangular gels of 0.4 - 0.6 mm edge lengths. (C) Oscillations measured in a single BZ gel while submerged in the experimental conditions (0.08 M MA, 0.1 M $NaBrO_3$, and 0.7 - 1.0 M HNO_3. (D) Measured gap distances over time for 4 rectangular BZ gels. Red data points represent gap distances separating the two lower gels, and black data points represent gap distances between the two upper gels. (E) Within the same experiment as part C, gap distances were measured for the gels on the right side (blue data) and for the gels on the left side (orange data). For both D and E, the closed data points represent measurements taken while the gels were in the fully reduced states, and the open data points represent measurements taken while the gels were in the fully oxidized states.

Note here that the gap distance separating two gels is generally smaller when both of the gels are in the oxidized, swollen state. The gap distance separating the two upper gels in Figure 5-14D decreased by 60 - 104 μm after 100 min of oscillation, and such results suggest that the gap distance separating the gel edges decreases over time. However, because this "aggregation" was an isolated incident that was not observed between any two gels throughout all five experiments, such results are more plausibly attributed to random motion. In fact, Figure 5-14E plots the gap distances separating the gels on the right side (blue data points) and the gels on the left

side (orange data points). The gels on the right side actually drifted apart, rather than aggregating towards each other. Thus, while some of the gels appeared to drift towards each other, other sets of gels appeared to drift apart. In summary, BZ chemotaxis among discrete gels was not observed in our experiments.

Although auto-chemotaxis of BZ gels represents an intriguing concept with potential applications for self-reinforcing or reconfigurable materials, such predictions may be difficult to realize without further modification of the material and/or experimental design. As a reminder, the theoretical model employed by Kuksenok et al. neglects the concentration of Br^- by assuming that $d[Br^-]/dt \approx 0$.[7] In our experiments, the actual concentration gradients for both $HBrO_2$ and Br^- are most likely comparable, and Br^- concentration cannot be neglected. Based on our knowledge and experimental observations of chemical signaling in BZ gels, both $HBrO_2$ and Br^- species accumulate between discrete BZ gels. Auto-chemotaxis did not occur because of this co-existence, for while the activator species may induce aggregation, the inhibitor species most likely prevents such aggregation.

5.7 Conclusions

In summary, we have demonstrated a synthetic material system that is capable of mechanically induced chemical propagation along complex trajectories. Engineering of these BZ material systems also provides certain analogies and implications for mimicking mechanotransduction in biological systems. Chemical signaling of mechanical cues is a critical component in biological phenomena ranging from cell-cell communication of locally imposed strain[29] to locomotion of an organism,[106] and some basic feedback mechanisms and resulting oscillatory characteristics can be replicated in BZ gels.

The ability to sense mechanical deformation and propagate chemical signals would be useful in applications involving artificial muscle and skin, whether for model robotic systems or therapeutic applications. While the mechanical actuation observed in our findings are negligible in comparison to the degree of actuation observed in real muscle tissue, recent findings suggest that organized BZ microgels can work together and exhibit amplified displacement.[119] Moreover, the capacity of BZ gel systems to sense mechanical stimuli at one location and generate propagating chemical signals to multiple distant locations is further enriched by the transmission of multiple modes of information in a single system, including gel color, volume, and redox state, that can be tuned and decoupled through the design of the metallopolymer and solution composition. The unique sensing and signaling characteristics of these complex gels thus provide several new avenues for basic and applied research in responsive and communicative materials.

Chapter 6

Conclusions

6.1 Major Findings

Shape and size influence BZ gel pattern formation

In Chapter 3, the effects of gel aspect ratio and absolute dimensions on pattern formation in N-isopropylacrylamide-co-Ru(bpy)$_3$ polymer gels undergoing the BZ reaction were studied. We demonstrated that oscillating chemical patterns within BZ gels can be modulated by changing the shape and size of the gel. At early reaction times, slight changes in the aspect ratio of the gel influenced BZ wave propagation and overall pattern formation. In contrast, robust target wave patterns were observed at late reaction times, regardless of gel aspect ratio. At certain lengthscales (gel edges < 0.6 mm), deviation from typical pattern formation occurred, even at late reaction times, and uniform color change was observed rather than traveling, chemical waves. We attributed such discrepancies to a switch in competition between the reaction and diffusion time scales for the experiment. In summary, we found an overall dependence of pattern formation, period, and amplitude of oscillation on absolute gel size.

BZ oscillations induce mechanical oscillations of the gel

At lengthscales < 0.6 mm, when the BZ reaction is limited by slow diffusion rates, uniform color change is synchronized with periodic gel swelling and shrinking. A swollen polymer network is observed when the gel is uniformly green (+3 Ru(bpy)$_3$ state), and a shrunken polymer network is observed when the gel is uniformly orange (+2 Ru(bpy)$_3$ state). Such volumetric changes of the gel occur because the overall oxidation state - and osmotic pressure - of the gel cycles according to the BZ redox reaction. As the osmotic pressure of the gel increases, water molecules from the external solution penetrate the polymer network and cause gel swelling. In Chapter 3, we recorded the synchronized BZ oscillations and mechanical swelling/shrinking of a BZ gel submerged in chemical reactants, and measured an average volumetric swelling of 22%. In other words, chemical oscillations drive synchronized mechanical oscillations of the material.

BZ oscillations can be mechanically triggered

In Chapter 4, we presented the first demonstration of mechanically triggered BZ oscillations in N-isopropylacrylamide-co-Ru(bpy)$_3$ gels. We showed that BZ oscillations can be triggered by applying a macroscopic, compressive stress to a quiescent BZ gel. Such results can either be achieved immediately within a quiescent BZ gel submerged in a chemical solution, or after the gel has attained a steady-state upon depletion of reagents. In the latter case, the BZ gels were submerged in chemical solutions and allowed to oscillate for many hours, during which time chemical reagents were being consumed while inhibitor species were generated. After oscillation had died out, uniaxial stress was used to trigger oscillations. In the compressed state, the BZ gel is able to utilize unreacted chemical reagents in the external solution. In other words, axial compression of the gel can be used to "resuscitate" the oscillatory functionality of the BZ material.

Leveraging this capacity to trigger chemical oscillations via applied pressure, we demonstrated sensor applications that involved discrete BZ gels, which are capable of both visually indicating the origin of mechanical loading and transmitting this signal away from the deformation site. Mechanical triggering of chemical oscillations in these gels affords novel approaches to creating pressure sensors based on self-oscillating gels.

Mechanical compression induces chemical transitioning between non-oscillatory and oscillatory regimes

To elucidate the underlying mechanism of mechanical triggering of oscillations in BZ gels, we quantified the chemical phase space for which mechanical triggering was possible. In doing so, we showed that oscillatory regimes may be described by the ratio of inhibitor species (Br^-) to reactant species (Ru(bpy)$_3$ and BrO_3). At high ratios of inhibitor to reactant species, oscillation is not possible, whereas a low ratio corresponds to the oscillatory regime of the BZ reaction. BZ oscillations can be mechanically triggered on and off at an intermediate ratio of inhibitor to reactant, when the chemical conditions are within the non-oscillatory regime but near the boundary dividing the oscillatory and non-oscillatory regimes. At these chemical conditions, macroscopic gel compression induces a chemical transition from the non-oscillatory to the oscillatory regime. Such transitioning is possible because the Ru(bpy)$_3$ catalyst is covalently bound to the polymer backbone, and compression decreases the overall gel volume, thereby increasing the catalyst concentration. Therefore, quantifying the oscillatory and non-oscillatory regimes resulted in a fundamental understanding of the underlying chemistry driving mechanically induced oscillations in BZ gels.

To understand if and how the mechanics of the BZ gel limits mechanically triggered oscillations, we varied the crosslinking density of the material. In doing so, we demonstrated that the required stress and strain for triggering oscillations depends on the polymer volume fraction of the polymer gel. Specifically, both the required stress and strain for triggering oscillations increased with decreasing polymer volume fraction. Swollen BZ gels, of low

polymer volume fraction, required relatively high stress to trigger oscillations. Thus, the threshold for pressure sensing in BZ gels may be tuned by adjusting the crosslinking density of the polymer. Additionally, such results suggest that the mechanism of mechanically triggering oscillations inherently depends on critical chemical conditions: there exists a critical $Ru(bpy)_3$ concentration for triggering oscillations that does not depend on polymer volume fraction. In conclusion, we found that the required mechanics for triggering BZ oscillations in a gel ultimately depend on critical chemical concentrations of reactant species.

BZ gels communicate chemical and mechanical information via inter-gel diffusion of $HBrO_2$

In Chapter 5, we demonstrated a synthetic system that can, in response to applied mechanical load, elicit a visible, chemical signal that propagates over long ranges and complex trajectories. This mechanically triggered signaling system comprises discrete N-isopropylacrylamide-co-$Ru(bpy)_3$ hydrogels capable of undergoing the BZ reaction. To elucidate the mechanisms governing signal propagation, we engineered systems in which chemical signals traverse sharp bends, split in opposing directions without attenuation, and terminate upon collision.

We showed that mechanical triggering can induce wave directionality in a series of discrete BZ gel discs that would otherwise oscillate in a disordered manner. Since signal amplitude does not decay with distance travelled away from the site of triggering, we concluded that $HBrO_2$ intermediates generated within the gel are above the concentration threshold required for activating oscillations in neighboring gels. Such results proved that signal transmission was achieved, in which a single gel source acts as a regulator for the entire series of gels. We also showed that the transmitted signal can change directions by travelling around bends. By quantifying the predicted diffusion times of $HBrO_2$ signaling molecules through solution, and by comparing such predictions with the actual diffusion times, we confirmed that the mechanism of gel to gel signaling is governed by diffusion. Beyond a critical gap distance (0.2 mm), signaling between gels is not possible since $HBrO_2$ is not a stable species in solution. In summary, we demonstrated that mechanically induced signal propagation is robust in that the signal does not attenuate with propagation over long ranges or around bends.

In Chapter 5, we also explored signal splitting and signal collision. To study signal splitting, we designed a series of discrete BZ gel discs that split into two separate branches of discs at a single gel node. We showed that the mechanically induced signal was capable of splitting into two opposite directions without decay in signal amplitude. In effect, we were able to show that the mechanically induced signal output may be doubled via signal splitting. To study signal collision, we cut the BZ gel into the shape of a ring, and locally triggered one end of the ring using macroscopic compression. In our experiment, the BZ signals annihilated upon collision. While this result was anticipated, we had originally hypothesized that signal amplification would occur when two signals collided. Because we did not observe signal

amplification at the site of collision, we concluded that doubling $HBrO_2$ concentration is not sufficient for increasing the amplitude of the signal output. Thus, signal output can be doubled via signal splitting, or extinguished via signal collision.

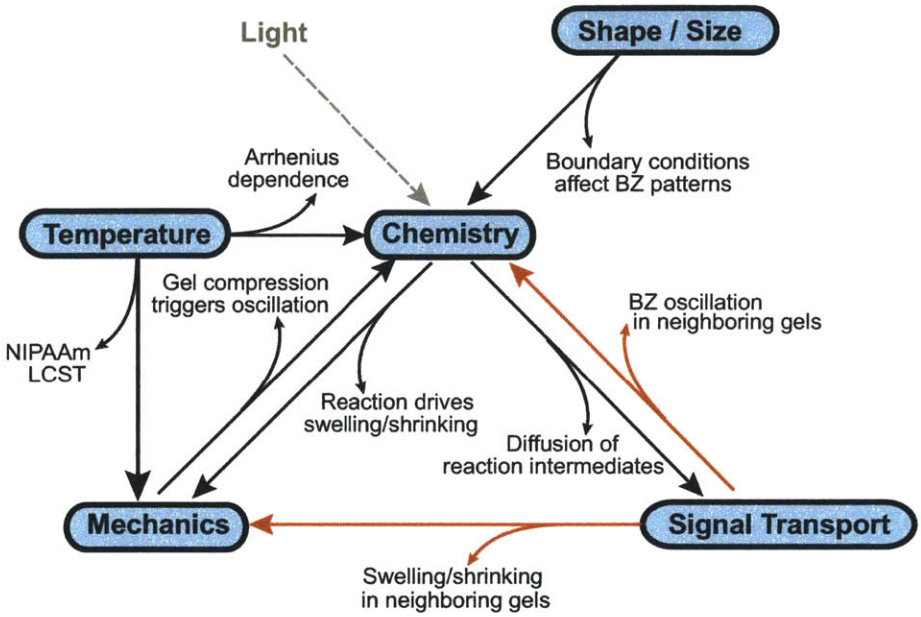

Figure 6-1: Flowchart summarizing stimuli-responsive behavior observed in BZ gels and the physical properties that were studied in this thesis. Solid arrows represent an observed relationship or novel result from this thesis. Black arrows indicate that the result was observed in a single BZ gel. Red arrows indicate that the result was observed in two or more BZ gels. Grey, dotted line indicates stimuli that were explored by other researchers.

Figure 6-1 summarizes some of the main results obtained in this thesis, and illustrates how these results fit within the context of other stimuli-responsive behavior observed in BZ gels. The solid arrows represent novel results or observed relationships that were explored in the thesis, while the grey, dotted line corresponds to cues that were explored by other researchers and not by us. Importantly, we have "closed the loop" in several areas of interest, meaning that we have demonstrated mutual coupling in chemomechanical phenomena. Previously, it was known that the temperature regulates the mechanical structure of NIPAAm hydrogels, and that temperature also affects the kinetic constants of the reactions via an Arrhenius relationship. In this thesis, we have closed the loop by demonstrating that BZ chemistry can drive mechanical oscillations of the gel, and that mechanical stimuli can drive chemical oscillations in the gel.

While the black arrows indicate that the result was observed within a single BZ gel, the red arrows indicate that the result was observed in two or more BZ gels. In this thesis, not only have we demonstrated how chemistry and mechanics can induce signal transport, but we have also shown how

signal transport can induce oscillations in neighboring gels. Importantly, chemical signaling among several BZ gels affects both the chemistry and the mechanics of the individual gels involved.

Comparison with theoretical models

Throughout the thesis work, comparisons between experimental results and BZ models or simulated predictions were made. In Chapter 3, we compared BZ patterns in gels of varying aspect ratio with simulated predictions of BZ patterns. We found that the simulated predictions were able to reproduce actual wave patterns at late reaction times, for most lengthscales. At lengthscales < 0.6 mm, the simulation results were unable to predict pattern inversion in high aspect ratio gels. Similarly, while the simulations were able to predict the observed period of oscillation in relatively large BZ gels, the model underpredicted the period of oscillation for gels < 0.6 mm.[4] We concluded that the BZ gel model has limitations at short length scales ($<$ 0.6 mm) because the model does not account for intermediate species, and does not distinguish between reaction and transport limited regimes.

In Chapter 4, theoretical evidence supporting the mechanism for mechanical triggering was developed. This analysis was based on existing theory for modeling the BZ dynamics in polymer gels. In our analysis, we showed that a change in the polymer volume fraction of the gel, induced by application of compressive stress to the material, will perturb the system of differential equations describing the BZ reaction. Specifically, the reaction rate describing the concentration of oxidized $Ru(bpy)_3$ is zero prior to gel compression, and is a non-zero, finite value after compression is applied to the gel. While our theoretical analysis provided a fundamental understanding of the mechanism for mechanical triggering, such theory was not able to describe the sensitive conditions required for achieving mechanically induced transitions between the oscillatory and non-oscillatory regimes.

In Chapter 5, we analyzed experimental data on mechanically induced signal collision in order to identify limitations within simulations that predict chemical signaling among sets of BZ gels. In particular, we showed that the concentration of inhibitor bromide is not constant within the spatial dimensions of our experiment. In contrast, the BZ theory developed for modeling signaling in BZ gels often assumes that $d[Br^-]/dt \approx 0$.[5,118] Our experimental results suggest that the inhibitor species cycles with a frequency comparable to the concentration of $Ru(bpy)_3$. Therefore, in order to validate simulated predictions that assume a constant Br^- concentration, further experimental manipulation is needed in order to negate the dynamic, inhibitory effects of Br^-.

6.2 Suggestions for future work

Addition of triggering agents to signaling networks of BZ gels

In this thesis, we have studied various aspects of mechanically induced signaling in BZ gel systems. In our experiments, we used the traditional BZ

reagents: malonic acid, sodium bromate, nitric acid, and transition metal catalyst. While we added bromide to force the system into a non-oscillatory regime, there are several other chemical species that may be added to the system. For instance, Bishop et al. explored shape effects in BZ materials under the influence of triggering agents. Such triggering agents include methanol or formaldehyde, and determine whether the BZ dynamics are governed by activator or inhibitor species, respectively.[59] Thus, by adding either methanol or formaldehyde in signaling networks of BZ gels, the chemical gradients may be purposefully manipulated. In Chapter 5, we showed that auto-chemotaxis of four discrete BZ gels was not possible. However, the addition of a triggering agent to such a system may alter the ultimate chemical gradients of the inhibitor or activator species. It is possible that artificial chemotaxis of BZ gels may be achieved by further manipulation of the chemical reagents added to the system and/or by changing the geometry of the BZ gels.

Fabricating patterned BZ gel composites

To further enrich the behavior of BZ gels, additional complexities may be incorporated within the NIPAAm gel system. Since most biological materials rely on their hierarchical structure in order to accomplish complex objectives, one might infer that a compartmentalized, non-uniform BZ gel material would also exhibit more elaborate stimuli-responsive behavior. Human skeletal muscle, for instance, relies on multiple phases and discrete components to achieve muscle contraction and movement. In particular, chemical reactions control molecular interactions between actin and myosin muscle proteins, and these interactions drive motion at both the molecular level and macroscale. Additionally, blood vessels are incorporated within the muscle tissue to provide chemical nutrients and enable signal transmission. Such architectural complexity is found in skeletal muscle, as well as human skin and plant tissue, and enable important biological functions. Therefore, biological materials are comprised of liquid and solid phases with distinct molecular components that interact via chemical reactions.

Heterogeneity can similarly be incorporated in the BZ gel system in multiple ways. Rather than submerging BZ gels in uniform chemical solutions, critical chemical reagents may be supplied to localized regions by embedding artificially constructed channels that mimic microvasculature in biological systems. To control synchronization in the BZ reaction, patterned BZ gels can be fabricated in which discrete units of $Ru(bpy)_3$ catalyst are separated by neutral, unreacting polymer. Here, the spacing between units of $Ru(bpy)_3$ would govern whether chemical signals are transmitted between the units or not. Heterogeneity can also be accomplished by introducing more than one type of responsive transition metal catalyst into the BZ system, or by incorporating other materials such as fibers with which the BZ catalysts may chemically interact with. Already, researchers have fabricated BZ gels with increasing complexity, and have engineered new and interesting material functionality. For example, Okeyoshi et al. fabricated artificial photosynthetic systems comprising NIPAAm-co-$Ru(bpy)_3$ nanogel composites containing either electrostatically absorbed Platinum nanoparticles or RuO_2

nanoparticles.[68,69] By embedding nanoparticles in NIPAAm-co-Ru(bpy)$_3$ gels, they have engineered the production of both hydrogen and oxygen. Given that BZ gels already respond to external changes in temperature, light, chemistry, and mechanical stimuli, increased material complexity can further enrich responsive behavior for interesting applications in biomimetics and soft robotics.

Demonstrating chemomechanics in other synthetic material systems

Another fascinating area of research that may be paired with continued BZ gel studies is the demonstration of chemomechanics in alternative material systems that are perhaps more biologically relevant. While BZ gels represent a useful class of materials for visualizing chemomechanics, the reaction is highly acidic and sensitive to specific chemical conditions that are not biologically compatible. However, the knowledge gained from studying BZ gel systems may be applied to other materials in which chemical oscillation is more difficult (but not impossible) to measure. As an example, Yoshida et al. have synthesized NIPAAm-co-MEP gels that self-oscillate due to an enzymatic reaction driven by adenosine triphosphate (ATP).[120] Here, the researchers applied knowledge of the BZ reaction in gels to another oscillating gel system that is more biologically relevant. In a different study, He et al. fabricated layered hydrogels with embedded microstructures, and harnessed the chemomechanical coupling of the system to achieve autonomous temperature regulation.[41] Thus far, researchers have not employed mechanical stimuli as triggers for such oscillating or regulatory systems. However, the knowledge gained from studying mechanically induced chemical oscillations and signal propagation in BZ gels can enable the design of biologically relevant materials that respond to external pressure.

6.3 Contributions

Prior to this work, other research groups had demonstrated that the BZ reaction can induce mechanical oscillations of the material.[45,58] Because BZ gels exhibit such strong chemomechanical coupling, we originally hypothesized that external mechanical perturbation could trigger the BZ reaction in gels. In fact, the conversion of mechanical to chemical energy is a natural phenomenon that few synthetic materials have been able to mimic robustly, and while biological materials - ranging from individual cells to entire organisms - can undergo chemical reactions in response to mechanical stimuli,[29–33] synthetic materials are limited in their functionality, and are rarely hydrated in chemical environments that provide access to chemical nutrients. To our knowledge, we have demonstrated that BZ gels are the first synthetic material capable of producing oscillating reactions in response to mechanical pressure. In demonstrating that BZ gels can sense mechanical pressure and respond by transducing such energy into chemical oscillations, we have opened up new avenues of research based on mechanical sensing in BZ gels. Our studies also facilitate the design of biologically relevant materials that

respond to mechanical impact, which could be used in self-healing applications and drug delivery devices that transport medicine upon injury or impact.

Historically, it has also been challenging to engineer synthetic materials that reproduce the mechanically induced signal transduction of biological systems, particularly the chemical transmission of mechanically induced signals over extended distances. In cellular biological systems, signaling systems often initiate by molecular recognition via site specific surface interactions that lead to processing and transmission of metabolic information. The presence of molecular inhibitors and activators in the biochemical environment aid in the regulation of such processes. In Chapter 5, we demonstrated mechanically induced signal transmission in sets of discrete BZ gels. While signal propagation in BZ gel systems does not depend on conformational surface interactions, we have shown that BZ gels can transmit information while maintaining a self-regulating chemical environment. These findings qualitatively mimic aspects of mechanotransduction among biological cells, and also describe intriguing new metallopolymer material systems that convert and convey information about metal ion redox state and mechanical deformation.

An interesting side contribution of this thesis was showing that the life time of BZ functionality may be extended by mechanically compressing the material. Previously, it was assumed that BZ gels self-oscillate in chemical solutions, and stop oscillating once the chemical energy has been consumed by reactions. We have shown that the oscillatory functionality can be restored or "resuscitated" by applying an external, macroscopic compression to the gel. Thus, while BZ oscillations in gels cease once sufficient chemical energy has been consumed via the BZ reactions, unreacted BZ reagents - or chemical "fuel" - still remains in solution. Taken from another perspective, we have shown how mechanical compression can effectively increase the overall conversion of chemical fuel into functional BZ oscillations.

Figure 6-2 summarizes the behaviors shared by BZ gels and biological materials, ranging from individual cells to entire organisms. Throughout this thesis, our studies were inspired by phenomena occuring in natural systems, and these phenomena included self-regulated oscillations, mechanical sensing, and signal transmission. In BZ gels, we showed that such phenomena is driven by chemical reactions occuring at the nanoscale, which subsequently drives overall system behavior at the macroscale, between sets of discrete BZ gels. Although the mechanisms of action for material behavior are different in BZ gels versus biological materials, the end results are remarkably similar.

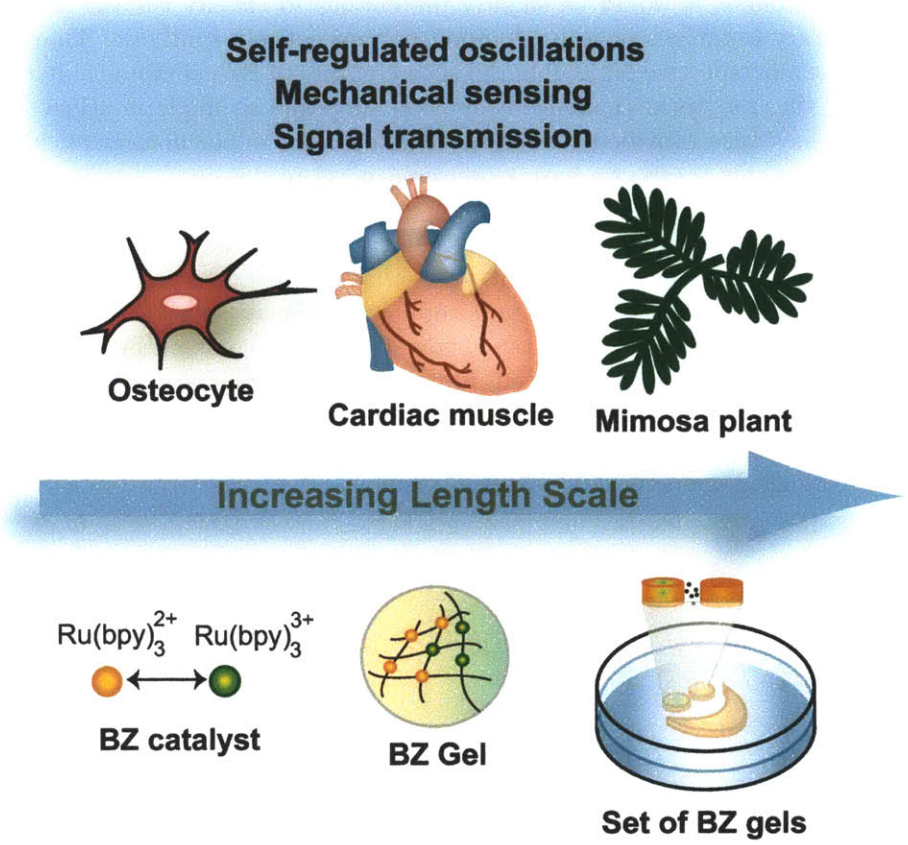

Figure 6-2: Illustration summarizing the similarities between biological materials and BZ gels. Biological materials (above arrow) exhibit interesting behaviors that have inspired the areas of focus in this thesis. BZ gels (below arrow) share the self-regulated oscillatory behavior, mechanical sensing, and signal transmission capability of natural systems, and such phenomena are exhibited by sets of BZ gels comprising BZ polymer and covalently bound BZ catalyst.

John J. Tyson from the Department of Biology at Virginia Polytechnic Institute and State University noted that the BZ reaction has been widely studied by biologists (in addition to chemists, mathematicians, physicists, and engineers). In *Frontiers in Mathematical Biology*, he wrote a paper entitled "What Everyone Should Know About the Belousov-Zhabotinsky Reaction," where he noted the following:

"For these reasons it is not pretentious to suggest that the BZ reaction be given status as an honorary organism, somewhere between viruses and bacteria!"

- Tyson, 1994, p. 584,[121]

Of course, it would be slightly pretentious to classify the BZ gel as an honorary organism since its components are entirely synthetic. That said, Tyson's perspective highlights the showy nature of BZ gel systems: not only have these systems challenged previous suppositions made in science, but they have also provided strikingly visual evidence of chemomechanical coupling. In this thesis, we have engineered novel responsive behavior by harnessing such chemomechanical coupling in BZ gel materials. We showed that chemical oscillations can drive mechanical oscillations, mechanical stimuli can trigger chemical oscillations, and that mechanical stimuli can induce chemical signal propagation and communication in sets of BZ gels. Our results can be used to facilitate understanding of complex biological phenomena, or to design advanced, functional materials that act as pulsating chemical or pressure sensors, and we hope that the foundational work provided in this thesis will inspire future studies that connect chemomechanics in biological and synthetic material systems.

Appendix A

Polyacrylamide-silica-ferroin BZ Gels

Portions of this work were performed in collaboration with Eva Cheung (MIT department of chemical engineering '11), and classmates for "Experimental Mechanics of Soft Condensed Matter" at MIT: William Polacheck, Hadi Nia, and Ting Ting Chen.

A.1 Introduction

While the majority of the work in this thesis was focused on a BZ gel system comprising poly(NIPAAm-co-Ru(bpy)$_3$), an alternate BZ gel comprising polyacrylamide was also fabricated. Here, we describe the synthesis and characterization of polyacrylamide-silica BZ gel composites containing electrostatically bound ferroin transition metal complex. The primary motivation for synthesizing an alternate BZ gel system was to compare chemomechanical similarities in different gel systems. A secondary motivation for studying polyacrylamide BZ gels was to observe BZ oscillations of high color contrast: ferroin metal complex can exhibit vibrant blue and red hues, corresponding to the +3 and +2 oxidation states, respectively.

Previously, Konotop et al. demonstrated that polyacrylamide-silica gel composites exhibit BZ self-oscillations.[58] In particular, when sodium silicate is added to the pre-polymer polyacrylamide solution, the silanol SiOH functional groups become negatively charged. The resulting polymer hydrogel exhibits a negatively-charged polymer backbone containing silica nanoparticles, and is able to absorb positively charged ferroin complex.[58]

Similar to NIPAAm BZ gels, polyacrylamide-silica gels containing ferroin catalyst are capable of undergoing mechanical oscillations that are driven by BZ oscillations. Interestingly, the chemical and mechanical oscillations of polyacrylamide BZ gels are out-of-phase: reduced ferroin catalyst corresponds to a relatively swollen polymer network while oxidized ferroin catalyst corresponds to a relatively shrunken polymer network.[58,122] The authors attributed such mechanical behavior to the periodic changes in physical crosslinking within the material. When the ferroin catalyst is uniformly oxidized, additional crosslinks form between ferroin and negatively charged

polymer, causing the polymer gel to shrink.[122]

A.2 Methods

A.2.1 Mechanical measurements

While the mechanical properties of polacrylamide have been reported in the literature,[58] literature values of the Young's elastic modulus can vary greatly depending on the experimental method used to extract this parameter. Furthermore, the mechanical properties of hydrogels such as polyacrylamide depend on the ratio of crosslinker to monomer as well as the duration of time that the hydrogel is allowed to swell in water. These details complicate the data reported in various literature sources and provide motivation for independently characterizing our polyacrylamide hydrogels. In addition, we aimed to characterize the mechanical properties of a polyacrylamide hydrogels polymerized with different concentrations of silica gel nanoparticles. Thus, we characterized the polyacrylamide system in order to confirm the mechanical properties of the gels. and to determine whether or not discrepancies between our experimental and literature values exist.

To extract the mechanical properties of polyacrylamide hydrogels, some approximations were incorporated. The mechanical behavior was assumed to exhibit an approximate classical linear elasticity. This approximation has been used for polyacrylamide systems in studies that have also shown that indentation experiments using both instrumented indentation and AFM-enabled indentation to quantify the Young's elastic modulus of polyacrylamide hydrogels. Using these methods, the modulus of polyacrylamide was shown to range between 10 and 340 kPa for 0.1 mol% to 5 mol% crosslinker, respectively.[123]

In order to use AFM indentation to extract the Young's elastic modulus of polyacrylamide gels, a Hertzian model was fit to force versus depth indentation data. This model assumes that the indented material behaves elastically, and agrees well with the equation below:

$$F = \frac{2Etan\phi}{\pi(1-\nu^2)} \tag{A.1}$$

where F is the applied load, E is the Young's Elastic Modulus, ϕ is the angle of the conical indenter, and ν is the Poisson's ratio which was assumed to be 0.5 (although note that this is not a correct assumption, and the gels are most likely compressible).

A.2.2 Polyacrylamide polymerization

Two different methods for polymerizing polyacrylamide gel were performed. In the first method, pre-polymer solution was sandwiched between a glass-bottomed petri dish and a glass coverslide. The glass-bottomed petri dish was activated using 3-aminopropyltrimethoxy silane (APTES) and glutaraldehyde such that the hydrogel would adhere to the glass-bottomed dish. The

glass coverslide was not activated and was easily removed after polymerization was completed at room temperature for 24 hours. This polymerization procedure was used to study the effects of sodium silicate on the elastic modulus of the adhered hydrogel. Three samples containing 1.72 wt%, 2.65 wt%, and 3.8 wt% sodium silicate were prepared using this method. (Note that the literature values for the elastic moduli of these samples varies between 0.6 and 2.4 kPa.[58]) In the second method, neither glass surface was activated such that the hydrogel did not adhere to either surface. The resulting hydrogel was then glued to a petri dish in order to observe BZ oscillations.

Following the synthesis procedures described by Konotop et al.[58], the typical pre-polymer recipe involved 40% acrylamide (2.5 mL), TEMED (51.7 μL), N,N'-methylenebisacrylamide (MBAAm) (15.2 mg), AMPS (79.2 mg), and sodium silicate (800 μL of 10.6% Na_2O and 26.5% SiO_2 solution). All chemicals were dissolved in water (7.5 mL) and 1 mL volumes of the resulting pre-polymer mixture were allowed to polymerize for one day at room temperature. The resulting gel was soaked in water for 3 days, and subsequently soaked in ferroin (12 mM) for 15 days. Before exposing the gel to the BZ reaction, the gel was thoroughly washed with water to remove unbound ferroin.[58]

A.2.3 AFM-enabled indentation

To characterize the Young's modulus of the hydrogel, indentation using AFM was performed on samples of hydrogel with varying weight percent sodium silicate. The cantilever tip with the lowest spring constant (nominal value of 0.1 N/m) was chosen since it has been suggested that for soft materials, the apparent elastic moduli varies as the cantilever stiffness. The apparent elastic moduli is closer to the expected values with a less stiff cantilever.

Due to the compliance of the cantilever, the AFM was first calibrated for the invOLs on a glass slide in deionized water to prevent electrostatic forces between the cantilever and glass slide from affecting the calibration. Roughly 1mL of water was added to the hydrogel sample to maintain hydration of the sample during the indent. Multiple indentations were performed on two locations in each sample of hydrogel using the the same loading and unloading conditions (scan rate 0.1Hz, velocity 1.95 μm/s, trigger point 6V). The LVDT position and delfection voltage from the photodiode were recorded during the indents.

A modified MATLAB script was used to analyze the raw LVDT and deflection data acquired from the indent. Load was calculated by multiplying the deflection data by the spring constant while the separation was calculated by subtracting the LVDT by deflection. From the load versus separation plot, an indentation elastic modulus was found by applying a Hertzian model to the loading portion of the curve. The indenter tip was assumed to be conical with an angle of 18 degrees. To find the contact point, the program fits the smoothed force data to two lines. The point when the slope increases becomes the contact point, and the maximum of the two points becomes the contact point used.

The drift associated with each curve was corrected by fitting a linear line

to the data prior to the found contact point and subsequently subtracting the value of the line evaluated at each point from the force at each point of the original curve. This correction in drift was found to increase the calculated stiffness by 1% to 2% of the uncorrected curve.

A.2.4 BZ Oscillations

When exposed to 0.08 M sodium bromate, 0.06 M malonic acid, and 0.6 M sulfuric acid, the polyacrylamide-silica gel containing absorbed ferroin undergoes the BZ self-oscillating reaction. To determine whether the polyacrylamide-silica gel undergoes localized swelling due to the BZ reaction, cantilever deflection was recorded as a function of time. To confirm the period of oscillation and wave velocity of this BZ system, the reaction was also recorded outside of the AFM. The amount of cross-linker, sodium silicate, and external reactants added to the system were held constant between these experiments.

To measure the BZ oscillations, we created a displacement function for the LVDT. We brought the LVDT into contact with the material surface and held the LVDT constant with time. By measuring the deflection of the cantilever tip as a function of time, we could measure changes in gel height as a function of time. We needed to make contact with the gel surface before monitoring deflection as a function of time, but we did not want to indent too much such that we could not observe oscillations in the gel. Consequently, we defined initial LVDT extension and iteratively modified this extension until we saw a slight but stable deflection of the cantilever tip. When defining the LVDT function, the "pre-indent" refers to the depth of indentation of the material after the cantilever tip comes into contact with the material surface. We initially set the pre-indent to 500nm, but the resulting cantilever deflection was 7V. After reducing the pre-indent by an order of magnitude but observing no change in the deflection of the cantilever tip, we realized that the LVDT was extending to the "trigger point" then following the defined load function. We reduced the trigger point from 6V to 1V and set the pre-indent to 50nm, and the resulting cantilever deflection was 1V. Reducing the pre-indent any further caused the deflection to be unstable, and we could not maintain contact with the surface.

Observing oscillations in the gel was further complicated by leaching of the ferroin into acid solution. Since the ferroin is red and the AFM laser is red, interference caused by the laser affected the intensity of the laser on the photodiode. Over time, the total photodiode voltage would drop, and we needed to replace the acid solution to retain a reasonable photodiode voltage.

A.3 Results

The composition of the tested polyacrylamide gels vary slightly in direct comparison to published data by Konotop et al. In particular, Konotop et al. has published the swelling ratio of polyacrylamide gels as a function of sodium silicate concentration for gels prepared with 0.5 mol% cross-linker. The amount of cross-linker used in this report, however, is 0.6 mol%. Figure

A-1A shows that our experimental hydrogels do not exhibit the same degree of swelling as the values reported by Konotop et al.[58] This discrepancy, however, is likely a result of our higher cross-linker content.

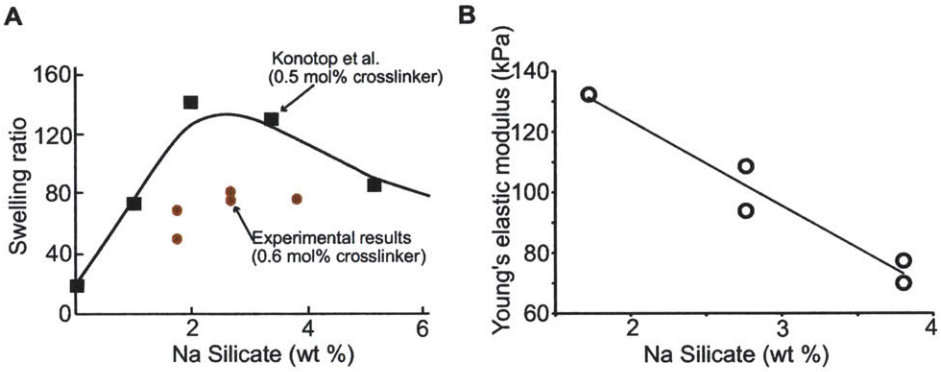

Figure A-1: (A) Swelling ratio as a function of sodium silicate concentration. The experimental results (shown in red) are consistently lower than the literature results (black). The swelling ratio was calculated using the following relationship: (mass of swollen gel - mass of dry gel)/mass of dry gel. (B) Mechanical properties of polyacrylamide composites as a function of sodium silicate content. The Young's elastic modulus for the composite decreases with increasing concentration of sodium silicate.

Indentation depth versus force curves using AFM were analyzed using the Hertzian equation for different concentrations of sodium silicate. As shown in the figure below, the Young's elastic modulus decreases as a function of increasing sodium silicate concentration. This result was anticipated because the literature values reported by Konotop et al. also follows this trend.[58]

In order to compare these values with the literature, several papers were examined. The Konotop et al. authors have reported the Shear relaxation modulus as a function of sodium silicate concentration.[58] For the concentrations of sodium silicate tested in our experiments, they report on Young's elastic modulus values that range between 0.6 and 2.4 kPa. While their experiment used less cross-linker than our experiments (0.5 mol% rather than 0.6 mol%), this difference should not be enough to create such disparity in elastic modulus values. Our method of extracting the elastic modulus is, however, very different than the methods which they have reported. The Konotop et al. authors used a uniaxial compression method rather than an AFM-based indentation.[58] While macroscale compression of materials is an accurate way of determining the elastic modulus, the Konotop et al. authors have not explicity stated in their paper the speed at which the hydrogel was compressed and other important parameters. Thus, we have investigated alternative literature sources which report the Young's elastic modulus for polyacrylamide.

Data for polyacrylamide prepared with 1 mol% cross-linker was reported to have an elastic modulus of approximately 87 kPa by Muniz et al.[124] According to Constantinides et al.,[123] for 0.5 or 0.6 mol% bis-crosslinker, the elastic modulus is approximately 35 kPa. The values 87 kPa and 35 kPa

should provide an upper value for the modulus values in our experiments because the sodium silicate causes the mechanical properties of the gel to become more compliant. The discrepancy between our data may be due to the duration of time allotted for the hydrogel to become fully hydrated. The data shown here were taken after one day of allowing the gel to swell in water. However, experimental observations indicate that the gel continues to swell after the first day. In order to confirm this observation, indentation experiments on a 2.65 wt% sodium silicate polyacrylamide composite were performed after the gel was allowed to swell in water for 17 days. While the elastic modulus of this hydrogel was approximately 100 kPa after one day of swelling in water, the elastic modulus was 26.4 +/− 2.3 kPa after 17 days of swelling in water. Thus, while the data in Figure A-1 allows us to qualitatively compare the relative Young's elastic modulus for hydrogels with different amounts of sodium silicate, the actual Young's elastic modulus for a 2.65 wt% sodium silicate gel at equilibrium is 26.4 kPa. This value is closer to the literature value of 35 kPa. Furthermore, we expect this hydrogel to have a lower modulus value than 35 kPa because it contains sodium silicate.

BZ Oscillations

The period of oscillation and the velocity of the BZ waves was determined by recording the BZ reaction within the gel under a stereomicroscope (without the AFM). The hydrogel was cut into an 8 mm in diameter disc. As shown in Figure A-2, the BZ reaction produces spiral patterns and also changes with time. Specifically, the left image has several locations on the gel in which the BZ waves originate. The waves propagate outwards in a spiral and collide with each other in certain areas. The right image corresponds to later times, when the BZ reaction has shifted and no longer originates from several locations in the gel. As a result, the waves collide with each other less frequently. Furthermore, the absorbed ferroin concentration within the gel noticeably decreases as a function of reaction time. The gel fades from red to pink, and the waves become less noticeable.

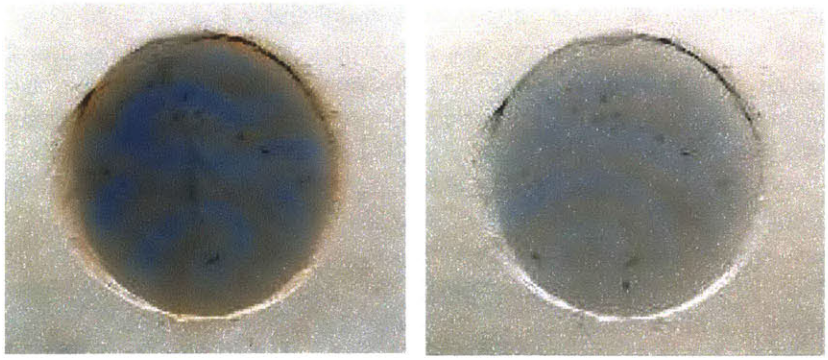

Figure A-2: BZ reaction in hydrogel composite as a function of time. The image on the left corresponds to early times, and the image on the right corresponds to late times.

In order to account for the random locations in which the BZ waves

originate, the period of oscillation was analyzed at 3 different locations. Figure A-3 shows the positions at which the waves were quantified and the resulting oscillations were plotted at each of these points. Interestingly, the period of oscillation was consistent over the chosen positions. This result suggests that a random location on the hydrogel may be chosen to analyze the BZ reaction. However, it should be noted that the amplitude of the local swelling of the BZ waves may change throughout the reaction because ferroin is obviously being desorbed from the hydrogel, causing the gel to fade from red to pink. The period of oscillation was 47.0 ± 6.1 seconds, and the velocity of the BZ waves was 2.0 ± 0.4 mm/minute, meaning that each wave travels approximately 2 mm every minute.

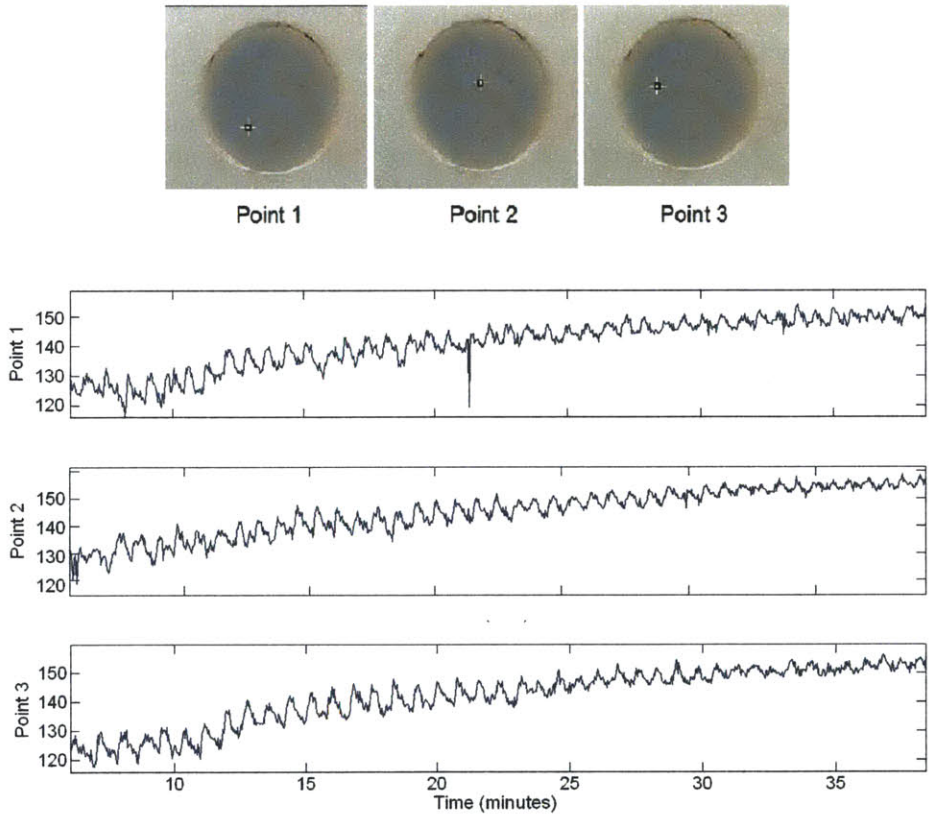

Figure A-3: BZ oscillations in the hydrogel at 3 different locations. The average RGB was quantified in the oscillating hydrogel and 3 different locations corresponding to the images shown above the 3 plots. The oscillations were consistent regardless of position.

To determine whether or not the hydrogel undergoes localized swelling due to the BZ waves, a hydrogel containing the same concentration of ferroin and sodium silicate (and equilibrated in water for the same duration) was glued to a petri dish and analyzed at a randomly chosen location using AFM. We assumed that the glue did not have any affect on the mechanical

properties of the gel because a cantilever with spring constant 21.48 pN/nm was used to indent the gel and obtain the Young's elastic modulus. The modulus was not greater than the value obtained for a hydrogel that was not glued to the petri dish, indicating that the glue did not penetrate the porous hydrogel to depths in which the experiment was performed. The cantilever deflection as a function of time was recorded in hopes of detecting the BZ self-oscillating reaction. By monitoring the cantilever deflection for a constant piezo extension, we observed erratic fluctuations in the cantilever deflection. It was not clear whether such fluctuations were indicative of mechanical oscillations in BZ gels.

Lastly, the Young's elastic modulus of the hydrogel did not change as a result of the acidic, BZ reaction. Before the acidic reactants were added to the hydrogel, the Young's elastic modulus (for the hydrogel in water) was 26.4 $\pm$ 2.3 kPa as measured for n=10 indentations. After undergoing the BZ reaction, 10 additional indentations were performed in the gel after the acidic reactants were replaced with water. The modulus was 24.2 $\pm$ 1.6 kPa, indicating that there was no degradation of the hydrogel due to the acidic conditions of the BZ reaction, and the hydrogel was able to retain its mechanical properties over the course of the oscillations.

Interaction between cantilever C and the glass slide was difficult to overcome (the deflection was always drifting). To troubleshoot this issue, the glass slide was submerged in water, and the calibrations were done in liquid. The spring constant was determined after the experiment by indenting a glass slide submerged in water.

A.4 Conclusions

The results from these experiments suggest that with careful consideration of the limitations of AFM in general and that of a specific AFM instrument, it is a possible to gain valuable mechanical properties of poroelastic gels. From simple indentation into the gels, it was found that the apparent elastic moduli calculated from a Hertzian model resulted in values close to reported literature values of similar gels. A Hertzian model was assumed because the indentation speed was slow enough to avoid viscous effects while the depth of indent was shallow enough to avoid substrate effects. Also, the loading and unloading portion of the indentation curves traced each other within error, which is characteristic of an elastic response. The discrepancies between the literature and experimental values my be attributed to the differences in sample preparation, stable adhesion to the petri dish during indentation, and degree of swelling of the hydrogels used in the experiment.

To more accurately characterize the mechanical properties of the hydrogel, the gel's indentation response to more compliant or stiff cantilevers could be used verify the accuracy of the apparent elastic moduli obtained from an AFM indentation experiment. Also, a larger range of cross-linker concentration could be tested to quantify the trend in sodium silicate concentration and stiffness.

In the last objective, the swelling characterization of the BZ oscillations,

some oscillations were observed using AFM but the oscillations were erratic and convoluted with drift as well as other parameters of the experiment. To obtain a more quantifiable data set to observe the mechanical swelling of the BZ oscillation, the drift in the piezo needs to be characterized, oscillations should be tested in several locations on the gel, and the problem of interference between the leaching of the ferroin into acid solution and the photodiode reception of the laser to acquire the sum needs to be addressed.

The polyacrylamide system was less complicated than the NIPAAm system to synthesize because it does not require special synthesis of a catalytic monomer. Furthermore, the material is less sensitive to oxygen and easier to handle after polymerization. Since the gel can easily be polymerized on activated glass such that the polymer backbone is adhered to the glass substrate, AFM measurements were used to determine the elastic moduli of this material at varying sodium silicate concentrations. However, the BZ reaction was difficult to monitor using the AFM because desorbing ferroin interfered with the AFM laser. Therefore, while the polyacrylamide system is easier to polymerize and easier to cut cleanly, the gradual desorption of ferroin from the gel matrix prevented long time experimental studies using this system. Ferroin desorption prevented visualization of patterns, especially at late reaction times. Furthermore, swelling/shrinking of the gel was never observed during the BZ reaction. Although chemomechanical behavior has been reported for this gel, it is unclear whether these results are repeatable or not. In conclusion, inherent problems with this hydrogel deter further progress using this material.

Appendix B

Additional data and protocols

B.1 Data from unpublished experiments

B.1.1 Heart shaped BZ gels

The images and studies in this section were performed in collaboration with Sally Lin (MIT department of material science & engineering).

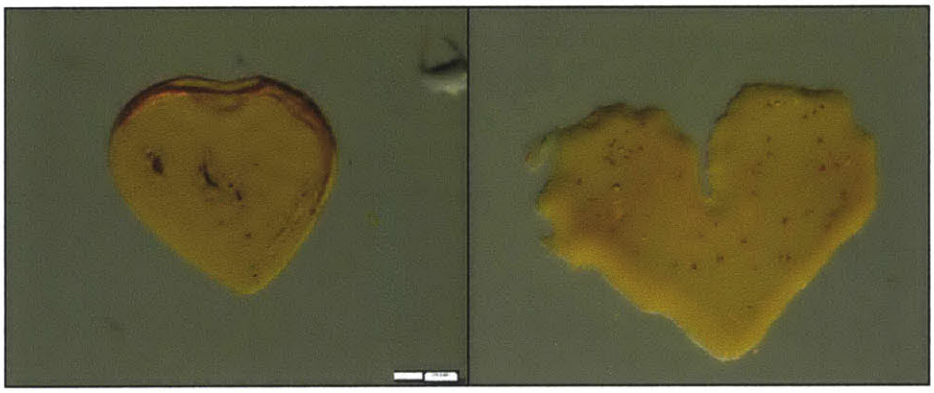

Figure B-1: Attempted preparation of a heart shaped BZ gel. (A) BZ gel polymerized through a heart shaped photomask. (B) BZ gel cut into a heart shape using a laser cutter.

Efforts were made to prepare BZ gels that were heart shaped. In order to fabricate gels with shapes that are more complex than rectangles and circles, UV polymerization was performed through customized masks. The masks were ordered from Fineline Imaging (as discussed in Chapter 2). When the BZ gel was polymerized under UV light, passed through a heart shaped photomaks, the resulting BZ gel lacked the "dimple" of a typical heart shape. Immediately after polymerization, the dimple was preserved; however, after hydrating the gel in water, the dimple disappeared almost completely. Shown in Figure B-1A is the hydrated BZ gel "heart," illustrating that the dimple is no longer discernable.

In addition to polymerizing gels through custom photomasks, a laser cutter was used to cut already hydrated BZ gel samples. Shown in Figure B-1B is an image of a BZ gel cut into a heart shape using a laser cutter. The edges of the gel were jagged due to small vibrations of the laser cutter instrument. The laser cutter was not able to cut complex BZ gel shapes at desired length scales (1 mm). However, the parameters of the laser cutter (speed and intensity) were not fully optimized. It is worth investigating whether speed and intensity of the laser may be optimized to refine the process of cutting BZ gels.

B.1.2 Perforated BZ gels

Experiments with perforated BZ gels were performed by Sally Lin (MIT department of material science & engineering) and Abe Cherukara. Analysis and BZ gel synthesis were performed by the author of this thesis.

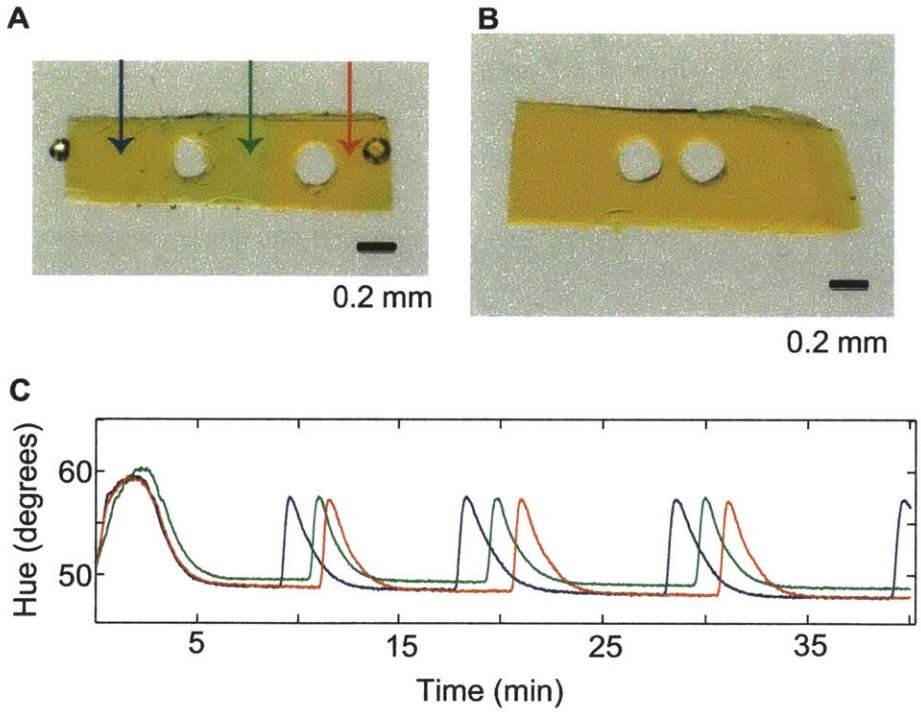

Figure B-2: BZ gels comprising 5 mM $Ru(bpy)_3$ and containing perforations. (A) Perforations were spaced over 0.2 mm apart. (B) Perforations were spaced under 0.2 mm apart. (C) Oscillations in the BZ gel pictured in part A: wave amplification was not observed between the perforations.

Several experiments were performed to study pattern formation in BZ gels with holes, or perforations. These experiments were motivated by simulations performed by Balazs et al. (unpublished). In their simulations, Balazs et al. predicted that $HBrO_2$ species would accumulate in the perforations, and such accumulation would cause wave amplification in the middle of the

gel (between the gel perforations). Shown in Figure B-2A-B are images of BZ gels comprising 5 mM $Ru(bpy)_3$ and cut into rectangles with two perforations. Both gels were submerged in BZ acid, and wave patterns were recorded using timelapse microscopy. Both gels exhibited typical wave patterns, in which the BZ wave travelled from one end of the gel towards the opposite side of the gel. (Such results were observed in rectangular BZ gels containing no perforations). To quantify the oscillations, three regions of the gel pictured in Figure B-2A were analyzed (see arrows for regions of interest). The oscillations shown in Figure B-2C show that wave amplification did not occur between the perforations (green line); rather, the wave amplitude of oscillation was consistent regardless of spatial location on the gel.

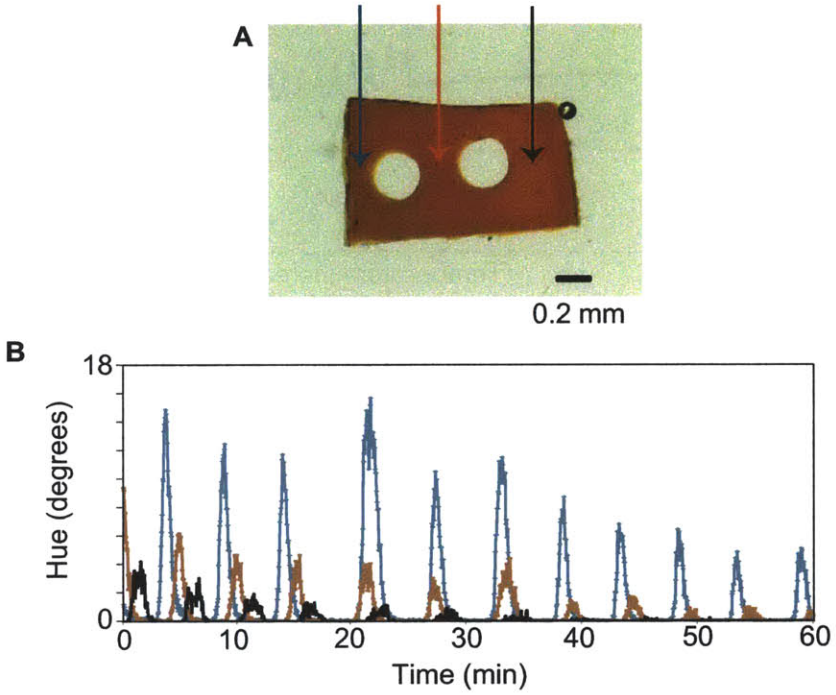

Figure B-3: BZ gels comprising 8 mM $Ru(bpy)_3$ and containing perforations. (A) Perforations were spaced approximately 0.2 mm apart. (B) Oscillations in the BZ gel show that wave amplification was not observed between the perforations.

Pattern formation in BZ gels comprising 8 mM $Ru(bpy)_3$ were also measured. Shown in Figure B-3 is another perforated BZ gel. Again, wave amplification did not occur between the gel perforations. In fact, the oscillatory amplitude appeared to decline from left to right in the gel. It is possible that the BZ gel was not of uniform $Ru(bpy)_3$ concentration. In any case, the data shown in Figures B-2 and B-3 suggest that BZ gels are unaffected by perforations.

B.1.3 Temperature triggering in BZ gels

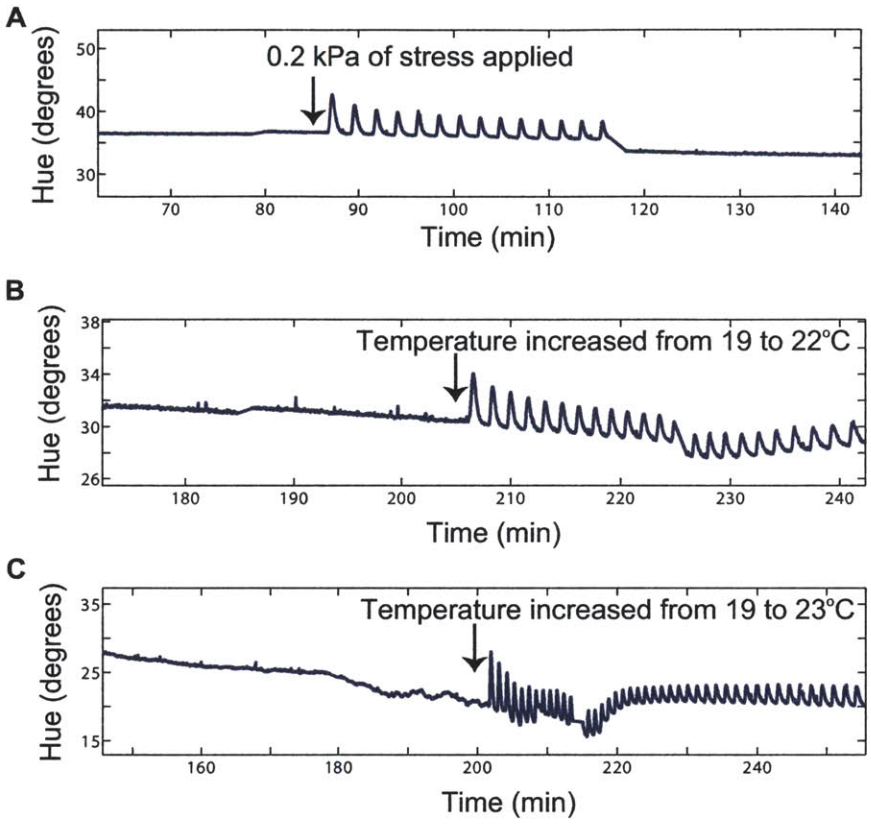

Figure B-4: Mechanical and/or temperature triggering of oscillations in BZ gels comprising 5 mM $Ru(bpy)_3$. (A) Gel of polymer volume fraction 0.25, and mechanically triggered under 0.2 kPa compressive stress. (B) Same experiment as part A, oscillations triggered when the temperature was increased from 19 to 22°C. (C) Gel of polymer volume fraction 0.11 and triggered when the temperature was increased from 19 to 23°C.

Shown in Figure B-4 are two separate experiments involving mechanical and/or temperature triggering. In Figure B-4A, a BZ gel disc of 1 mm diameter (and polymer volume fraction 0.25) was submerged in BZ solution (0.2 M MA, 0.14 M BrO_3, 0.7 M HNO_3, and 3 mM Br^-). The gel failed to oscillate under the presence of bromide inhibitor. Eventually, around 85 min, 0.2 kPa of compressive stress triggered oscillations in the gel. When the compressive stress was removed, oscillations ceased. Next, temperature was used to trigger oscillations in the gel. The temperature was gradually increased from 19°C to 21 °C and no oscillations occurred. Oscillations were triggered when the temperature was increased further, to 22°C (see Figure B-4B). The gel dimensions were measured before and after the temperature was increased, and the temperature induced a 16.7% strain and 27% change in overall gel volume at 22°C.

In a separate experiment, a BZ gel disc of 1 mm diameter (and polymer volume fraction 0.11) was submerged in BZ solution (0.2 M MA, 0.14 M BrO_3, 0.7 M HNO_3, and 3 mM Br^-). Again, the gel failed to oscillate under the presence of bromide inhibitor. Only 13 kPa of compressive stress was applied to the gel, so oscillations were never mechanically triggered in this gel. (Recall that over 25 kPa of compressive stress is required to trigger oscillations in gels with polymer volume fractions of 0.11). The temperature of the system was gradually increased in order to trigger oscillations in the gel. In this experiment, oscillations were not triggered until the temperature of the system reached 23°C (see Figure B-4C). Here, the strain induced by the temperature increase was only 9.4 %, while the volume change was 23 %. These experiments demonstrate that oscillations can be triggered in BZ gels by increasing the system temperature. Physically, the increase in temperature induces BZ gels to shrink because of the thermosensitive properties of the NIPAAm backbone. Essentially, both increasing the system temperature and application of compressive stress to BZ gels accomplishes the same goal of decreasing the overall gel volume and increasing the concentration of $Ru(bpy)_3$ to trigger oscillations.

B.1.4 Patterned BZ gels

Note that some of the data in this section were acquired by Abe Cherukara (as indicated).

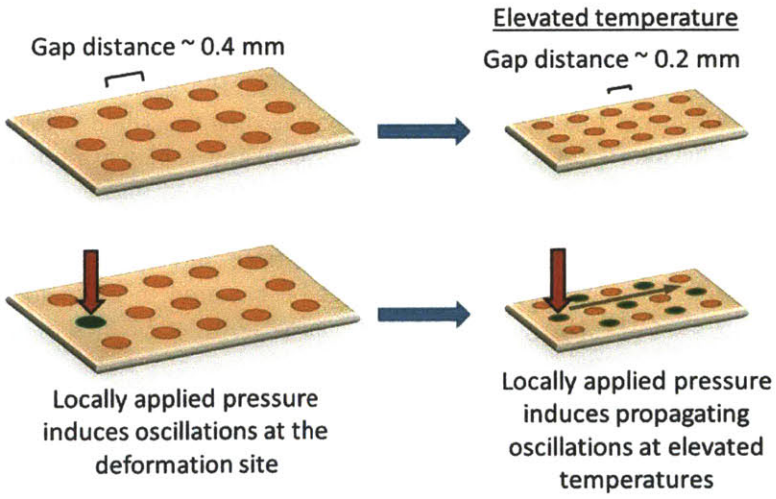

Figure B-5: Schematic of patterned BZ gels. The illustration shows how a patterned BZ gel has the potential to respond to changes in chemistry, temperature, and mechanical stress. The gap distances separating the $Ru(bpy)_3$ patches (orange circles) are altered by temperature changes of the system, causing mechanically induced signaling at elevated temperatures.

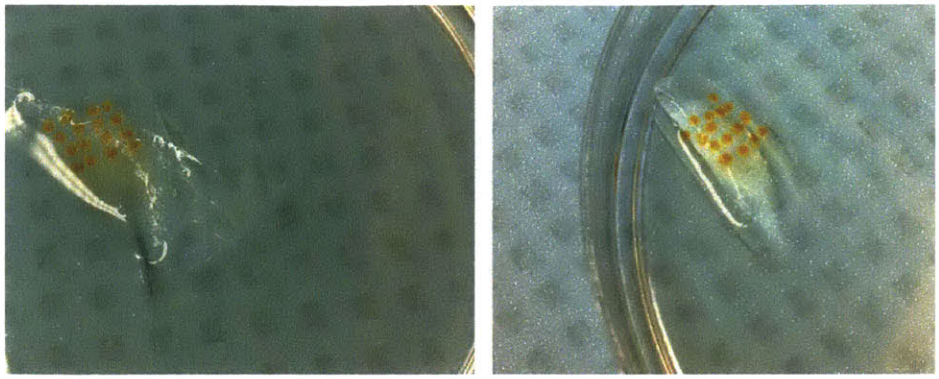

Figure B-6: Patterned BZ gels in which the $Ru(bpy)_3$ catalyst has been confined to circular patches. Gels were prepared by Abe Cherukara.

In order to study signal propagation in materials with tunable gap distances, "heterogeneous," or patterned BZ gels were fabricated. The gels were designed such that disc shaped gels comprising NIPAAm-co-$Ru(bpy)_3$ were confined within non-reactive NIPAAm gel containing no $Ru(bpy)_3$ catalyst. Shown in Figure B-6 is a schematic outline of the experimental goals. Because NIPAAm is a thermosensitive polymer, the gel will shrink with increasing temperature, thereby decreasing the gap distances separating $Ru(bpy)_3$ patches (orange circles). Above the critical gap distance (at low temperatures), only part of the system can oscillate in response to mechanical stimuli. However, below the critical gap distance (at higher temperatures), the entire system will oscillate in response to mechanical stimuli due to signal propagation among communicating $Ru(bpy)_3$ patches. Therefore, this system incorporates various elements from the thesis: temperature, mechanics, chemistry, and signal transmission.

Shown in Figure B-6 are images of patterned BZ gels. Here, BZ gel containing $Ru(bpy)_3$ was synthesized and hydrated as described previously. Next, Abe Cherukara cut the BZ gel into discs using a biopsy punch. NIPAAm pre-polymer liquid (lacking $Ru(bpy)_3$) was poured into a Petri dish containing the BZ gel discs. After arranging the BZ gel discs into a four by four grid, the NIPAAm pre-polymer was polymerized under UV light. While these particular patterned gels have not yet been tested in BZ acid, such images show that the BZ gel discs can be succesfully embedded within a non-reactive polymer gel.

In the following discussion and accompanying figures, we test similar patterned BZ gels in BZ acid, and expose the gels to either mechanical or temperature stimuli.

Shown in FigureB-7 is an experiment involving only two NIPAAm-co-$Ru(bpy)_3$ discs. The entire patterned gel was submerged in BZ acid (0.2 M MA, 0.1 M BrO_3, 0.7 M HNO_3), and oscillations were observed in the right disc alone. After 40 min, the temperature of the system was increased from 16 to 21^{o}C, and oscillations were observed in both discs. Since the gap distance separating the two discs decreased upon temperature increase, oscillations in the left disc may have been induced by chemical signal transmission from

the right disc. However, since temperature can also trigger oscillations in discs (discussed previously), it was not clear whether oscillations in the left disc were induced by chemical signaling or temperature triggering.

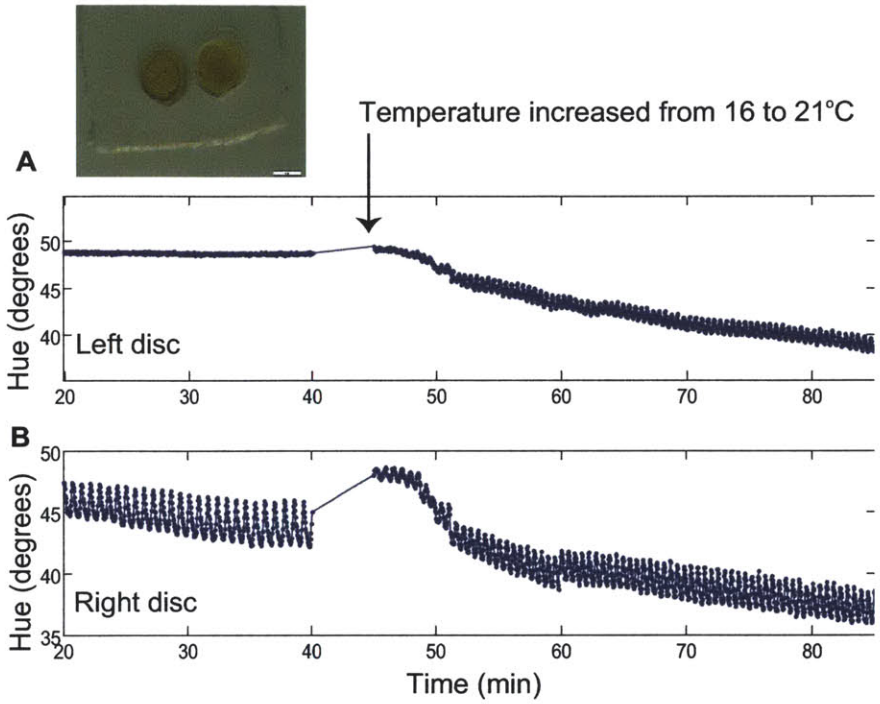

Figure B-7: Patterned BZ gel containing two discs comprising NIPAAm-co-$Ru(bpy)_3$. (A) Oscillations in the left disc, before and after the temperature was increased. (B) Oscillations in the right disc, before and after the temperature was increased.

In the next experiment, three BZ gels comprising NIPAAm-co-$Ru(bpy)_3$ were embedded in the NIPAAm gel. The resulting patterned gel (fabricated by Abe Cherukara) was submerged in BZ acid (0.1 M MA, 0.16 M BrO_3, 0.7 M HNO_3) for 20 h (overnight) to force all three BZ gel discs into a non-oscillatory state. After 20 h, the patterned gel was not oscillating (see data in Figure B-8A). Disc 1 (the left disc) was mechanically compressed using a glass slide, and oscillations were triggered in only disc 1. Discs 2 and 3 were not affected by the mechanical compression and did not oscillate (see Figure B-8B). By itself, this Figure shows that patterned gels can locally respond to mechanical compression by exhibiting BZ oscillations.

We continued the experiment and increased the temperature of the system while Disc 1 was mechanically compressed. Shown in Figure B-9A are oscillations in discs 1-3, after the temperature was increased from 17 to 21°C. Of course, disc 1 was already oscillating due to the mechanical compression. Interestingly, however, disc 2 began to oscillate almost 15 min after the temperature was increased. Disc 3 began to oscillate approximately 5 minutes after disc 2 started oscillating. Again, it was not clear whether chemical signaling from the mechanically compressed disc (disc 1) induced oscillations

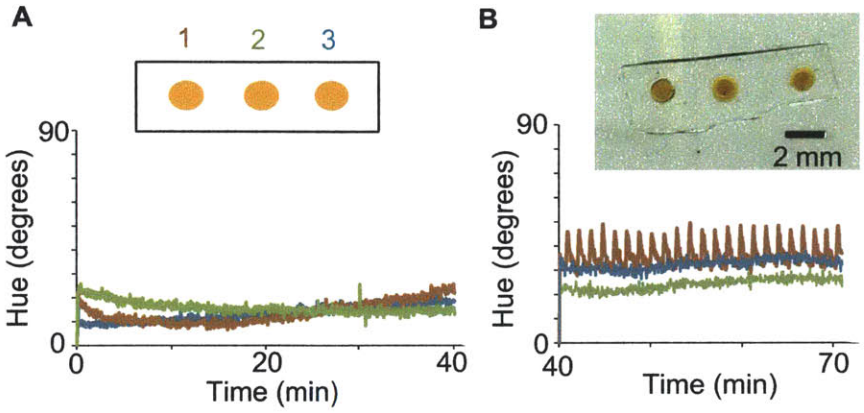

Figure B-8: Patterned BZ gel containing three discs comprising NIPAAm-co-$Ru(bpy)_3$. (A) In the absence of mechanical compression, all three BZ gel discs were non-oscillatory. (B) When disc 1 (dark red) was mechanically compressed, oscillations were triggered in disc 1. Discs 2 and 3 did not oscillate (green and blue, respectively).

in disc 2-3 or whether the temperature increase triggered oscillations. In addition, note the image shown in Figure B-9A. When the temperature of the system increased, the gel began to shrink and turn opaque. Due to light scattering by the microscope light, the images of the NIPAAm gel appeared black.

In an attempt to de-couple the mechanical and temperature stimuli, compressive stress was removed from disc 1, and the source of heating was shut off. Although the temperature of the system never cooled back down to 17°, Figure B-9B shows that disc 1 stopped oscillating almost immediately after compression was removed. On the other hand, discs 2 and 3 continued to oscillate. After approximately 15 min, disc 2 stopped oscillating, while disc 3 continued to oscillate for 35 min. It was not clear whether local temperature gradients caused the certain discs to oscillate. Initially, it was our aim to only trigger oscillations using mechanical stress, but the results in Figure B-9 show that temperature did trigger oscillations in the discs as well. Additional experiments should be performed in order to distinguish between temperature and mechanical triggering and induced signal propagation.

Overall, our results demonstrate that it is challenging to de-couple mechanical and temperature stimuli, since both types of stimuli result in an overall decrease in the gel volume and can trigger oscillations in BZ gels. Furthermore, we note that there are several synthesis issues regarding the preparation of patterned BZ gels. The first issue is that the patterned gels curl in BZ acid. Shown in Figure B-6 are patterned BZ gels that have curled up in water. Such curvature of the gel increases when the gels are submerged in BZ acid, making it difficult to image the samples. A second issue is that the gels become difficult to handle due to stickiness in BZ acid. A third issue is that the gels become opaque and are difficult to image when they darken

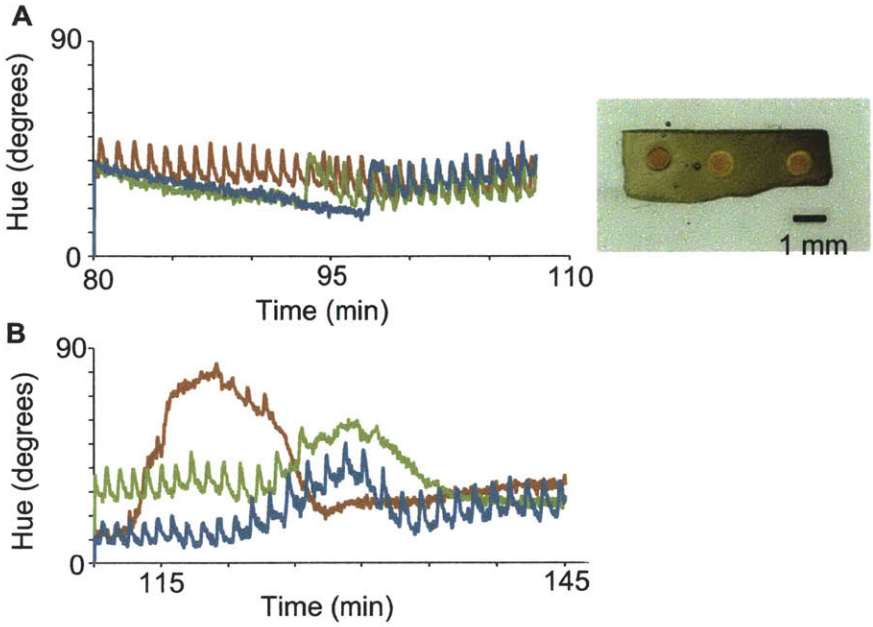

Figure B-9: (A) Hue of discs 1-3, while disc 1 was mechanically compressed and after temperature was increased to 21^{o}. (B) Hue of discs 1-3 after mechanically compression was removed and heating source was shut off.

under the microscope light. We were not able to add Br^{-} directly to the BZ solution because the gel shriveled up and turned opaque. In three instances, the gels turned opaque immediately upon addition of BZ acid. And as shown in Figure B-9, the gel also turned opaque when the temperature of the system was increased. Future experiments involving patterned BZ gels should address these difficulties.

Appendix C

Protocols

Heat-initiated BZ gel polymerization

1. Separately weigh out desired NIPAAm monomer, $Ru(bpy)_3$ monomer, AIBN, and MBAAm.
2. Mix solids in vial with methanol.
3. Use sonicator, if necessary, to fully dissolve all solids.
4. If solids do not dissolve, filter the pre-polymer liquid.
5. Place Petri dish (with lid over turned and underneath the main dish) inside glass crystalling dish.
6. Seal glass dish with large rubber stopper and parafilm.
7. Purge glass vessel of air by pumping nitrogen gas through the system for approximately 2 min.
8. Bubble nitrogen through pre-polymer liquid for 4 min (vent using a needle).
9. Carefully purge air from an empty syringe equipped with a long needle using nitrogen gas.
10. Using the syringe needle, carefully transfer pre-polymer liquid into the purged, glass dish.
11. Inject pre-polymer liquid between the Petri dish lid and main polystyrene dish.
12. Place entire crystallizing dish in oven at 60°C for 18 h.
13. Remove dish from oven, and inject methanol into the system using a syringe needle.
14. Eventually, remove the rubber stopper seal, and continue to submerge the polymer gel in methanol.
15. Soak the gel in methanol for one week, exchanging the solvent for fresh methanol each day (save discarded methanol washes).
16. Gradually hydrate gel by soaking the gel in methanol/water mixtures. Each day, exchange the old mixture with the following solutions: 75%/25%, 50%/50%, 25%/75%, and 0%/100% methanol/water.

UV-initiated BZ gel polymerization

1. Turn on UV lamp (allow 5 min for warm up). Ensure lab coat, gloves, and UV eye protection are worn at all times.
2. Separately weigh out desired NIPAAm monomer, $Ru(bpy)_3$ monomer, dimethoxy-2-phenylacetophenone, and MBAAm.
3. Mix solids in vial with methanol.
4. Use sonicator, if necessary, to fully dissolve all solids.
5. If solids do not dissolve, filter the pre-polymer liquid.
6. Pipette pre-polymer liquid into the Petri dish lid, and place Petri dish bottom on top of liquid such that liquid is evenly sandwiched.
7. Place the Petri dish under the UV lamp, and shield UV rays from other lab members.
8. Allow 1.5 5 min for polymerization to occur.
9. Soak polymerized gel in excess methanol.
10. Rinse unreacted monomers for one week by soaking the gel in methanol. Each day, exchange old methanol with fresh solvent.
11. Gradually hydrate gel by soaking the gel in methanol/water mixtures. Each day, exchange the old mixture with the following solutions: 75%/25%, 50%/50%, 25%/75%, and 0%/100% methanol/water.

BZ reaction in gels

1. Using a surgical blade or biopsy punch, cut gel to desired size and shape.
2. Place gel in new Petri dish and submerge gel in water.
3. Prepare BZ solution.
4. Vigorously mix BZ solution using vortexer to prevent bubble formation.
5. De-gas BZ solution by bubbling nitrogen gas through sealed vial (using a needle as the outlet).
6. Place solution under vacuum.
7. Pipette excess water out of Petri dish so BZ gel is no longer submerged.
8. Use syringe (no needle) to remove solution from vial.
9. Place filter on syringe, and slowly eject BZ solution on top of BZ gel.
10. Push BZ gel to bottom of Petri dish if the gel floats.
11. Remove any bubbles that stick to the gel (use needle to gently manipulate gel placement).
12. Focus microscope.
13. Open CellSens software.
14. Adjust scale bar to match microscope magnification.
15. Using CellSens timelapse imaging, acquire images as desired.

BZ solution recipe:

(ALWAYS ADD ACID TO WATER NOT WATER TO ACID!)

a. (mg malonic acid) = (desired Molarity) x (solution volume in mL) x 104.03 mg/mL
b. (mg sodium bromate) = (desired Molarity) x (solution volume in mL) x 150.89 mg/mL
c. (mL water) = (solution volume in mL) − (mL nitric acid)
d. (mL nitric acid) = (desired Molarity) x (solution volume in mL) / (1.0 M stock solution)

Examples:

Common preparation for large amplitude oscillations:

a. (mg malonic acid) = 0.0625 M x 5 mL x 104.03 mg/mL = 32.5 mg
b. (mg sodium bromate) = 0.085 M x 5 mL x 150.89 mg/mL = 64.1 mg
c. (mL water) = 5 − 4.5 mL = 0.5 mL
d. (mL nitric acid) = 0.9 M x 5 / (1.0 M stock solution) = 4.5 mL

Common preparation for mechanically triggered experiments:

e. (mg malonic acid) = 0.1 M x 5 mL x 104.03 mg/mL = 52 mg

f. (mg sodium bromate) = 0.16 M x 5 mL x 150.89 mg/mL = 120.7 mg
g. (mL water) = 5 mL − 3.5 mL = 1.5 mL
h. (mL nitric acid) = 0.7 M x 5 mL / (1.0 M stock solution) = 3.5 mL

Image analysis of BZ reaction

1. Save timelapse movie as an uncompressed avi file with lower resolution.
2. Open file in ImageJ.
3. Draw a straight line on the scale bar, and select Analyze → Set scale
4. Enter known length of scale bar, then unselect line.
5. Split images into red, green, and blue: Select Image → Color → RGB split.
6. For each set of R, G, and B data, select the desired area of interest,[1] then open Plugins → Stacks → Measure Stack.
7. Copy data into Excel or Matlab.
8. Plot Hue by calculating values based off of R, G, and B vector data.

The following equations were used to plot hue:[88]

$$\alpha = R - 0.5(G + B) \tag{C.1}$$

$$\beta = \frac{\sqrt{3}}{2}(G - B) \tag{C.2}$$

$$Hue = 180 * atan2(\beta, \alpha)/\pi \tag{C.3}$$

Image analysis of mechanical oscillations in gels

1. Save timelapse movie as an uncompressed avi file with lower resolution.
2. Open file in ImageJ.
3. Draw a straight line on the scale bar, and select Analyze → Set scale
4. Enter known length of scale bar, then unselect line.
5. Split images into red, green, and blue: Select Image → Color → RGB split.
6. Analyzing the blue images only, go to Image → Adjust → Threshold.
7. Manually determine threshold that accurately fills in projected gel area (with distinct gel edges).
(Typical threshold values were 0,115 or 0, 60).[2]

[1] Use point selection tool if analyzing a single spot on the BZ gel. Use elliptical tool to select a larger area of the BZ gel to analyze (i.e. if average hue of an area is of interest).

[2] Analysis results should be manually compared to the actual gel dimensions, because at low concentrations of $Ru(bpy)_3$, the gel edges are poorly defined.

Mechanical triggering of oscillations in BZ gels

1. Cut BZ gel into desired shape and size.
2. Place BZ gel on bottom of Petri dish and submerge in BZ acid.
3. If gel oscillates, then add small amount of NaBr to BZ acid. (e.g., 10-30 μL of 0.7 M NaBr)
4. Record steady-state of gel using timelapse imaging for approx. 30 min.
5. Gently place glass slide of known mass on top surface of the gel (use tweezers to center gel with center of glass slide).
8. Record timelapse images of gel under compression for at least 15 m.
9. If oscillations are not triggered, replace glass slide with heavier slide, or add additional slides to the stack.

Mechanical resuscitation of oscillations

1. Cut BZ gel into desired shape and size.
2. Place BZ gel on bottom of Petri dish and submerge in BZ acid.
3. Allow gel to oscillate for approx. 1 h.
4. Cover system with Petri dish lid and shield from light.
5. Leave system covered for 20 h (overnight).
6. Remove lid and turn on light. Record timelapse images of gel for 1 h.
7. Gently place glass slide of known mass on top surface of the gel (use tweezers to center gel with center of glass slide).
8. Record timelapse images of gel under compression for at least 15 m.
9. If oscillations are not triggered, replace glass slide with heavier slide, or add additional slides to the stack.

Fabrication of patterned BZ gels

1. Using a biopsy punch, carefully punch gel discs from hydrated BZ gel.
2. Place BZ gel discs in Petri dish.
3. Turn on UV lamp (allow 5 min for warm up). Ensure lab coat, gloves, and UV eye protection are worn at all times.
4. Prepare pre-polymer NIPAAm.
5. Pipette pre-polymer liquid into the Petri dish.
6. Re-arrange BZ gel discs in desired pattern (use a fine needle).
7. Place the Petri dish under the UV lamp, and shield UV rays from other lab members.
8. Allow 1.5 5 min for polymerization to occur.
9. Soak polymerized gel in excess methanol.
10. Rinse unreacted monomers for one week by soaking the gel in methanol. Each day, exchange old methanol with fresh solvent.
11. Gradually hydrate gel by soaking the gel in methanol/water mixtures. Each day, exchange the old mixture with the following solutions: 75%/25%, 50%/50%, 25%/75%, and 0%/100% methanol/water.

Pre-polymer recipe

a. 260 mg NIPAAm monomer
b. 34 mg UV initiator
c. 12 mg MBAAm crosslinker
d. 1 mL Methanol
e. Drop of DMSO (25-50 μL) - optional

Bibliography

[1] Tokarev, I. and Minko, S. *Soft Matter* **5**(3), 511–524 (2009).

[2] Roy, I. and Gupta, M. N. *Chemistry & biology* **10**(12), 1161–1171 (2003).

[3] Chen, I., Kuksenok, O., Yashin, V., Balazs, A., and Van Vliet, K. *Adv. Funct. Mater.* **22**(12), 2535–2541 (2012).

[4] Chen, I., Kuksenok, O., Yashin, V., Moslin, R., Balazs, A., and Van Vliet, K. *Soft Matter* **7**(7), 3141–3146 (2011).

[5] Kuksenok, O., Yashin, V., and Balazs, A. *Soft Matter* **3**(9), 1138–1144 (2007).

[6] Kuksenok, O., Yashin, V., and Balazs, A. *Soft Matter* **5**, 1835–1839 (2009).

[7] Kuksenok, O., Dayal, P., Bhattacharya, A., Yashin, V. V., Deb, D., Chen, I. C., Van Vliet, K. J., and Balazs, A. C. *Chemical Society Reviews* (2013).

[8] Yoshida, R., Onodera, S., Yamaguchi, T., and Kokufuta, E. *J. Phys. Chem. A* **103**(43), 8573–8578 (1999).

[9] Liu, F. and Urban, M. W. *Progress in Polymer Science* **35**(1), 3–23 (2010).

[10] Ahn, S.-k., Kasi, R. M., Kim, S.-C., Sharma, N., and Zhou, Y. *Soft Matter* **4**(6), 1151–1157 (2008).

[11] Stuart, M. A. C., Huck, W. T., Genzer, J., Müller, M., Ober, C., Stamm, M., Sukhorukov, G. B., Szleifer, I., Tsukruk, V. V., Urban, M., et al. *Nature materials* **9**(2), 101–113 (2010).

[12] Kakugo, A., Sugimoto, S., Gong, J. P., and Osada, Y. *Advanced Materials* **14**(16), 1124–1126 (2002).

[13] Kitamura, K., Tokunaga, M., Iwane, A. H., and Yanagida, T. *Nature* **397**(6715), 129–134 (1999).

[14] Epstein, I. R. and Showalter, K. *The Journal of Physical Chemistry* **100**(31), 13132–13147 (1996).

[15] Zhabotinsky, A. M. In *Proc. Acad. Sci. USSR*, volume 157, 392–395, (1964).

[16] Degn, H. *Journal of Chemical Education* **49**(5), 302 (1972).

[17] Tyson, J. *Oscillations and Traveling Waves in Chemical Systems, edited by Field, R.J. and Burger, M.* Wiley, (1985).

[18] Scott, S. *Oscillations, Waves, and Chaos in Chemical Kinetics.* Oxford University Press, (1994).

[19] Ruoff, P. and Noyes, R. M. *The Journal of chemical physics* **84**, 1413 (1986).

[20] Aller Pellitero, M., Alvarez Lamsfus, C., and Borge, J. *Journal of Chemical Education* (2013).

[21] Petrov, V., Gaspar, V., Masere, J., and Showalter, K. *Nature* **361**(6409), 240–243 (1993).

[22] Bialkowski, J., Karaman, S., Otte, M., and Frazzoli, E. *Algorithmic Foundations of Robotics X* , 365–380 (2013).

[23] Steinbock, O., Tóth, A., Showalter, K., et al. *Science (New York, NY)* **267**(5199), 868 (1995).

[24] Epstein, I. R. *Proceedings of the National Academy of Sciences* **103**(43), 15727–15728 (2006).

[25] Shanks, N. *Foundations of Chemistry* **3**(1), 33–53 (2001).

[26] Winfree, A. et al. *Science (New York, NY)* **266**(5187), 1003 (1994).

[27] Goldbeter, A. et al. *Nature* **420**(6912), 238–245 (2002).

[28] Brandman, O. and Meyer, T. *Science Signalling* **322**(5900), 390 (2008).

[29] Huo, B., Lu, X., Costa, K., Xu, Q., and Guo, X. *Cell Calcium* **47**(3), 234–241 (2010).

[30] Kohl, P., Hunter, P., and Noble, D. *Prog. Biophys. Mol. Biol.* **71**, 91–138 (1999).

[31] Volkov, A., Foster, J., and Markin, V. *Plant, Cell, & Environment* **33**(5), 816–827 (2010).

[32] Malone, M. *New Phytol.* **128**(1), 49–56 (1994).

[33] Braam, J. *New Phytologist* **165**(2), 373–389 (2005).

[34] Beyer, M., Clausen-Schaumann, H., et al. *Chem. Rev* **105**(8), 2921–2948 (2005).

[35] Kuckling, D. *Colloid & Polymer Science* **287**(8), 881–891 (2009).

[36] Miyata, T., Nakamae, K., Hoffman, A., and Kanzaki, Y. *Macromolecular Chemistry and Physics* **195**(4), 1111–1120 (1994).

[37] Tanaka, T., Nishio, I., Sun, S., and Ueno-Nishio, S. *Science* **218**, 467–469 (1982).

[38] Capadona, J. R., Shanmuganathan, K., Tyler, D. J., Rowan, S. J., and Weder, C. *Science* **319**(5868), 1370–1374 (2008).

[39] Schmidt, D. J., Cebeci, F. C., Kalcioglu, Z. I., Wyman, S. G., Ortiz, C., Van Vliet, K. J., and Hammond, P. T. *ACS nano* **3**(8), 2207–2216 (2009).

[40] Chia, K.-K., Rubner, M. F., and Cohen, R. E. *Langmuir* **25**(24), 14044–14052 (2009).

[41] He, X., Aizenberg, M., Kuksenok, O., Zarzar, L. D., Shastri, A., Balazs, A. C., and Aizenberg, J. *Nature* **487**(7406), 214–218 (2012).

[42] Yoshida, R., Takahashi, T., Yamaguchi, T., and Ichijo, H. *J. Am. Chem. Soc.* **118**, 5134–5135 (1996).

[43] Shinohara, S.-i., Seki, T., Sakai, T., Yoshida, R., and Takeoka, Y. *Chemical Communications* (39), 4735–4737 (2008).

[44] Ito, Y., Nogawa, M., and Yoshida, R. *Langmuir* **19**(23), 9577–9579 (2003).

[45] Yoshida, R., Tanaka, M., Onodera, S., Yamaguchi, T., and Kokufuta, E. *J. Phys. Chem. A* **104**(32), 7549–7555 (2000).

[46] Tabata, O., Hirasawa, H., Aoki, S., Yoshida, R., and Kokufuta, E. *Sensors and Actuators A: Physical* **95**(2), 234–238 (2002).

[47] Murase, Y., Maeda, S., Hashimoto, S., and Yoshida, R. *Langmuir* **25**(1), 483–489 (2008).

[48] Sakai, T., Hara, Y., and Yoshida, R. *Macromolecular rapid communications* **26**(14), 1140–1144 (2005).

[49] Hara, Y., Sakai, T., Maeda, S., Hashimoto, S., and Yoshida, R. *The Journal of Physical Chemistry B* **109**(49), 23316–23319 (2005).

[50] Hara, Y. and Yoshida, R. *Langmuir* **21**(21), 9773–9776 (2005).

[51] Maeda, S., Hara, Y., Sakai, T., Yoshida, R., and Hashimoto, S. *Advanced Materials* **19**(21), 3480–3484 (2007).

[52] Hara, Y. and Yoshida, R. *The Journal of Physical Chemistry B* **112**(29), 8427–8429 (2008).

[53] Tateyama, S., Shibuta, Y., and Yoshida, R. *The Journal of Physical Chemistry B* **112**(6), 1777–1782 (2008).

[54] Hara, Y. and Yoshida, R. *The Journal of chemical physics* **128**, 224904 (2008).

[55] Suzuki, D., Sakai, T., and Yoshida, R. *Angewandte Chemie* **120**(5), 931–934 (2007).

[56] Hidaka, M. and Yoshida, R. *Journal of Controlled Release* **150**(2), 171–176 (2011).

[57] Aihara, R. and Yoshikawa, K. *J. Phys. Chem. A* **105**(37), 8445–8448 (2001).

[58] Konotop, I., Nasimova, I., Rambidi, N., and Khokhlov, A. *Polymer Science Series B* **51**(9), 383–388 (2009).

[59] Bishop, K. and Grzybowski, B. *Physical review letters* **97**(12), 128702 (2006).

[60] Yuan, P., Kuksenok, O., Gross, D. E., Balazs, A. C., Moore, J. S., and Nuzzo, R. G. *Soft Matter* **9**(4), 1231–1243 (2013).

[61] Smith, M. L., Slone, C., Heitfeld, K., and Vaia, R. A. *Advanced Functional Materials* (2013).

[62] Suzuki, K., Yoshinobu, T., and Iwasaki, H. *Chemical physics letters* **349**(5), 437–441 (2001).

[63] Munuzuri, A., Innocenti, C., Flesselles, J., Gilli, J., Agladze, K., and Krinsky, V. *Physical Review E* **50**(2), 667–670 (1994).

[64] Hara, Y. and Yoshida, R. *Macromolecular Chemistry and Physics* **210**(24), 2160–2166 (2009).

[65] Hara, Y. and Yoshida, R. *Macromolecular rapid communications* **30**(19), 1656–1662 (2009).

[66] Hidaka, M. and Yoshida, R. *Journal of Controlled Release* **150**(2), 171–176 (2011).

[67] Ueno, T. and Yoshida, R. *The Journal of Physical Chemistry A* **115**(21), 5231–5237 (2011).

[68] Okeyoshi, K. and Yoshida, R. *Advanced Functional Materials* **20**(5), 708–714 (2010).

[69] Okeyoshi, K., Suzuki, D., and Yoshida, R. *Langmuir* **28**(2), 1539–1544 (2011).

[70] Yashin, V. and Balazs, A. *Macromolecules* **39**(6), 2024–2026 (2006).

[71] Kuksenok, O., Yashin, V., and Balazs, A. *Phys. Rev. E* **78**, 041406 (2008).

[72] Dayal, P., Kuksenok, O., and Balazs, A. C. *Proceedings of the National Academy of Sciences* **110**(2), 431–436 (2013).

[73] Dayal, P., Kuksenok, O., Bhattacharya, A., and Balazs, A. C. *Journal of Materials Chemistry* **22**(1), 241–250 (2012).

[74] Toiya, M., González-Ochoa, H. O., Vanag, V. K., Fraden, S., and Epstein, I. R. *The Journal of Physical Chemistry Letters* **1**(8), 1241–1246 (2010).

[75] Delgado, J., Li, N., Leda, M., González-Ochoa, H. O., Fraden, S., and Epstein, I. R. *Soft Matter* **7**(7), 3155–3167 (2011).

[76] Yashin, V., Van Vliet, K., and Balazs, A. *Physical Review E* **79**(4), 46214 (2009).

[77] Balazs, A. *Materials Today* **10**(9), 18–23 (2007).

[78] Sottos, N., White, S., and Bond, I. *J.R.Soc. Interface* **4**, 347–348 (2007).

[79] Ghosh, P. and Spiro, T. *Journal of the American Chemical Society* **102**(17), 5543–5549 (1980).

[80] Schultze, X., Serin, J., Adronov, A., and Fréchet, J. *Chemical Communications* **2001**(13), 1160–1161 (2001).

[81] Schwindeman, J. A., Woltermann, C. J., and Letchford, R. J. *Chemical Health and Safety* **9**(3), 6–11 (2002).

[82] Sykes, R. A., Mani, M. M., and Hiebert, J. M. *Journal of Burn Care & Research* **7**(4), 343–347 (1986).

[83] Kumaraswamy, J., Hirusappa, R., Naidu, J., and Raghavendra, R. *International Journal of Oral and Maxillofacial Pathology* **2**(2), 13–19 (2011).

[84] Sun, T., Wang, G., Feng, L., Liu, B., Ma, Y., Jiang, L., and Zhu, D. *Angewandte Chemie International Edition* **43**(3), 357–360 (2003).

[85] Matzelle, T., Geuskens, G., and Kruse, N. *Macromolecules* **36**(8), 2926–2931 (2003).

[86] Yoshida, R., Takahashi, T., Yamaguchi, T., and Ichijo, H. *Advanced Materials* **9**(2), 175–178 (2004).

[87] Yashin, V. and Balazs, A. *Science* **314**(5800), 798 (2006).

[88] Hanbury, A. *Pattern Recognition Letters* **29**(4), 494–500 (2008).

[89] Yoshida, R., Takei, K., and Yamaguchi, T. *Macromolecules* **36**(6), 1759–1761 (2003).

[90] Sasaki, S., Koga, S., Yoshida, R., and Yamaguchi, T. *Langmuir* **19**(14), 5595–5600 (2003).

[91] Yoshida, R., Otoshi, G., Yamaguchi, T., and Kokufuta, E. *The Journal of Physical Chemistry A* **105**(14), 3667–3672 (2001).

[92] Yoshida, R. *Advanced Materials* **22**, 3463–3483 (2010).

[93] Mikhailov, A. and Showalter, K. *Physics Reports* **425**(2-3), 79–194 (2006).

[94] Yamaguchi, T., Kuhnert, L., Nagy-Ungvrai, Z., M. S., and Hess, B. *Journal of Physical Chemistry* **95**(15), 5831–5837 (1991).

[95] Murase, Y., Maeda, S., Hashimoto, S., and Yoshida, R. *Langmuir: the ACS journal of surfaces and colloids* **25**(1), 483 (2009).

[96] Yoshida, R., Kokufuta, E., and Yamaguchi, T. *Chaos: An Interdisciplinary Journal of Nonlinear Science* **9**, 260 (1999).

[97] Rustici, M., Branca, M., Caravati, C., and Marchettini, N. *Chemical Physics Letters* **263**(3-4), 429–434 (1996).

[98] Rustici, M., Caravati, C., Petretto, E., Branca, M., and Marchettini, N. *J. Phys. Chem. A* **103**(33), 6564–6570 (1999).

[99] Amemiya, T., Yamamoto, T., Ohmori, T., and Yamaguchi, T. *Journal of Physical Chemistry A* **106**, 612–620 (2002).

[100] Munuzuri, A., Innocenti, C., Flesselles, J., Gilli, J., Agladze, K., and Krinsky, V. *Physical Review E* **50**(2), 667–670 (1994).

[101] De, R., Zemel, A., and Safran, S. *Biophysical Journal* **94**(5), L29 – L31 (2008).

[102] Vogel, V. and Sheetz, M. *Nature Reviews Molecular Cell Biology* **7**(4), 265–275 (2006).

[103] Fukuda, H., Tamari, N., Morimura, H., and Kai, S. *J. Phys. Chem. A.* **109**, 11250–11254 (2005).

[104] Rubinstein, M. and Colby, R. *Macromolecules* **27**(12), 3184–3190 (1994).

[105] Shiota, T., Ikura, Y. S., and Nakata, S. *The Journal of Physical Chemistry B* (2013).

[106] Park, S., Goodman, M., and Pruitt, B. *Proceedings of the National Academy of Sciences* **104**(44), 17376–17381 (2007).

[107] Chen, C. *Journal of cell science* **121**(20), 3285–3292 (2008).

[108] Geiger, B., Spatz, J., and Bershadsky, A. *Nature Reviews Molecular Cell Biology* **10**(1), 21–33 (2009).

[109] Bacchus, W., Lang, M., El-Baba, M., Weber, W., Stelling, J., and Fussenegger, M. *Nature Biotechnology* **30**(10), 991–996 (2012).

[110] Hiyama, S., Suda, M., Egashira, R., Enomoto, A., Moore, M., and Nakano, T. *Journal of the Institute of Electronics, Information and Communication Engineers* **89**(2), 162 (2006).

[111] King, J. S. and Insall, R. H. *Trends in cell biology* **19**(10), 523–530 (2009).

[112] March, J. C. and Bentley, W. E. *Current opinion in biotechnology* **15**(5), 495–502 (2004).

[113] Field, R. J. and Noyes, R. M. *The Journal of Chemical Physics* **60**, 1877 (1974).

[114] Goldbeter, A. et al. *Nature* **420**(6912), 238–245 (2002).

[115] Adamatzky, A. *Chaos, Solitons & Fractals* **21**(5), 1259–1264 (2004).

[116] Toth, R., Stone, C., Adamatzky, A., de Lacy Costello, B., and Bull, L. *Chaos, Solitons & Fractals* **41**(4), 1605–1615 (2009).

[117] Harned, H. *Chem. Rev.* **40**(3), 461–522 (1947).

[118] Yashin, V. and Balazs, A. *The Journal of Chemical Physics* **126**, 124707 (2007).

[119] Suzuki, D., Kobayashi, T., Yoshida, R., and Hirai, T. *Soft Matter* **8**, 11447–11449 (2012).

[120] Yoshida, R. and Uesusuki, Y. *Biomacromolecules* **6**(6), 2923–2926 (2005).

[121] Levin, S. A. *Frontiers in mathematical biology.* Springer-Verlag, (1994).

[122] Konotop, I. Y., Nasimova, I., Rambidi, N., and Khokhlov, A. *Polymer Science Series B* **53**(1-2), 26–30 (2011).

[123] Constantinides, G., Kalcioglu, Z. I., McFarland, M., Smith, J. F., and Van Vliet, K. J. *Journal of biomechanics* **41**(15), 3285–3289 (2008).

[124] Muniz, E. C. and Geuskens, G. *Macromolecules* **34**(13), 4480–4484 (2001).